A Semi-Analytical Weight Estimation Method for Oval Fuselages in Novel Aircraft Configurations

R.K. Schmidt

Master of Science Thesis

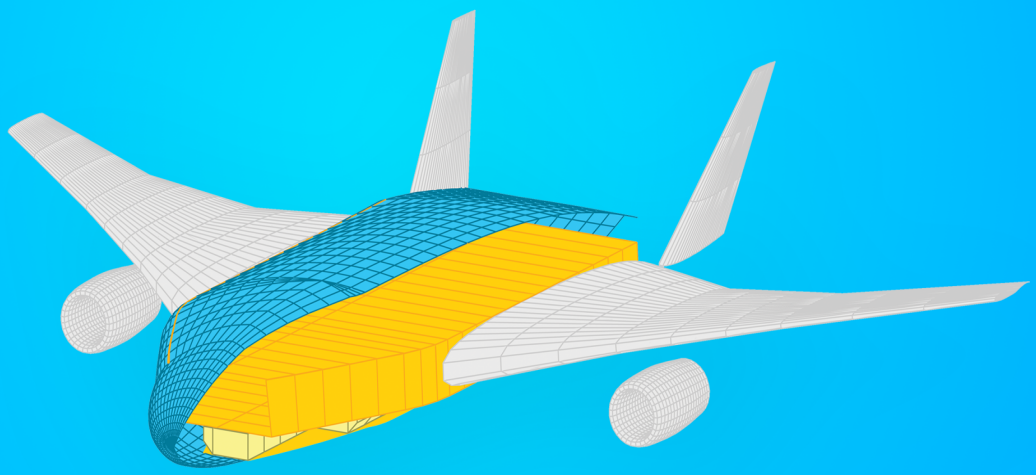

TU Delft Delft University of Technology

A Semi-Analytical Weight Estimation Method for Oval Fuselages in Novel Aircraft Configurations

Master of Science Thesis

For the degree of Master of Science in Aerospace Engineering at Delft University of Technology

R.K. Schmidt

October 25, 2013

Faculty of Aerospace Engineering · Delft University of Technology

Delft University of Technology
Department of
Aerospace Engineering

The undersigned hereby certify that they have read and recommend to the Faculty of Aerospace Engineering for acceptance a thesis entitled

A Semi-Analytical Weight Estimation Method for Oval Fuselages in Novel Aircraft Configurations

by

R.K. Schmidt

in partial fulfillment of the requirements for the degree of

Master of Science Aerospace Engineering

Dated: October 25, 2013

Supervisor(s):

dr.ir. R. Vos

Reader(s):

prof.dr.ir. L. Veldhuis

dr.ir. F.J.J.M.M. Geuskens

Abstract

The aircraft industry faces a number of challenges to continue its success in the future. While the industry has seen revolutions in the fields of propulsion, materials and flight controls, the general aircraft layout has not changed since the shift from the first flying machines to the tube-and-wing configuration which has dominated the skies for the last decades. Research in aircraft design is focusing on novel aircraft configurations in search for a step change in terms of overall transport efficiency. Where conceptual aircraft design of conventional aircraft rely heavily on empirical methods, so-called Class 2 methods, to evaluate the performance of a design. Since these methods are based on statistical data they are not accurate when used for novel aircraft. Therefore there is a strong need for methods that are valid for the conceptual aircraft design of these aircraft. The method proposed in this thesis is a semi-analytical method for estimating the weight of a fuselage constructed using the oval fuselage concept.

The oval fuselage concept is a concept for a wide unobstructed pressurized cabin that can be used for Blended Wing Body (BWB) aircraft or conventional aircraft. A parameterization of the oval fuselage is presented along with a method for estimating the weight of the oval fuselage for conventional and unconventional aircraft. It is demonstrated that the oval cross section can be used for the design of conventional tube-and-wing aircraft with a single-deck or twin-deck layout as well as for blended-wing-body aircraft. It is also shown that the oval cross section allows for additional design freedom of the fuselage shape without introducing any bending loads in the fuselage skin panels.

The weight estimation of the fuselage is based on the combination of pressurization loads, steady-state maneuver loads, aerodynamic loads and landing loads. Each of the structural members of the inner structure is sized based on two-dimensional structural analysis satisfying requirements on bi-axial strength, global buckling, crippling, dimpling, and wrinkling. The outer structure is sized using a global buckling criteria adapted from cylinders and a local buckling criteria based on buckling of slender plates. Empirical methods are used to calculate the nonstructural weight and additional weight. Examples are presented of various oval-fuselage incarnations and associated weight predictions.

A verification of the structural analysis method by a finite-element analysis is done and it is shown that the made assumptions for the analysis of the structure are valid within the application of aircraft fuselage design. The weight estimation method is compared with weight

prediction methods from the open literature and with weight data of existing aircraft. The accuracy of the weight estimation is similar to the accuracy of empirical methods for circular fuselages. A sensitivity analysis is performed which gives insight in the design of oval fuselages. In a comparison study between a canard, Prandtl and tube-and-wing configuration it is shown that the fuselage weight is significantly lower in the canard and Prandtl configuration compared to the tube-and-wing configuration. Examples are shown of oval fuselages in aircraft designs and a weight estimation is performed on these fuselage to form a basis for future research on this subject.

Acknowledgements

This thesis is written as part of the Master Program in System Engineering and Aircraft Design at the Faculty of Aerospace Engineering of Delft University of Technology. This report forms the final step in completing this program and with this final step also the end of my time as a student. I am happy that I have been able to contribute to the body of knowledge in the field of novel aircraft design during my Master Program and during my year at the CleanEra research group. The faculty of Aerospace Engineering has a large pool of bright minds from whom I often got help from when faced with difficult problems.

First of all, I would like to thank my supervisor dr.ir. Roelof Vos for his support, ideas and invaluable advise along the course of this research project. I also would like to thank prof.dr. J. Arbocz for his advice on buckling of thin walled structures. Furthermore, I would like to thank Arne, Niels and Reno with whom I worked on the foundations of the Initiator. You guys helped me out with all kinds of little bugs that popped up in the computer programs we daily use for our research. I would also like to thank my committee: prof.dr.ir. Leo Veldhuis, dr.ir. Roelof Vos and dr.ir. François Geuskens.

Many thanks to all my friends and fellow students of the FPP department and especially the students of Room 1 who made this busy period also a very amusing period. A special thanks goes to my parents, who have always been a tremendous support and have always encouraged me to chase my dreams.

Delft, University of Technology — R.K. Schmidt
October 25, 2013

List of symbols

Symbol	Unit	Definition
A	[m^2]	Area
A	[-]	Stress amplitude
b	[m]	Span
B	[m]	Width of the fuselage at a specific point
b_j	[m]	Width of a stiffened panel strip
c	[m]	Chord
$C_{\text{fr,circ}}$	[-]	Shanley frame constant
c_b	[-]	Coefficient of bending
c_l	[-]	Sectional lift coefficient
D	[N/m]	Plate bending stiffness
D	[m]	Diameter of a circular fuselage
e	[m]	Eccentricity of the horizontal member
E	[N/m^2]	Young's modulus
F	[N]	Force
G	[N/m^2]	Shear modulus
H	[m]	Total height of the center section
h_1	[m]	Height between the top of the fuselage center section and the ceiling
h_2	[m]	Cabin height
h_3	[m]	Height of the bottom of the fuselage center section and the floor
h_{oval}	[m]	Total height of the oval cross-section
I	[m^4]	Moment of inertia
k	[-]	Buckling coefficient
K	[-]	Constant
k	[N/m]	Spring stiffness
k_x	[-]	Cylindrical shell coefficient
L	[m]	Length
M	[Nm]	Sectional moment
N	[N/m]	Line load
Q	[m^3]	Moment of area
q	[N/m]	Shear flow
r	[m]	Radius (of a circular shell part)

Symbol	Unit	Definition
R	[-]	Stress ratio
S	[-]	Shear force
S	[m^2]	Wing area
t	[m]	Thickness
v	[m]	Deflection
w_c	[m]	Half of the width of the horizontal member (ceiling)
w_f	[m]	Half of the width of the horizontal member (floor)
x	[m]	Longitudinal axis
y	[m]	Lateral axis
z	[m]	Vertical axis
Z	[-]	Batdorf curvature parameter
α	[rad]	Angle between cabin floor or bottom, section top or bottom
α	[rad]	Spring stiffness
$\bar{t}$	[m]	Smeared thickness
β	[rad]	Outward angle of the wall
δ	[m]	Deflection
Δp	[N/m^2]	Pressure differential
ϵ	[-]	Fineness ratio of the fuselage center section
γ	[rad]	Angle of isosceles triangle
κ	[rad]	Angle between the fuselage section and the XZ-plane
λ		Characteristic parameter of the differential equation
ν	[-]	Poisson's ratio
ϕ	[rad]	Angle spanned over the arc
ρ	[kg/m^3]	Density
σ	[N/m^2]	Normal stress
τ	[N/m^2]	Shear stress
θ	[-]	Correlation factor
ζ	[-]	Upsweep ratio

List of subscripts

Subscripts	Definition
0	At zero cycles
1	The arc spanning the top of the fuselage
2	The arc spanning the side of the fuselage
3	The arc spanning the bottom of the fuselage
b	Due to bending
ceiling	Of the ceiling
circ	Circular
core	Of the core material
cr	Critical
crimping	Due to crimping
dimpling	Due to dimpling
eq	Flat plate equivalent
face	Of the face sheet
fl	Floor
fr	Frame
frame	Of the frame
global	Due to global buckling
hoop	In circumferential direction
j	Stiffened panel strip
lat	In lateral direction
long	In longitudinal direction
oval	Oval
p	Due to pressure
section	Of the section
shear	Of the section used for shear
shell	Of the shell
sk	Skin
stringer	Of the stringer
wall	Of the wall
wing	Relating to the main wing
wrinkling	Due to wrinkling

Subscripts	Definition
y	Yield

Glossary

List of Acronyms

BWB	Blended Wing Body
NS	Navier-Stokes
RANS	Reynolds-Averaged Navier-Stokes
AVL	Athena Vortex Lattice

Table of Contents

Chapter 1

Introduction

The aircraft industry faces a number of challenges in order to be successful in the future. The industry will continue to grow, the oil price will continue to rise and the political climate is demanding a reduction of transport aircraft noise and emissions. This powers a continuous search for gains in the operational efficiency of transport aircraft and lower their footprint on the environment. The industry has seen revolutions in the fields of propulsion with the shift from propellers to turbofans, in the fields of structures with the shift from wood to metal to composite and in the field of aircraft systems with the shift from cables and hydraulics to an all electric aircraft. Yet the general aircraft configuration has not changed since the shift from the first flying machines to the tube-wing configuration which has dominated the skies for the last decades. Research on a conceptual level has shown that the blended wing body (BWB) and aircraft with pressurized non-circular fuselages have great potential to provide a step change in terms of aerodynamic efficiency, structural weight and noise levels for transport aircraft [1, 2]. To fulfill this promise a fuselage is needed that is structurally efficient, allows for aerodynamic shape optimization and offers great flexibility in cabin configuration. The research presented in this thesis focuses on these three problems and specifically the efficiency and operative empty weight of the oval fuselage both in BWB aircraft as aircraft with pressurized non-circular fuselages.

A non-cylindrical fuselage has a number of advantages over circular fuselages. The diameter of a circular fuselage is primarily dictated by the height of the human body, whereas with the oval fuselage the designer is free to choose the cabin width. This makes it possible to design non-circular fuselages for conventional aircraft that are wider, shorter and take advantage of aerodynamic shaping. Examples of fuselages with non-circular cross sections are shown in Figure 1-1.

The reason to choose a non-circular cross section over a circular cross section is threefold:

- A shorter and wider fuselage reduces the longitudinal bending loads, which could result in a reduction in structural weight.

(a) Blended wing body aircraft [3]

(b) Hybrid Wing Body aircraft [4]

(c) Double-bubble tube-and-wing aircraft [2]

(d) Elliptical fuselage [5]

Figure 1-1: Examples of aircraft with non-circular fuselages

- A fuselage with a flatter non-circular cross section makes geometric integration or blending with the connected components such as wings and engines easier. This could potentially reduce wetted area and reduce interference drag.
- Taking into consideration the total fuselage structural weight, a wider fuselage that is able to generate lift reduces the lateral bending due to lift and could possibly reduce the weight of the main wings.

1-1 Historical background of non-circular fuselages

Non-circular fuselages are not a new trend, actually the first series of fuselages have been non-circular. Only since the advent of pressurized passenger cabins aircraft designers have resorted to circular fuselages due to their inherent efficiency in resisting pressurization loads. The current development and research in the field of non-circular fuselages is largely thrived by the development of the BWB transport aircraft in which a structurally efficient non-circular lift generating pressurized cabin is the key to its feasibility.

The BWB aircraft concept evolved from the concepts of the flying wing, flying fuselage and lifting body that were conceived in the early days of flight as the idea of the optimal aerodynamic shape. Besides aerodynamic benefits it features inherent low material cost and low manufacturing cost due to the absence of a tail making it an attractive concept. The currently proposed configuration can be seen as a combination of the Junkers, Horten, Burnelli and Northrop aircraft designs ranging from the 1950s to 1980s as can be seen in Figure 1-2.

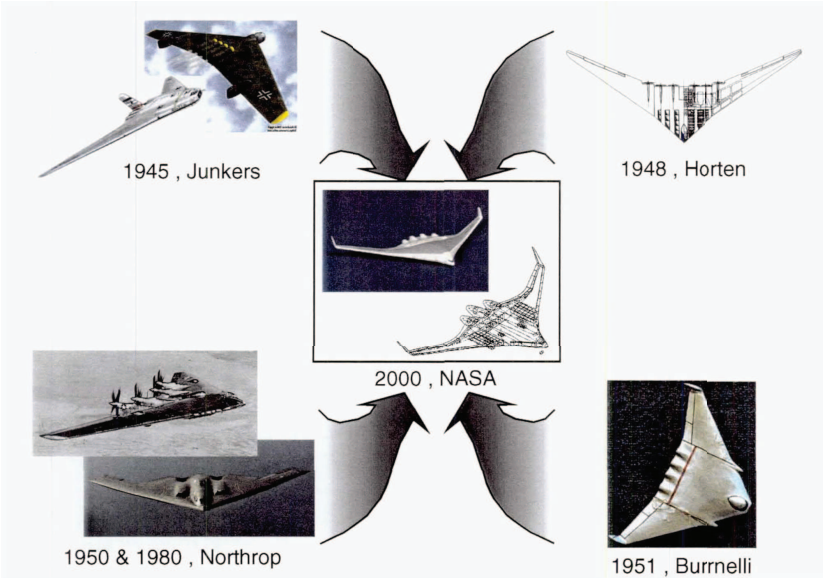

Figure 1-2: Historical concept development of the BWB [6]

The tailless configuration is also not new and there has much research been done in the area of control. The challenges of control and stability were solved but often penalized the competitive performance. Lessons learned in the past on the control are collected in Nickel's work [7]. He pointed out that that a tailless passenger aircraft would be impossible to design. His rationale is that an aircraft with without a tail would be feasible only if the longitudinal unstable fuselage would be removed as well. In his opinion it would be impossible due to a maximum wing thickness of 2 meters and relative high development cost associated with a novel aircraft. Nowadays this concept is more feasible using advances in control and stability such as fly-by-wire making it possible to handle unstable flight characteristics and advanced aerodynamic predictions making it possible to achieve thicker bodies without the occurrence of shock waves.

For these reasons in 1994 a team from NASA, industry and university focused on the concept of a to investigate the feasibility of a BWB aircraft using present technology. The results of a conceptual study showed a significant improvement over conventional aircraft, a 15% reduction of take-off weight and a 27% reduction in fuel burn per passenger for a 800 passenger aircraft with a range of 7000 nautical miles [8]. Subsequent studies also confirmed these results and concluded similar efficiency improvement for smaller aircraft [9, 10, 11].

Subsequent research performed by Pertuze et. al. [2] and Hange et. al. [4] predict that future generations of aircraft could have highly integrated structural components including non-circular fuselages in a tube-and-wing configuration.

1-2 Advances in non-circular fuselage design

The current state of the art in non-circular fuselage design consist of two main concepts: (1) the integrated panel concept and (2) the multi-bubble concept. A drawback of these designs is that both feature poles and walls passing through the cabin limiting cabin configurations

and lacking passenger acceptance. The oval fuselage has been conceived as an alternative to the current state of the art in non-circular fuselages. The concept is shown in Figure 1-4. It sets itself apart from other non-cylindrical fuselage designs in a number of ways. The large unobstructed cabin and cargo area eases the emergency egress and gives the airliners flexibility for the seating configuration and cargo placement. Due to the presence of a structural box passing around the cabin synergy can be found by integrating the carry-through wing box here. This would also result in an unobstructed cargo space, increasing the cargo volume. The design has less unique parts and joints compared to the current state of the art which results could result in reduced manufacturing costs.

Three different concepts, shown in Figure 1-4, are proposed for carrying these loads in the most efficient manner:

Multibubble and outer skin

This concept consists of a pressure vessel constructed out of multiple cylinders or spheroids connected to each other and loaded by the internal cabin pressure. The multi-bubble structure is efficient in carrying the pressurization load with circular or spherical shells of small radii. Complementary to the inner shell structure, it uses an outer shell to provide the required aerodynamic shape. These two structures are connected to each other at multiple points. The double bubble is as seen in Figure 1-1c is an a example of a multibubble specifically designed for a tube-and-wing aircraft configration. [12]

Integrated skin and shell

The integrated panel uses curved sandwich panels to carry the pressurization loads in bending. This concept uses a single sandwich structure that copes with all the loads. A study by Mukhopadhyay et al. showed that by vaulting the sandwich panels the lightest integrated shell structure is achieved. [13]

Oval fuselage

In this concept cabin cross-section is defined by a single trapezoidal structure as a wingbox made from sandwich panels. A single arc spans over the top of the box, a single arc spans over the bottom to include the cargo bay and two arc at each side of the box form the sides. This way the arcs are able to withstand the presssure difference and the box is dedicated to withstanding the bending loads of the wing efficiently. One of the advantages over the other concepts is that this concept generates a unobstructed space in the cabin. [14]

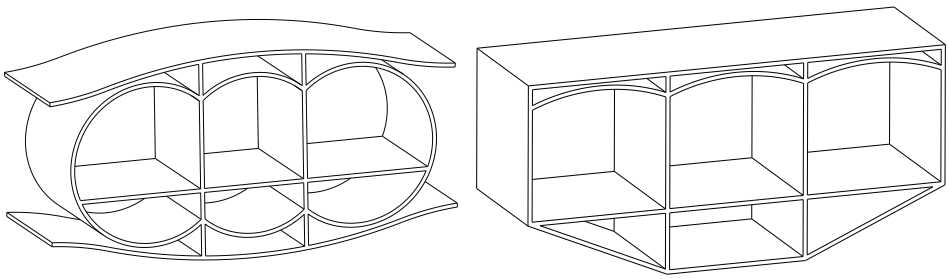

(a) The multi-bubble structure **(b)** The integrated panel structure

Figure 1-3: State of the art non-circular fuselages

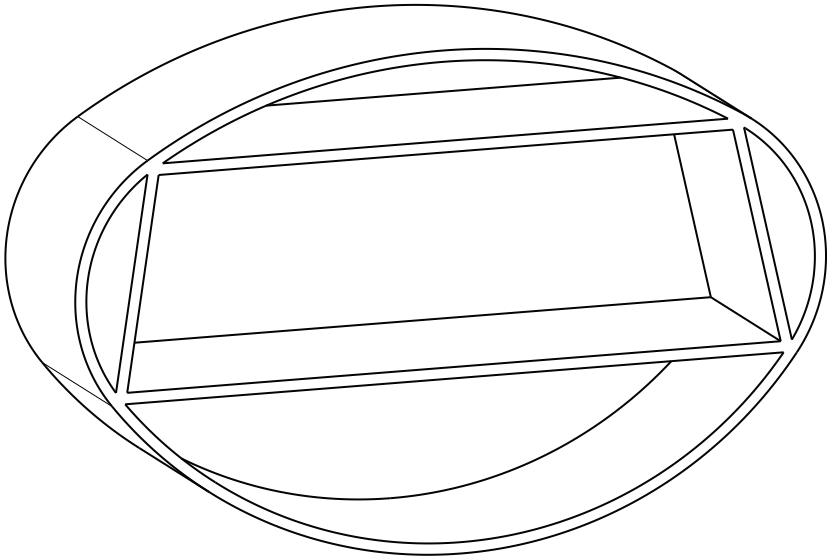

Figure 1-4: The oval fuselage

The estimation of the efficiency and operative empty weight of these fuselages currently primarily based on detailed finite element analysis of a section. A semi-analytical proprietary method is used for the design of the double bubble fuselage in [2] similar to the semi-analytical method for circular fuselages described by Chambers et. al. [15]. The aforementioned structural concepts for non-circular fuselages have been analyzed in [14, 16, 17]. Mukhopadhyay et. al found that a two- and three-fold multibubble shows lower sectional weight compared to the integrated panel method as can be seen in Figure 1-5 and 1-6. Vos et. al found that in a conceptual design the oval fuselage concept surpasses the multibubble concept by a 14% lower operational empty weight. The quality of these results is difficult to determine as no validation of the used method is performed by Vos et al. The lack of any standard cases to compare with makes it difficult to compare different fuselage concepts. As Mukhopadhyay et. al. only studies the weight as the performance index, the effects on aerodynamics of the aircraft not considered. This is incorrect since previous BWB aircraft designs have pointed out that the coupling between disciplines is very strong and this interaction cannot be neglected [1].

1-3 Existing fuselage weight estimation methods

Existing fuselage weight estimation methods are often based on empirical data. Using this empirical data a set of key variables are selected which have the greatest influence on the fuselage weight. These key variables are then combined in a single mathematical with the fuselage weight as the outcome. These methods are accurate for the estimation of the fuselage weight when the fuselage is similar to the fuselages that have been used for the derivation of the empirical relation. It can be seen from the empirical relations available in open literature (Appendix A) that the aircraft speed, wing geometry, load factor, cabin pressure and fuselage geometry are important parameters for the estimation of the fuselage weight.

A great improvement has been made by Chambers et al. [15] in the estimation in the fuselage

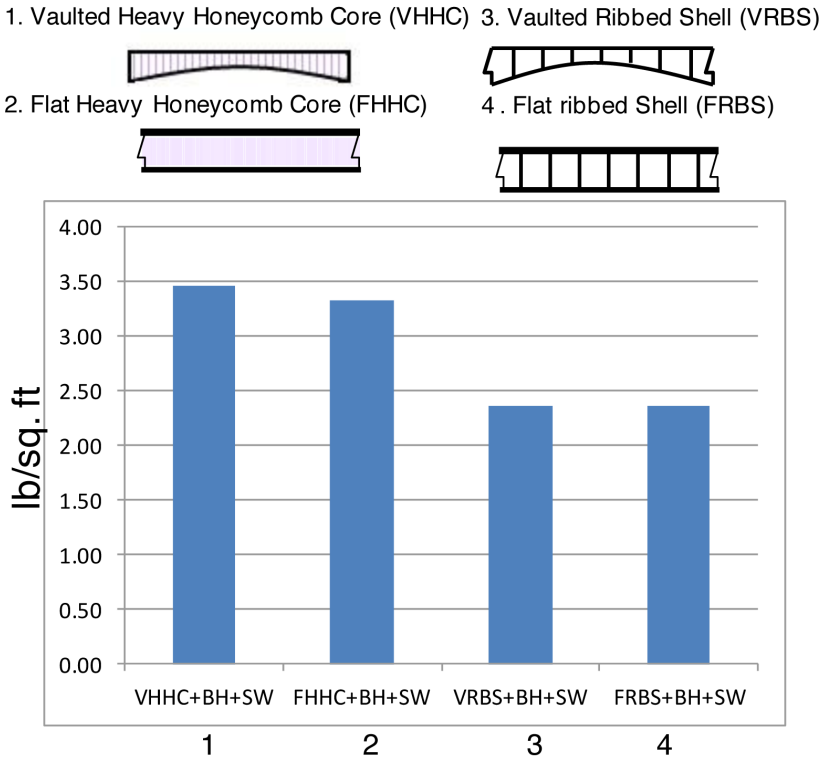

Figure 1-5: Comparison of the weight of a integrated panel fuselage [17]

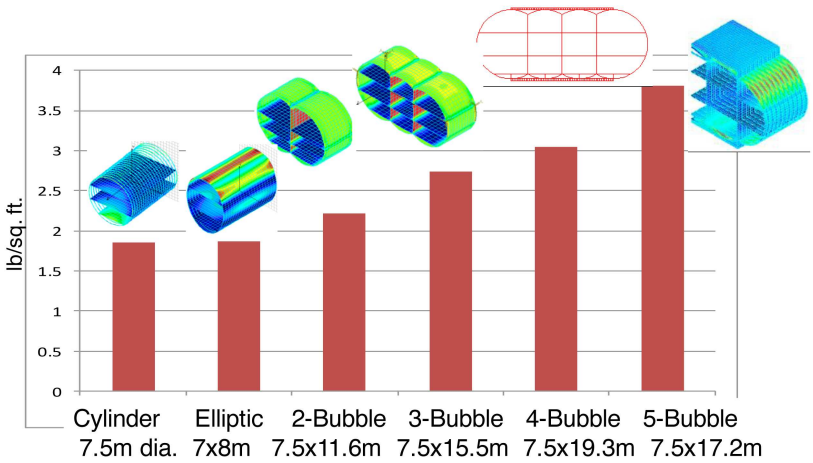

Figure 1-6: Comparison of a multibubble fuselage [16]

weight for circular fuselages with the analytical fuselage and wing weight estimation. However this method is, like the empirical methods, not suitable for the weight estimation of the non-circular fuselage in novel aircraft configuration. It would violate assumptions which are valid for conventional aircraft but not for novel aircraft. An example is the ratio between skin, stringer and frame, this is rather constant for circular fuselages in a tube-and-wing configuration. For the oval fuselage this is unlikely. If the skin thickness would increase due to a large arc radius, less stringers would be required due to the increased bending stiffness of the skin itself.

Another great example is the work of Laughlin et al. [18] where the weight of an integrated panel fuselage in a BWB is estimated using a design routine coupled with a finite element analysis. Although interesting insights were obtained, due to the high fidelity of the structural analysis model lengthy computational times were required making the method less applicable for the use in initial aircraft sizing.

1-4 Initiator

There is a strong trend towards computer aided aircraft design. In combination with multidisciplinary design optimization it plays a central role in the design of novel aircraft configurations and aircraft structures. As Potsdam et al. states in [1], the design requires a high level of integration. Close cooperation between disciplines is required due to the increased close coupling of changes in the aircraft design in comparison to conventional aircraft design. Multidisciplinary optimization is therefore the favored design methodology in these studies, as is used in the aforementioned research using Boeing's proprietary code WingMOD [8], NASA's Flight Optimization System [19, 20] and the European Computational Design Engine from the MOB research program [21].

The Delft University of Technology has started laying the foundation of such a similar design framework. Starting with the Design and Engineering Engine [22] the foundation was laid for a multidisciplinary design framework capable of generating an optimal aircraft design for a BWB aircraft with a multi-bubble fuselage. This has now evolved to a modular design framework, called the Initiator, capable of analyzing aircraft configurations of canard, Prandtl, conventional, three surface and BWB aircraft using the same methods for each aircraft. The goal of this framework is to be able to estimate the optimal design for each configuration and comparing its performance and operational efficiency from simple top level requirements. Due to modular architecture of the framework the design of an aircraft with an oval fuselage could adopt existing analysis modules for the determination of the wing weight for example.

1-5 Thesis goal

It has been discussed above that there is a research gap concerning the weight estimation of non-circular fuselages in transport aircraft taking into account the multidisciplinary interplay between structure, aerodynamic forces and cabin design. Although the oval fuselage concept clearly has benefits over current state of the art fuselages, little research has been performed on this subject. If the operative empty weight of this concept could be analyzed in an aircraft

design together with the Initiator, new insights on the performance of the aircraft with an oval fuselage can be determined. Therefore the goal of this thesis is:

Determine a method for the estimation of the operative empty weight of a pressurized oval fuselage in novel passenger aircraft configurations.

Since this research is part of a larger research project which is aimed at finding an optimum initial design for a number of aircraft configurations using a computer program (the Initiator), computational cost, modularity and flexibility is of importance. Therefore the research question is:

How can the weight of a pressurized oval fuselage for the application in conventional and novel passenger aircraft configurations be estimated in a way that is suitable for the use in the Initiator?

The subquestions that should be answered to be able to answer the research question include:

- How can an oval fuselage be parameterized in order to make it suitable for conceptual shape optimization?
- How is the oval fuselage different from a circular fuselage and how does this affect the weight estimation?
- How can the weight estimation method be verified to gain confidence in the method?

1-6 Thesis approach

In this thesis the problem is approached a bottom-up approach is taken. The novel fuselage concept is analyzed as a combination of elements of which the behavior is known. Using a first principles physical approach an structural sizing problem is set up. In this manner the reliance on empirical methods is minimized.

After a parameterization is determined that is efficient and appropriate for the problem at hand, the loads acting on the structure are determined. Since the fuselage is a primary aircraft structure, it is highly stressed and the sizing of the fuselage should be dependent on the loads acting on it. Therefore before diving into the weight estimation method it should be clear how the loads act on the fuselage. Next a method is determined to size these structural members similar to a circular fuselage. Although an oval fuselage is more complex than a circular fuselage, it shares similarities such as circular stiffened panels, cabin floors and cut-outs. Other than the weight of the structural members, a method for the estimation of non-structural weights is determined. These methods together result in the estimated fuselage weight.

In order to gain confidence in the established method, a number of checks are performed to verify the method such that conclusions could be drawn with more confidence. These tests include verification by a higher fidelity on a detailed part of the method and a verification with reference data on the complete method.

1-7 Thesis outline

The thesis outline is almost analogue to the thesis approach. First a parametrization is set up in Chapter 2,. Next the first part of the weight estimation is discussed. In Chapter 3 a discussion of the loads acting on the fuselage structure are discussed. Using the loads the structural members are sized in Chapter 4. In addition to the structural weight, a method is presented for the calculation of the additional weight and non-structural weight of the fuselage in Chapter 5. For sake of completeness, a short documentation is provided of the computer program, describing the possibilities, dependencies and examples of computer input in Chapter 6. This model and the made assumptions are then thoroughly tested and verified in Chapter 7. Preliminary results are obtained from a number of test cases in Chapter 8. The thesis is concluded with a summary of the findings in Chapter 9 and recommendations in Chapter 10.

Part I

Fuselage weight estimation

Chapter 2

Parametric desciption of the Oval Fuselage

The oval fuselage was first introduced by Vos et al. [14] as an alternative to the current state of the art of non-cylindrical pressurized fuselages, namely the multi-bubble fuselage and the integrated panel fuselage. An example of a section of an oval fuselage is shown in Figure 2-1. This concept sets itself apart from other non-cylindrical fuselage designs in a number of ways.

1. The large unobstructed cabin and cargo area eases the emergency egress and gives the airliners flexibility for the seating configuration.

2. The trapezoidal structure passing around the cabin can double as the carry-through wing box structure of a wing. Additionally, this would result in a unobstructed cargo space.

3. The design has less unique parts and joints, as the width of the fuselage increases, compared to current state of the art which could results in potential reduced manufacturing costs.

2-1 The oval cross-section

The oval fuselage consists of four connected circular shells (the outer skin) and a trapezoidal box which connects these individual circular shells. The trapezoidal box consists of two horizontal members and two "vertical" members. The lower and upper horizontal members double as floors, while the "vertical" members serve as the interior wall element. In this concept, the passengers are situated in the unobstructed space enclosed by the trapezoidal box and cargo is situated in the space below this floor. In addition, designs can be generated where passengers are situated on two floors.

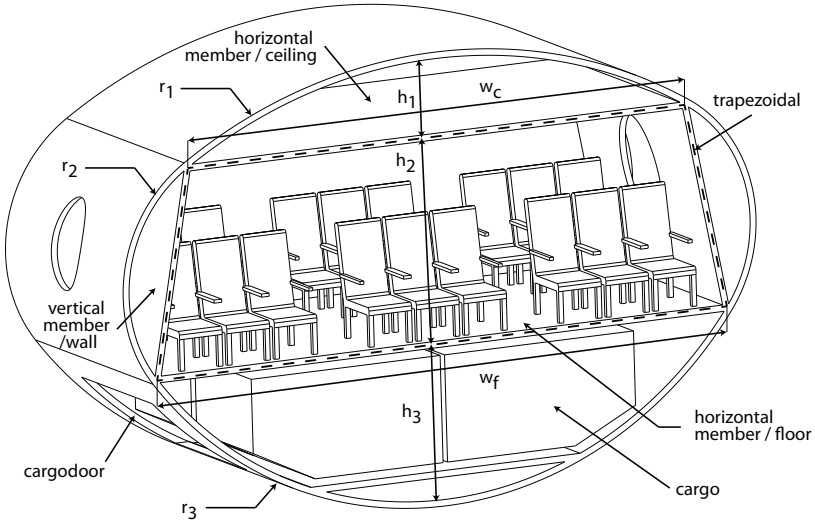

Figure 2-1: The oval fuselage concept

To construct the cross-sectional design, it is necessary to define the top height h_1, the center height h_2, the bottom height h_3, and the width of cabin floor w_f. The width of the cabin ceiling w_c follows from these dimensions such that the circular shells are tangent to each other. Since the circular shells are tangent to each other, they can be replaced by four equilateral triangles where the leg of one triangle coincides with the leg of the neighboring triangle. When only one half of a oval fuselage section is considered the problem is reduced to three isosceles triangles as shown in Figure 2-2. The geometric relationship between these dimensions can be derived by first defining the characteristic angles. The angles FAB, EDC and CBC' are defined as,

$$\alpha_1 = \tan^{-1} \frac{w_c}{h_1} \tag{2-1}$$

$$\alpha_2 = \tan^{-1} \frac{w_f}{h_3} \tag{2-2}$$

$$\beta = \tan^{-1} \frac{w_c - w_f}{h_2}. \tag{2-3}$$

where h is the height and w is the width. The angles ABF and ECD in Figure 2-2 are defined as ,

$$\theta_1 = \frac{\pi}{2} - \alpha_1 \tag{2-4}$$

$$\theta_2 = \frac{\pi}{2} - \alpha_2. \tag{2-5}$$

Using these angles and the isosceles property of the three triangles, the angles of the isosceles triangle CBG, γ_1 and γ_2, are defined as,

$$\gamma_1 = \frac{\pi}{2} - (\alpha_1 - \theta_1) - \beta \tag{2-6}$$

$$\gamma_2 = \frac{\pi}{2} - (\alpha_2 - \theta_2) + \beta. \tag{2-7}$$

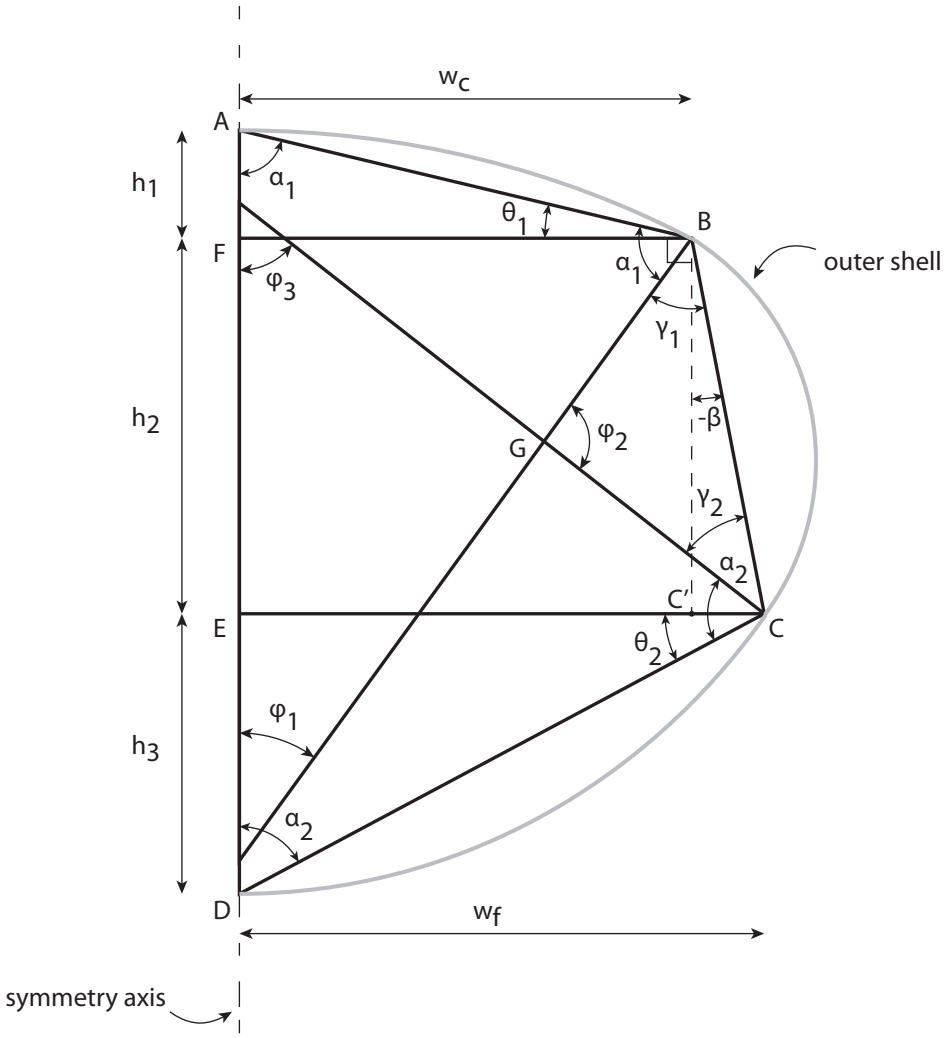

Figure 2-2: Overview of geometric variables of an oval fuselage section

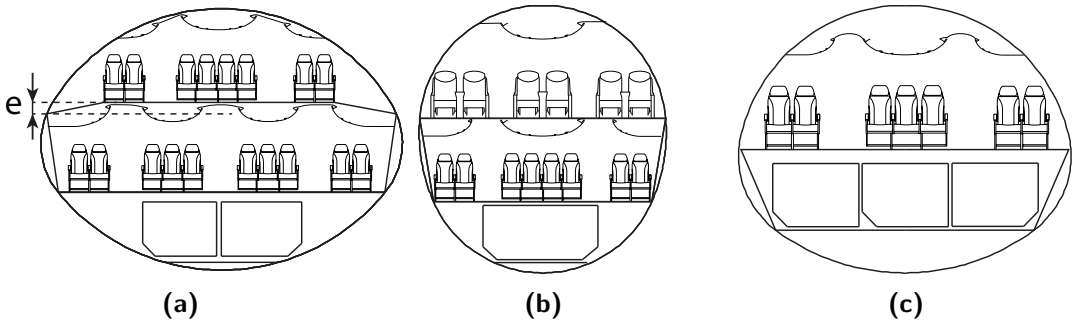

Figure 2-3: An example of various two-dimensional oval fuselage sections

Since the two angles of the isosceles triangle CBG are equal,

$$\gamma_1 = \gamma_2, \tag{2-8}$$

in combination with Equation 2-1 to 2-8 gives,

$$2\alpha_2 - 2\alpha_1 - 2\beta = 0 \tag{2-9}$$

$$\tan^{-1}\frac{w_f}{h_3} - \tan^{-1}\frac{w_c}{h_1} - \tan^{-1}\frac{w_c - w_f}{h_2} = 0. \tag{2-10}$$

Using this parametrization various cross-sectional configurations are possible. From a designer's point of view, this cross-section gives an extra degree of freedom compared to a circular cross-section. This is exemplified in Figure 2-3 where three incarnations of oval cross sections are shown. Figure 2-3a shows a wide body oval fuselage with two passenger decks. The ceiling member of the trapezoid is an eccentric beam. Although this eccentric beam will heavier compared to a normal beam, it reduces the radius of the upper circular shell while maintaining the cabin height which could potentially reduce the overall weight of the fuselage. Figure 2-3b shows an oval fuselage which is higher than its width with two passenger decks. Figure 2-3c shows an oval fuselage with a single deck. In this configuration the cargo bay is enclosed by the trapezoidal structure.

2-2 Three-dimensional shapes for the oval fuselage

The oval cross-section can be extruded to construct a tubular fuselage but also more complex shapes can be constructed with the oval cross-section. To construct a three-dimensional body, the variation in h_1 and h_3 can be varied by defining a crown curve and belly curve of the fuselage. One could for example specify an airfoil shape over the centerline of the fuselage in addition to a cabin height, h_2, and a planform shape of the cabin floor to obtain the three-dimensional oval fuselage.

This three-dimensional shape is constructed from four sets of geometric shapes and combined to construct complex shapes. These sets consist of a series of cylinders, spheres and tori which all resist the pressurization load in pure tension. The following four sets of geometric shapes are identified:

1. The oval cylindrical shape consisting of three cylindrical sections, shown in Figure 2-7.
2. The spherical set consisting of a spherical part on the top and bottom and a toroidal shape on the side, shown in Figure 2-8.
3. The toroidal set consisting of three toroidal parts at the top, bottom and side, shown in Figure 2-9.
4. The lofted nose ahead of the cabin and the rear fuselage behind the aft pressure bulkhead, Figure 2-10.

2-3 The crown and belly curve

As discussed in Section 2-2, the variation in h_1 and h_3 define the crown and belly curve. The crown and belly curve, or center section, can be defined in different ways. Where a circular fuselage can be described by a drooped down nose, tubular center and swept up tail, for an oval fuselage it is beneficial to have the ability of local refinement of the camber and thickness of the center section. Airfoil shapes and the "CST"-method [23] lend themselves well for these purposes. From a structural point of view the shape definition of circular fuselages result in an almost constant h_1 and h_3 resulting in a direct minimization of radii for r_1 and r_3 and therefore reducing the pressurization loads. The parametrization of such an curvature can be defined by the nose fineness ratio ϵ_{nose}, aft fineness ratio ϵ_{aft}, nose droop down ratio ζ_{nose} and aft upsweep ratio ζ_{aft}. These ratio's are defined by the dimensions from Figure 2-4 and the following relations:

$$\epsilon_{\text{nose}} = \frac{L_{\text{nose}}}{H_{\text{fuselage}}} \tag{2-11}$$

$$\epsilon_{\text{aft}} = \frac{L_{\text{aft}}}{H_{\text{fuselage}}} \tag{2-12}$$

$$\zeta_{\text{nose}} = \frac{H_{\text{nose}}}{H_{\text{fuselage}}} \tag{2-13}$$

$$\zeta_{\text{aft}} = \frac{H_{\text{aft}}}{H_{\text{fuselage}}}. \tag{2-14}$$

The fuselage nose center curvature is constructed using a half ellipse as a basic shape. This basic shape is then drooped down by translating the center curve by

$$z = \frac{H_{\text{nose}}}{L_{\text{nose}}^3} x_{\text{nose}}^3. \tag{2-15}$$

The fuselage aft section curvature is constructed from two polynomials starting from x_{nose} to L_{fuselage}. The fuselage aft crown curve follows the line

$$z = \frac{H_{\text{fuselage}}}{2} - \frac{H_{\text{aft}}}{L_{\text{aft}}^3} x_{\text{aft}}^3 \tag{2-16}$$

and the fuselage aft belly curve follows the line

$$z = -\frac{H_{\text{fuselage}}}{2} - \frac{H_{\text{fuselage}} - H_{\text{aft}}}{L_{\text{aft}}^3} x_{\text{aft}}^3. \tag{2-17}$$

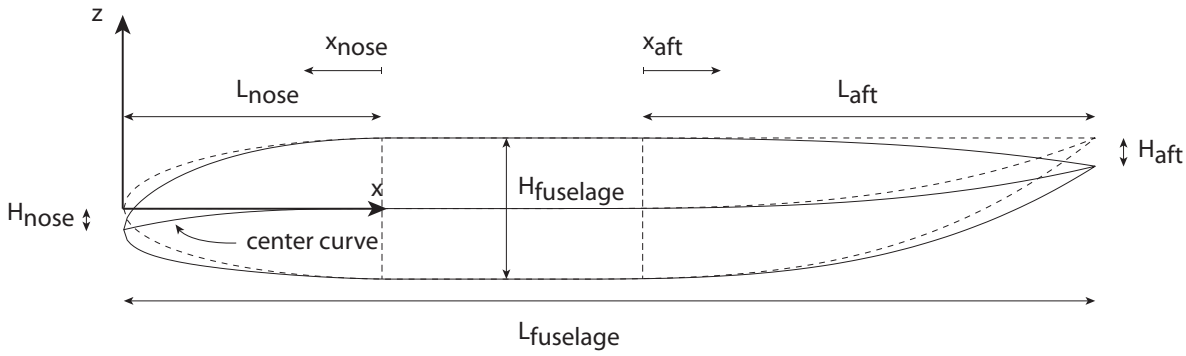

Figure 2-4: A parametrization for the center section of the fuselage

2-4 Constructing the cabin floor

The translation between the two-dimensional sections to the three-dimensional geometry is made using the cabin floor as a basis. This inside-out approach is adopted from Hoogreef et al. [24] and modified for a new three-dimensional definition.

The steps for constructing the cabin floor is as follows.

1. First the center section is defined using either a class shape transformation, airfoil curve or fuselage crown and belly parameterization.
2. Next using the floor position and cabin height the front and aft limit of the cabin are found.
3. The cabin floor is then constructed using various cabin widths at different relative cabin lengths determined by the designer.

The construction of the fuselage planform is best explained by example. Consider the case where one wants to construct an area ruled oval fuselage. The cabin floor should be 16 m wide at its widest point at 30% and 80% of the cabin length, 9 m at the front of the cabin and 14 m at the back of the cabin. To reduce the cross-sectional area of the fuselage, the width of the fuselage is reduced to 13 m at 50% of the cabin length. The fuselage itself should have a length of 55 m. Note that the width is defined as a ratio of the cabin length instead of a absolute length. This is chosen for easier incorporation in optimization algorithms because a valid set of parameters yielding the fuselage geometry is easier found.

The construction starts with the crown and belly curve discussed in Section 2-3. For this example a nose fineness ratio of 30%, an aft fineness ratio of 65%, height of 8.5 m, a nose droop ratio of 15% from the center and an aft droop ratio of 20% from the top. The crown and belly curve are shown in Figure 2-5.

Only a portion of the fuselage is constructed as being a oval fuselage. The front of the cabin is determined by the height of the cabin floor and the height of the cabin itself. The solid red lines in Figure 2-5 indicate a cabin floor positioned at $z = -1.15$ m and a cabin height of 2.4 m. These lines are the floor and ceiling of the trapezoid structure. Where the red line intersects the blue line defines a cabin having a maximum length.

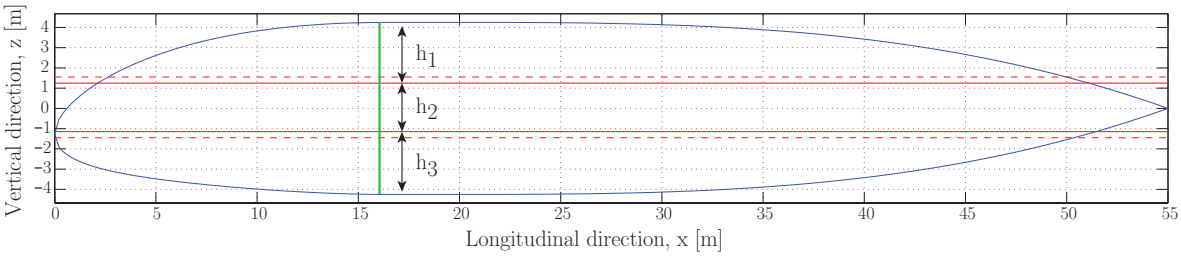

Figure 2-5: The crown and belly curve of constructed using the parameterization from Section 2-3

It can readily be seen that if these intersections would be used, h_1 and h_3 would be zero resulting in arc of infinite radius or practically flat panels. It is known that this will significantly increase the weight of the pressurized structure and therefore a minimum height of h_1 and h_3 is defined. The dashed red lines in Figure 2-5 describe the floor and ceiling offset by 0.3 m. Now the intersection of these lines with the center section define the limits of the cabin. In this case the front of the cabin is positioned on the centerline where $x = 2.7$ m and the aft of the cabin is position on the centerline where $x = 50$ m.

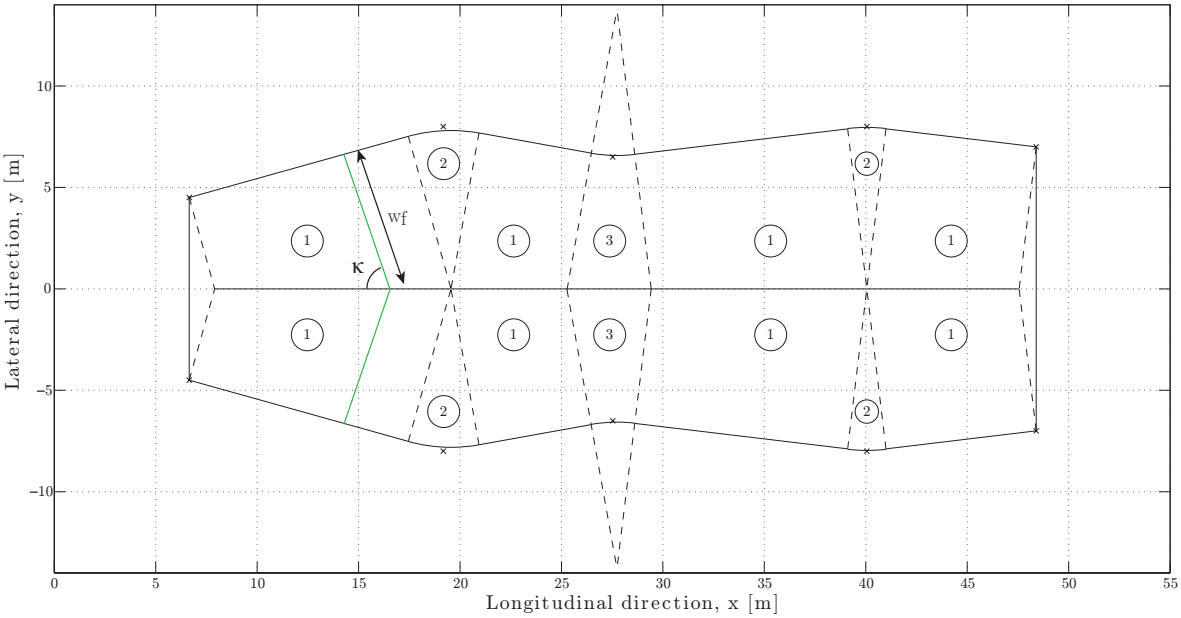

Figure 2-6: The outline of the cabin floor of an incarnation of the oval fuselage, the numbers correspond to the number in the enumerated list of Section 2-2

Using the cabin front and aft position the absolute x-position of the corner points is obtained: $x = 16.9$ m and $x = 40.5$ m for the widest points and the pinched section at $x = 26.2$ m. The location of these points are indicated as crosses in Figure 2-6. From these points the parameters for the shell geometry are derived conform the four geometrical shapes identified in Section 2-2. The numbers on the cabin floor correspond to the numbers in the enumerated list of Section 2-2. It can be seen that cabin floor is curved in the same manner as the outer shell revolves about its axis. For the toroidal geometry, number 3 in Figure 2-6, the point of revolution does not lie on the XZ-plane. The radius of revolution and thus the center point

is free. In this case it is chosen to be three times the cabin height, thus 7.2 m.

From the dimensions of the cabin floor and the orientation of the geometrical parts the variables are obtained. These variables are the angle κ, width of the floor w_f, the cabin height h_2, crown height h_1 and belly height h_3.

2-5 Examples of the oval fuselage geometry

By combining these geometrical sets, complex unobstructed cabin spaces can be realized. Two examples of such fuselages are shown in Figure 2-11. The first example is a typical BWB fuselage with a narrow nose and a wide center (Figure 2-11a). The second example is an area-ruled fuselage, where the fuselage is "pinched" at the wing intersection, (Figure 2-11b).

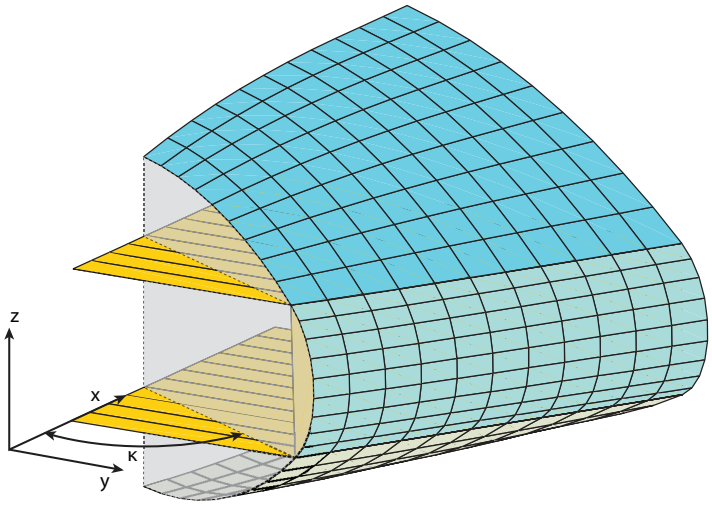

Figure 2-7: An example of the extruded shape consisting of three cylindrical parts.

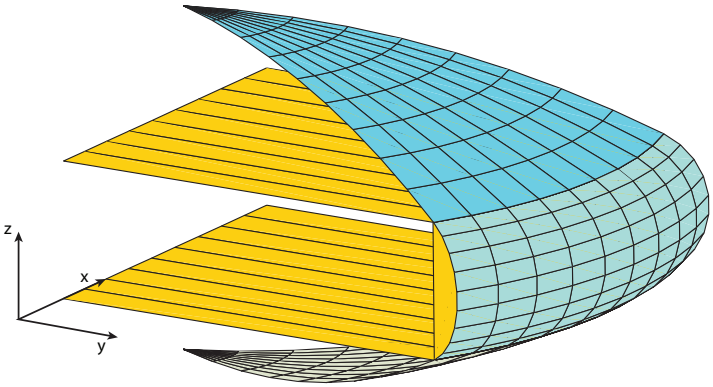

Figure 2-8: An example of the revolved shape consisting of two spherical parts and one toroidal part.

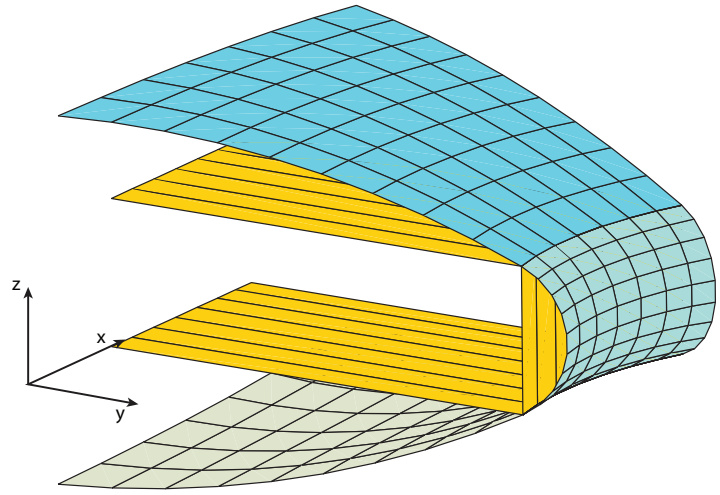

Figure 2-9: An example of the revolved shape consisting of three toroidal parts.

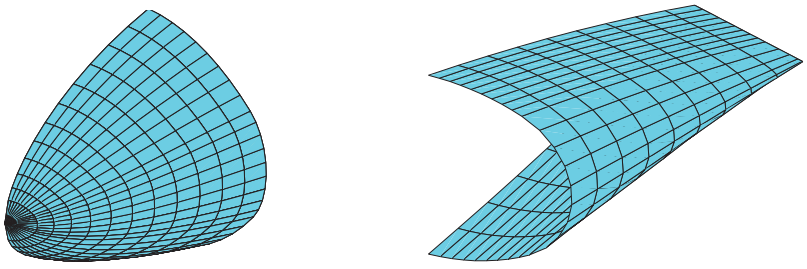

(a) The geometry of the nose of the fuselage.

(b) The geometry of the rear of the fuselage.

Figure 2-10: An example of the noncylindral shaped nose of the fuselage and rear of the fuselage

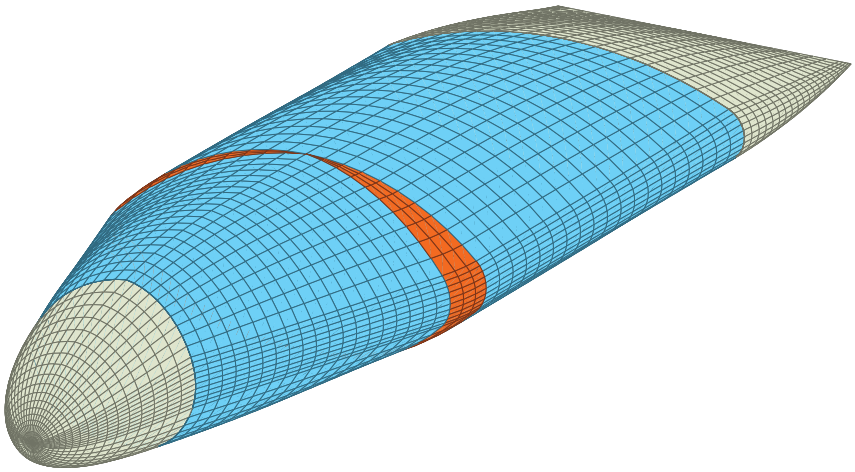

(a) An example of a blended wing body fuselage

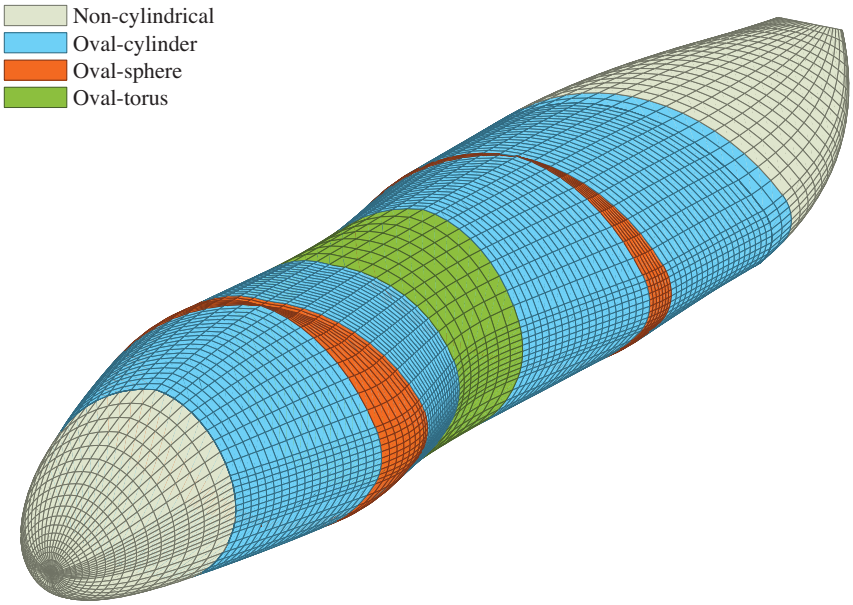

(b) An example of an area ruled fuselage

Figure 2-11: The three dimensional shape of fuselages constructed using the oval fuselage parametrization.

Chapter 3

Loads acting on the fuselage

The method for estimating the weight of the fuselage is based on the structural analysis of an oval fuselage. The first step of this structural analysis is the determination of the loads acting on the structure. The loads that are taken into account are the pressurization loads, aerodynamic loads and the inertial loads. The aerodynamic loads and inertial loads are subdivided into loads caused by the aircraft components attached to the fuselage and the fuselage itself.

This chapter derives the forces that act on the individual structural components of the fuselage due to aerodynamic loads and inertial loads. This chapter starts with the definition of the load cases that are considered followed by the pressurization loads. Next a comparison is made between a selection of aerodynamic models that can be used for determining the aerodynamic loads and a derivation is presented to determine the inertial loads acting on the fuselage. The aerodynamic loads and inertial loads are then combined to determine the longitudinal bending and shear in each structural member.

In this chapter and the subsequent chapter, the terms *stress* and *line load* are often used. To avoid any misunderstanding, the term stress is used when force per unit area is discussed. The term line load is used when force per unit length is discussed. When the load in a structural member having a certain thickness is discussed, the relation between stress and line load is,

$$N = \sigma t = \frac{F}{A}t, \tag{3-1}$$

where N is the line load, σ the stress, F the normal force, t the thickness of the structural member and A the area over which the force acts.

The term *shear* and the term *shear flow* are analogue to stress and line load. Their relation is described as,

$$q = \tau t = \frac{S}{A}t, \tag{3-2}$$

where q is the shear flow, τ is the shear stress, t is the thickness of the structural member, S is the shear force and A is the area over which the shear force acts.

3-1 Loads acting on the fuselage

The fuselage is stressed by many loads acting on the fuselage structure in varying magnitude during its operational life. While in the detail design of aircraft structures numerous load cases are taken into account, only a limited amount of load cases are considered in the present analysis. The load cases are constructed from the steady-state maneuvering loads during the cruise phase and a hard landing.

In the present case, a combination of the loads acting on the fuselage in lateral, longitudinal and vertical direction are considered that occur during the cruise and landing phase of the mission and at different aircraft weights. In addition, a safety factor can be included. These primary loads on the fuselage result in the following stresses:

- tensile stresses in the shell due to pressurization
- axial reaction stresses in the trapezoidal structure due to pressurization and wing root bending moment
- longitudinal stresses in the shell and the trapezoidal structure due to the distributed weight of the fuselage
- axial and shear stresses in the horizontal members (sandwich panels) due to the distributed transverse load of furnishing, passengers and cargo

Loads that are neglected are torsion loads caused by forces generated by the tail surfaces of the aircraft and the loads associated with the attachments of components of significant weight. Since only the flight states corresponding to steady-state cruise and hard landing are taken into account, other off-design flight states are neglected in the present analysis.

For the cruise phase it is assumed that the limiting load case occurs with the aircraft at maximum take-off mass (MTOM) and for the landing phase the limited load case occurs with the aircraft at design landing mass (DLM). To prevent any stress relieves that would not occur during operation, a combination of different pressure differentials, load factors, wing weights and fuel weights are employed that result in eight load cases for the cruise phase and two load cases for the landing phase. An overview of the combination of loads that make up the ten load cases are shown in Table 3-1. A hard landing is modeled as a predefined downward acceleration where the landing gears provide concentrated reaction loads acting on the fuselage. In this way all landing gears touch down simultaneously.

The load cases 1-8 consist of all the combinations of loads during cruise. These include the minimum and maximum load factor, no pressurization and maximum pressurization, minimum fuel weight and maximum fuel weight. The load cases 9-10 consist of the combination of loads during a hard landing. Here the minimum landing fuel is assumed and both no pressure and a minimal pressure differential is considered.

3-2 Pressurization

The pressurization of the cabin causes a load in both outer shell and the trapezoidal structure. This load acting on the outer shell of the cabin is calculated using membrane theory [25]. The

Load case	Aircraft weight	Load factor	Differential pressure	Fuel weight
1	MTOM	Max	Max	Max
2	MTOM	Max	Max	Min
3	MTOM	Min	Max	Max
4	MTOM	Min	Max	Min
5	MTOM	Max	0	Max
6	MTOM	Max	0	Min
7	MTOM	Min	0	Max
8	MTOM	Min	0	Min
9	DLM	Landing	Min	Min
10	DLM	Landing	0	Min

Table 3-1: The combination of loads that make up the load cases

load in the outer shell of a pressurized cylinder is given by,

$$N_{\text{p,long}} = \frac{\Delta p r}{2} \tag{3-3}$$

$$N_{\text{p,hoop}} = \Delta p r \tag{3-4}$$

where N is the line load, Δp the differential pressure, r the radius of the cylinder.

The resultant forces at each junction of the shells are carried in compression by the horizontal member and in tension by the "vertical" member for fuselage sections where the width is larger than the height and tension and compression respectively for sections where the height is larger than the width. In Figure 3-1a the resulting forces are schematically shown. The forces acting on the members of the structure are determined from force equilibrium at the nodes as. Consider node A in Figure 3-1b, the horizontal and vertical force equilibrium are

$$-N_{p,\text{ceiling}} - \Delta p(r_1 - r_2)\cos\alpha_1 - N_{p,\text{wall}}\sin(-\beta) = 0, \tag{3-5}$$

$$\sin\alpha_1 \Delta p(r_1 - r_2) - N_{p,\text{wall}}\cos(-\beta) = 0. \tag{3-6}$$

These two equation have two unkowns and are solved for$N_{p,\text{ceiling}}$ and $N_{p,\text{wall}}$. To obtain$N_{p,\text{floor}}$ a similar force equilibrium is determined for the node B in Figure 3-1a. The horizontal force equilibrium is

$$-N_{p,\text{floor}} + N_{p,\text{wall}}\sin(-\beta) - \Delta p(r_3 - r_2)\cos\alpha_3 = 0. \tag{3-7}$$

The solution for the line load in the ceiling $N_{p,\text{ceiling}}$, in the wall $N_{p,\text{wall}}$ and in the floor $N_{p,\text{floor}}$ are

$$\begin{aligned} N_{p,\text{ceiling,inplane}} &= -\Delta p(r_1 - r_2)\left(\cos\alpha_1 + \sin\alpha_1 \tan(-\beta)\right) \\ N_{p,\text{wall}} &= \quad \Delta p(r_1 - r_2)\frac{\sin\alpha_1}{\cos\beta} \\ N_{p,\text{floor,„inplane}} &= -\Delta p(r_3 - r_2)\left(\cos\alpha_3 + \sin\alpha_3 \tan\beta\right) \end{aligned} \tag{3-8}$$

where α is the subtended angle of the arc and β is the angle of the slanted "vertical" member. The subscripts 1, 2 and 3 denote the upper, side and lower arc respectively. It was shown in Figure 2-7 that when the section was positioned at an angle away from the YZ plane, the

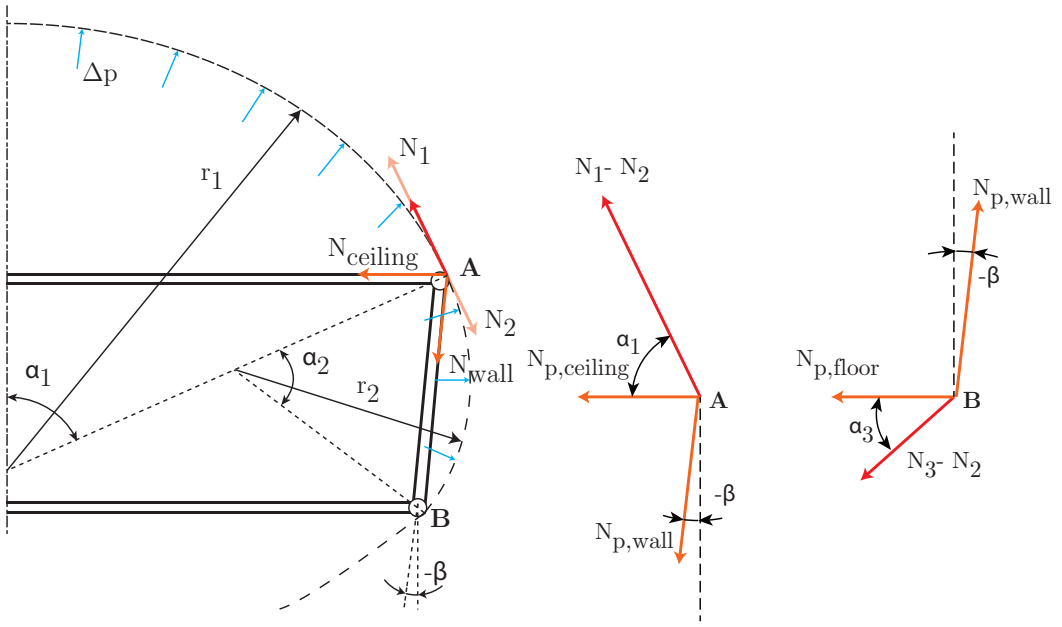

(a) Schematic representation of reaction forces due to pressurization on the trapezoidal structure

(b) Forces at the node A and B

Figure 3-1: Forces due to the pressurization of the fuselage

floor and ceiling of the trapezoid structure would follow a direct line to the centerline where as the outer shell is at an angle κ. This reduces the axial force acting on the trapezoidal structure by a factor $\sin\kappa$, thus

$$N_{p,\text{ceiling}} = \sin\kappa N_{p,\text{ceiling,inplane}} \tag{3-9}$$

$$N_{p,\text{floor}} = \sin\kappa N_{p,\text{floor,inplane}} \tag{3-10}$$

Using these equations it is also seen that when all radii are equal (the outer shell forms a perfect circle) the axial loads in the members is zero. Note that this analysis neglects the effect of any deformations of the structural members, this effect is discussed in Chapter 7.

It was shown in Section 2-2 that the geometry consists of tori, spheres and cylinders. The pressurization loads in tori and spheres are different than in cylinders. The load in a sphere is in all directions equal to the longitudinal load of the cylinder meaning that the maximum load in a sphere is only half of the maximum load in a cylinder. The load in the outer half of a torus is smaller than the load of a cylinder while the inner half of a torus has a larger pressurization load.

For the present analysis the pressurization of the spherical and toroidal parts is simplified to behave as if these were cylinders. This simplification neglects the reduced load in spherical parts and the load variations in toroidal parts. Since the meridian radius is relatively large in these parts and the majority of the fuselage consists of cylindrical parts, this assumptions deemed reasonable.

3-3 Aerodynamic loads

All aircraft components are either directly or indirectly connected to the fuselage. During flight all these component experience a resultant force due to the flow passing over the component's surface. At steady flight the forces on all the aircraft components together are equal to the weight of the aircraft. Since the position where lift and drag is generated is not necessarily equal to the position where weight and thrust respectively act, there is bending throughout the aircraft structure. The determination of the aerodynamic force generated by the surface of an aircraft component requires an aerodynamic analysis. The scope of this analysis will be limited to major components such as a lifting fuselage and lifting surfaces. Different aerodynamic models can be used to determine these aerodynamic forces and this sections presents a comparison of a few of these models along with a discussion of how fuselage loads are derived from this.

First the requirements are summed up in Section 3-3-1 followed by different options in Section 3-3-2. In Section 3-3-3 these models are compared to wind tunnel data of straight wings, swept wings and a BWB UAV. Using these test cases a suitable model is selected in Section 3-3-4.

3-3-1 Requirements for an aerodynamic solver

The fuselage weight estimation uses the aerodynamic solver to obtain the aerodynamic forces acting on each aircraft component to balance lift and weight. Therefore the model should be able to calculate the lift distribution, total lift and trimmed state of the aircraft in an accurate and precise manner with minimum computational cost. Accuracy is required to have a good representation of the aerodynamic forces acting on the aircraft and the aerodynamic efficiency of the aircraft. Precision is required to give a smooth design space for the optimization routines of the Initiator. Low computational cost is required since the weight estimation will be evaluated multiple times per iteration. The calculation time of one iteration should be on the order of few seconds on a normal desktop computer.

Although the aircraft will cruise at Mach 0.85, solving the flow for this Mach number is relatively difficult. The model that is able to approximate this will be favored.

The aerodynamic force of interest is both the lift force generated by each aircraft component and the root bending moment of the wing attached to the trapezoidal structure of the fuselage. For transport aircraft in general the ratio between the lift and drag of a lifting surface is around 20, thus the magnitude of the drag force is a factor 20 smaller than the lift force. Although the drag force affects the aerodynamic moment as the lift force does, the drag force causing compression and tension on the wingbox is neglected.

3-3-2 Candidate aerodynamic analysis methods

In the field of computational fluid dynamics several models have found their application in modern aircraft engineering. Starting from the most general form, the motion of a fluid in space is described by the full Navier-Stokes (NS) equations describe the motion of a fluid. These equations are rather complex and it is practically impossible to solve analytical. Using

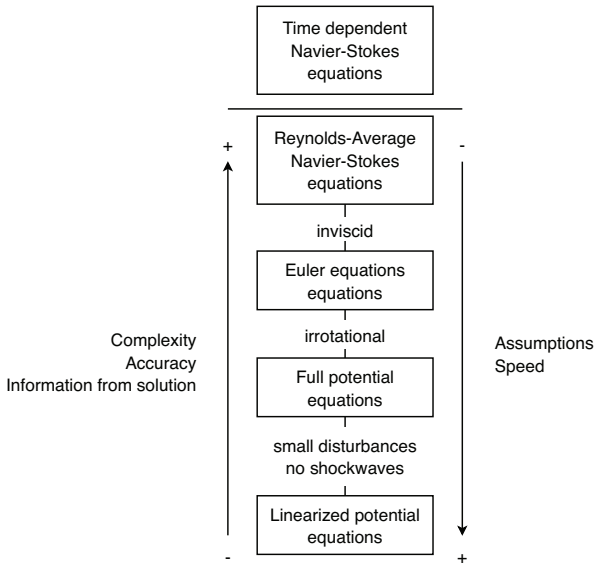

Figure 3-2: Classes of aerodynamic solvers. Adapted from [26]

powerful computers these equations can be solved numerically. By making simplifications, solving these equation becomes easier. The resulting sets of equations are listed in Figure 3-2. It can be seen that the model closest to the full NS equations is the Reynolds-Averaged Navier-Stokes (RANS) equations. In this model the equations and flow properties are averaged in time and turbulent fluctuations are modeled using a turbulence model. By assuming a inviscid flow the viscosity terms in the NS equations are removed to form the Euler equations. By assuming the flow is irrotational one ends up with the full potential equations and by making the last assumption that only small disturbances are present results in the linearized potential equations.

With the requirement that the calculation time of a single analysis should be in the order of a few seconds eliminates the methods that require a calculation through the complete domain (or mesh) and favor the methods that only require the definition of the surface of the body. The set of equations that is most simplified is the set of linearized potential equations. It assumes that the flow is irrotational and assumes that disturbances are small. It also assumes inviscid flow which makes it unable to determine the friction drag and pressure drag and it is unable to accurately predict high subsonic speeds. However by correcting for these effects, these methods seem very efficient in this stage of the design.

There are several applications bases on the linearized potential equations. These numerical methods can be divided in the Lifting Line method, the Vortex Lattice method and the 3D panel method.

Lifting line method

The numerical lifting line method is based on Prandtl's classical lifting line theory [27] where the wing is replaced by a very simple vortex filament spanning from tip to tip and coinciding with the line of aerodynamic centres. As Helmholtz theory explains, these vortices cannot end in free-stream and therefore a horseshoe-shaped vortex is proposed extending from the

wing tip downstream to infinity. At first a single horseshoe-shaped vortex was used and later on a large number of these horseshoe-shaped vortices were superimposed to represent a wing. These individual vortex strengths are calculated by imposing a flow-tangency condition on the three-quarter chord position on the wing. Using these vortex strengths the sectional lift distribution, induced velocity and induced drag can be calculated.

This method gives reasonable results for straight wings with moderate to high aspect ratios. The advantage of this method is that it is the fastest of the three since it only requires discretization in span wise direction. However, for swept wings and wing with low aspect ratios the method is less accurate [28]. It also does not take thickness and viscosity into account.

Vortex Lattice method

The vortex lattice numerical method extends the lifting line method by placing a series of lifting lines in the plane of the wing. This way a vortex sheet is formed over the wing with a corresponding wake sheet. The individual vortex strengths are determined for the case where a flow-tangency condition is imposed on the wing surface modelled as a (cambered) surface with no thickness. Similar to the lifting line method, the aerodynamic properties can be calculated from these strengths. This method gives good results for general wings. However, it does not take thickness and viscosity into account.

Tornado [29] and Athena Vortex Lattice (AVL) [30] are two readily available programs that use the vortex lattice method. These two programs differ in platform. Where Tornado is written in MATLAB, AVL is written in FORTRAN.

Three dimensional panel method

In contrast to the previous two methods, the three-dimensional panel method takes the thickness of the wing into account. The panel method covers the surface of the wing with singularities such as point sources, doublets and vortices of unknown strength. For lifting bodies also a paneled wake is modeled. By solving the unknown strengths, pressure distributions are calculated and integrated to yield aerodynamic coefficients. This method gives good results for general wings and bodies. Due to the high number of panels, this method is the slowest of the three. It also has the disadvantage that it does not take viscous effects into account.

VSAERO is an example of an 3-D panel method that uses the linearized potential equations. It couples its inviscid, irrotational flow solver with an on-body stream wise boundary layer. This way the boundary layer thickens the body to account for differences in the pressure distribution due to viscosity. It also models a relaxed wake.

Using different test cases three models will be compared, from low to high fidelity these models are:

1. Tornado with the Raymer drag prediction
2. AVL with the XFOIL 2D viscous solver
3. VSAERO with stream wise boundary layer coupling

3-3-3 Test case definition

A comparison is made between the aerodynamic models under consideration and wind tunnel data. Additionally to the wind tunnel data a higher fidelity model is consulted to provide an extra check. The wind tunnel data that is used consists of measurement of simple straight and swept wings from the NACA (former NASA) [31], [32] and wind tunnel data of a low subsonic BWB model [33]. The higher fidelity model is MATRICS-V, a full potential flow model with an integral boundary method which is tested for the swept wings from Sivells et al. by Mariens in [34]. All tests are at low Mach numbers and therefore compressibility corrections are not required. The models will be tested on their performance in calculating total lift, span wise lift distribution, lift-induced drag and profile drag. The geometry of each wing is shown in Figure 3-3. Figure 3-3a shows the geometry of a tapered wing with a symmetrical NACA0015 airfoil for the wing root and NACA0102 airfoil for the wing tip. Figure 3-3b shows the geometry of a wing of similar dimension with the cambered NACA2415 airfoil for the wing root and NACA2412 airfoil for the wing tip. A similar wing but with a larger sweep angle of 15° and 30° result in the the wings of Figure 3-3c and 3-3d respectively. Figure 3-3e shows the geometry of a BWB model which is tested at the Delft University of Technology. This wing shape consist of five different airfoils and a small positive twist distribution. This test case resembles the geometry for which the fuselage weight estimation will be used. The wing geometry presented in Figure 3-3f is a straight tapered wing with a NACA4420 airfoil for the wing root and a NACA4412 airfoil for the wing tip.

3-3-4 Test case results and aerodynamic solver selection

The ability of the aerodynamic solvers to predict the lift and the root bending moment is of primary importance for the fuselage weight estimation. Therefore only the predicted total lift and lift distribution is compared. More information about the predicted drag of the three models can be found in Appendix C.

The total lift coefficient for a range of angles of attack is shown in Figure 3-5 and 3-6. All three methods follow the wind tunnel data closely for the NACA-00-0-0, which has the simplest geometry. As camber is added the AVL, VSAERO and Tornado all overestimate the lift whereas MATRICS-V still follows the experimental data. Figure 3-5c and 3-6a show that differences between the experiments and both vortex lattice methods reduce when the camber is combined with sweep, whereas MATRICS-V and VSAERO underestimate and overestimate lift respectively when camber is combined with sweep. Although Figure 3-6c should show similar differences as Figure 3-6a, an offset can be seen in the VSAERO estimation. For the blended wing body of Figure 3-6b a similar offset is noticed from VSAERO. Other offsets suggest a difference in the definition of the angle of attack of such an aircraft.

The lift distributions shown in Figure 3-7 and 3-8 show different trends than those seen for the total lift. Unfortunately no experimental data of the lift distribution is available. In general the AVL and VSAERO are in agreement for the straight wings but large deviations are seen for the blended wing body aircraft. The vortex lattice methods are in agreement but differ from the three-dimensional panel method. VSAERO predicts more lift on the inner wing and less lift on the outer wing. This difference is of importance for the use of the aerodynamic analysis for determining the wing root bending.

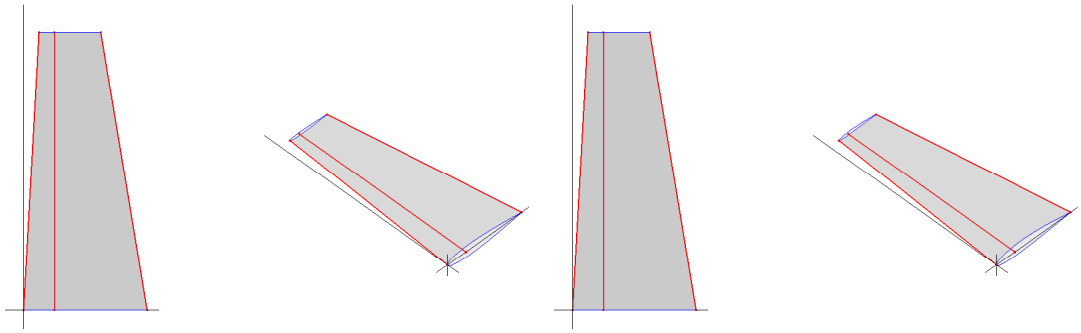

(a) The NACA-00-0-0 wing

(b) The NACA-24-0-0 wing

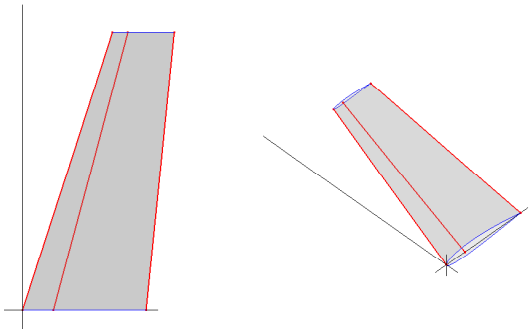

(c) The NACA-24-15-0 wing

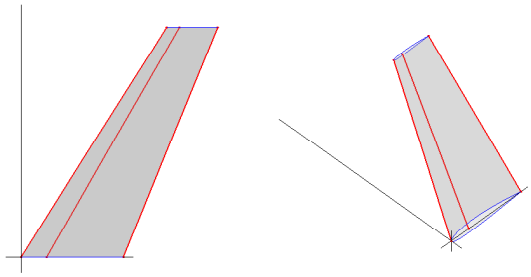

(d) The NACA-24-30-0 wing

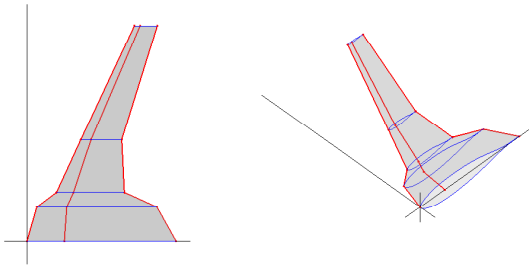

(e) The blended wing body

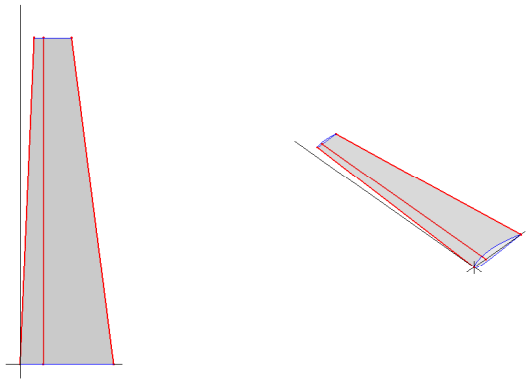

(f) The NACA-2.5-10-44.20 wing

Figure 3-3: Geometry and the quarter-chord-line of the test cases

To get insight in the effect of the differences in lift distribution on the wing root bending moment a *bending moment coefficient* is defined by,

$$c_b = \frac{\int_y^{\frac{b}{2}} c_l c \mathrm{d}y}{S}$$

where c_b is the bending moment coefficient, y is the spanwise location on the wing at c_b is calculated, b is the wing span, c_l is the local lift coefficient, c is the local chord and S is the wing area. The bending moment distribution as a function of the wing span is shown in Figure 3-9 and 3-10. It is seen that AVL is in general the most conservative solver since it overestimates the bending moment at the wing root.

The computational cost of the testes aerodynamic solver varies from 8 seconds for Tornado and 42 seconds for VSAERO and only 0.3 seconds for AVL. These differences between the three models can be expressed in numbers. The lift slope and bending moment coefficient are calculated and presented in Table 3-2. It can be seen that the difference in the lift slope between deviations of AVL with the experimental data is slightly better than MATRICS-V. The bending moment at $y = 0.10\frac{b}{2}$ is on the conservative side for AVL compared to Tornado and VSAERO. The AVL solver has the lowest computational cost and predicts lift and bending accurately. It is therefore favored to be used in the fuselage weight estimation.

Using the AVL aerodynamic analysis the aerodynamic forces on each aircraft component at the steady cruise flight phase are determined. Using the method described in Section 3-5 these forces are translated to forces acting on the fuselage. The fuselage weight estimation uses the lift and moment of each component for the calculation of the longitudinal moment and shear distribution of the fuselage. This wing bending moment acting on the trapezoidal structure is calculated from the lift distribution of the main wings. An overview is shown in Figure E-11.

	Experiment	MATRICS-V		VSAERO		AVL-XFOIL		Tornado	
	C_{L_α} [deg^{-1}]								
NACA 00-0-0	0.074	-	-		6%	0.075	2%	0.076	3%
NACA 24-0-0	0.073	0.070	-4%	0.078	7%	0.075	4%	0.076	5%
NACA 24-15-0	0.876	-	-		16%	0.914	4%	1.071	22%
NACA 24-30-0	0.070	0.067	-4%	0.075	7%	0.070	0%	0.070	1%
ZEFT BWB	0.079	-	-	0.077	-2%	0.073	-8%	0.070	-11%
NACA 2.5-10-44.20	0.085	-	-	0.095	11%	0.087	1%	0.088	3%
	Bending moment coefficient at $y = 0.10\frac{b}{2}$, percentages w.r.t. AVL-XFOIL								
NACA 00-0-0	-	-	-	-	-	0.565	-	0.565	1.7%
NACA-24-0-0	-	-	-	-	-	1.170	-	1.123	-4.0%
NACA-24-15-0	-	-	-	1.187	-1.0%	1.198	-	1.147	-4.2%
NACA-24-30-0	-	-	-	1.165	0.1%	1.164	-	1.111	-4.5%
ZEFT BWB	-	-	-	0.030	-6.4%	0.032	-	0.032	0.2%
NACA 2.5-10-44.20	-	-	-	-	-	0.512	-	0.479	-6.4%

Table 3-2: Overview of the lift slope and bending moment determined from experiment and from calculations

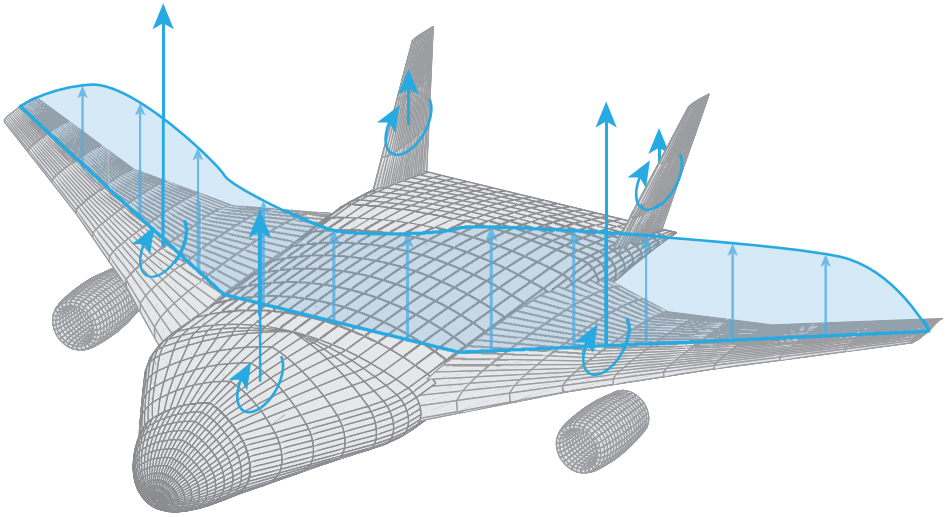

Figure 3-4: The concentrated lift forces and moments of each aircraft component and the lift distribution of a BWB

3-4 Inertial loads

The inertial loads acting on the fuselage structure either originate from the fuselage itself or from components attached to the fuselage. The inertial loads originating from the fuselage itself include the empty weight of the fuselage, the passengers and the cargo. The empty weight of the fuselage is evenly distributed by its planform. The inertial load of the passengers is evenly distributed by the cabin floor. The inertial load of the cargo is considered as a series of point forces at the centroid of the cargo container. If a bulk cargo floor is present the inertial load of the bulk cargo is evenly distributed by the cargo floor similar to the cabin floor.

The connected components that are taken into account are engines, main landing gears, fuel tanks and lifting surfaces. These lifting surfaces include main wings, horizontal stabilizers, vertical stabilizers, canards and winglets. How these inertial loads translate to the forces acting on the fuselage is explained in Section 3-5.

3-5 The fuselage beam

The loads acting on the fuselage structure are projected to distributed load and concentrated loads acting on a one-dimensional beam. This surrogate beam stretches from the front of the fuselage to the end of the fuselage and lies in the XZ-plane, as shown in Figure 3-11. Three types of loads are modeled in this beam:

1. A concentrated load
2. A linear distributed load
3. A non-linear distributed load

A concentrated load is simply projected onto the beam without any transformations. These loads include unit load devices (ULD's), landing gear when these are directly attached to the fuselage and engines directly attached to the fuselage.

Linear distributed loads consist of all the connected aircraft components and the aerodynamic loads of these components as well as the aerodynamic loads acting on the fuselage itself. How this distribution is determined can be explained with the help of Figure 3-12. In this figure the wing is attached to the fuselage. The loads of the wing are transferred to the fuselage through the wing box, its front and aft spar are illustrated as beams. It can be seen in the side view (Figure 3-12b) that due to the sweep of the wing the force also induces a moment. The moment through the center of the wingbox attachment C is

$$M = F\left(x_F - \frac{x_2 - x_1}{2}\right) \tag{3-11}$$

where M is the moment induced by the force, x_1 is the position of the front spar, x_2 is the position of the rear spar, x_F is the position of the applied force, F force applied by the wing. The distributed load is then linear between x_1 and x_2. At x_1 this is

$$f_1 = \frac{F}{x_2 - x_1} - \frac{6M}{(x_2 - x_1)^2}$$

and at x_2 this is

$$f_2 = \frac{F}{x_2 - x_1} + \frac{6M}{(x_2 - x_1)^2}$$

where f is the distributed load acting on the fuselage beam due to the applied force. When aerodynamics loads are transformed to linear distributions the moment aerodynamic moment is added to M. The aerodynamic forces of the fuselage itself are distributed along the entire length of the beam.

Non-linear distributions such as the fuselage weight itself and the passengers weight are derived from their planform assuming a constant weight per area. These non-linear distributions are also shown in Figure 3-11 and these are transformed to distribution per unit length by multiplication of the local width of the fuselage and the width of the cabin for the fuselage weight and passengers weight respectively.

3-6 Longitudinal bending of the fuselage

Using the surrogate beam discussed in the previous discussion the moment at every longitudinal position of the fuselage is known. The stress normal to the section is calculated using beam theory, Eq. 3-12. In this equation M $M$is the moment acting on the section, κ is the angle between the fuselage XZ-plane and the section plane (also shown in Figure 2-7), Δz is the vertical distance from the section centroid, $\bar{t}$ is the total smeared thickness of the structural members and I_{section} is the inertia of the section.

$$N_b = \frac{M \sin \kappa \Delta z_{\max}}{I_{\text{section}}} \bar{t} \tag{3-12}$$

An elaborate derivation of the moment of inertia of an oval fuselage section is found in Appendix B.

In this manner the line load due to bending is determined. In the horizontal members this stress is constant, however this stress varies in the outer shell and the wall of the trapezoid structure. Different stresses will be used for the sizing of the structural members, as will be discussed in more detail in Chapter 4.

3-7 Shear

The shear in the each fuselage section are induced by the weight of the fuselage, the lift generated by the fuselage and the forces induced by the weight and lift acting on the structural components attached to the fuselage. The shear stress in the section has a parabolic shape where the highest shear stress is concentrated about the neutral axis.

Let q be the shear flow such that $q = \tau \bar{t}$ where τ is the shear stress in the section and $\bar{t}$ is the smeared thickness of the structural element of the section. Using this definition the shear load acting on the section is independent of the thickness.

The oval fuselage section is classified as a multi-cell thin walled section and the determination of the shear flow is rather complicated due to the complex construction of arcs. The shear flow problem is simplified by assuming that the shear flow in the horizontal members of the trapezoid structure have a small contribution on the total shear flow and the 'vertical' member of the trapezoid structure is unified with the outer arc. The oval cross-section that is loaded by the shear force The shear flow is given by,

$$q = q_0 - \frac{S}{I_{\text{shear}}} Q \tag{3-13}$$

where

$$Q = \int z \mathrm{d}A = \int z \bar{t} \mathrm{d}s = \int r^2 \bar{t} \cos\alpha \mathrm{d}\alpha \tag{3-14}$$

In these equations, S is the shear force, z is the distance from the neutral axis to a point of interest on a structural member, Q is the moment of area about the neutral axis, r is the radius of the arc and α is the angle along the arc.

Due to symmetry of the section the shear flow at the top and bottom of the section is zero. By starting at a position where the shear flow is known, for example at the top (point A in Figure 3-13), $q_0 = 0$. The shear flow is calculated starting at the top of the section at point A.

$$q_1 = -\frac{S}{I_{\text{shear}}} r_1 \bar{t}_1 \left(z_{\text{c}} - z_{\text{c}_1}\right) \alpha + r_1^2 \bar{t}_1 \sin\alpha \tag{3-15}$$

$$q_2 = q_1 - \frac{S}{I_{\text{shear}}} r_2 \bar{t}_{2,\text{w}} \left(z_{\text{c}} - z_{\text{c}_2}\right) \left(\alpha - \alpha_1\right) + r_2^2 \bar{t}_{2,\text{w}} \left(\sin\alpha - \sin\alpha_1\right) \tag{3-16}$$

$$q_3 = q_2 - \frac{S}{I_{\text{shear}}} r_3 \bar{t}_3 \left(z_{\text{c}} - z_{\text{c}_3}\right) \left(\alpha - \alpha_2\right) + r_3^2 \bar{t}_3 \left(\sin\alpha - \sin\alpha_2\right) \tag{3-17}$$

In these equations, z_c is the position of the shear section centroid and z_{c_1}, z_{c_2} and z_{c_3} are the centroids of the top, side and bottom arc respectively. The thicknesses $\bar{t}_1$, $\bar{t}_2$ and $\bar{t}_3$ are the smeared thicknesses of the top, side and bottom. The $\bar{t}_{2,\mathrm{w}}$ is the smeared thickness of the side arc and the wall together and the thickness $\bar{t}_{\mathrm{w}}$ refers to the thickness of the vertical member itself.

The shear stress of the upper and lower arc are then determined using,

$$\tau_{\mathrm{hoop,long_1}} = \frac{q_1}{\bar{t}_1}, \tag{3-18}$$

$$\tau_{\mathrm{hoop,long_3}} = \frac{q_3}{\bar{t}_3}. \tag{3-19}$$

The shear stress acting in the 'vertical' trapezoidal member and the side arc distributed according to their relative thickness as,

$$\tau_{\mathrm{hoop,long_2}} = \frac{q_2 \bar{t}_2}{\bar{t}^2_{2,\mathrm{w}}}, \tag{3-20}$$

$$\tau_{\mathrm{lat,long_w all}} = \frac{q_2 \bar{t}_{\mathrm{wall}}}{\bar{t}^2_{2,\mathrm{w}}}. \tag{3-21}$$

It is clear that the shear flow is not constant over the structural members. For the sizing of the structural members the average shear flow over a structural members is used. This average shear flow takes on different values for each load case.

3-8 Wing bending

The function of the trapezoidal structure is to carry the pressurization loads from the outer shell. However, when the oval fuselage is used in a mid-wing configuration the trapezoidal structures doubles as a wing box. The bending load of the wing is transferred from the wing box. The line load couple acting on the horizontal members of the trapezoid induced by the bending of the wing are defined by,

$$N_{\mathrm{wing}} = \pm \frac{F_{\mathrm{wing}} y_{\mathrm{wing}}}{h_2 L_{\mathrm{wing}}},$$

where N_{wing} is the line load acting on the trapezoidal structure, F_{wing} is the force of the wing,y_{wing} is the arm length from the center of force to the wing root, h_2 is the cabin height and L_{wing} is the distance between the front and rear spar at the wing root location.

The force acting on the wing is different at each load case. For each load case the weight of the wing structure, fuel tank and attached engines is taken into account as well as the amount of lift the wing at each load case.

3-9 Total load acting on the structure

A summation is given of the load cases that are accounted for in the fuselage weight estimation. A method is discussed to determine the total longitudinal bending loads, shear loads,

distributed transfers loads and axial loads in lateral direction which act on each fuselage cross-section. A basic method is presented to translate these line load to line loads acting on the individual members of the structure. These line loads are used in the next chapter to determine the minimal necessary geometry of the structural members to withstand these loads.

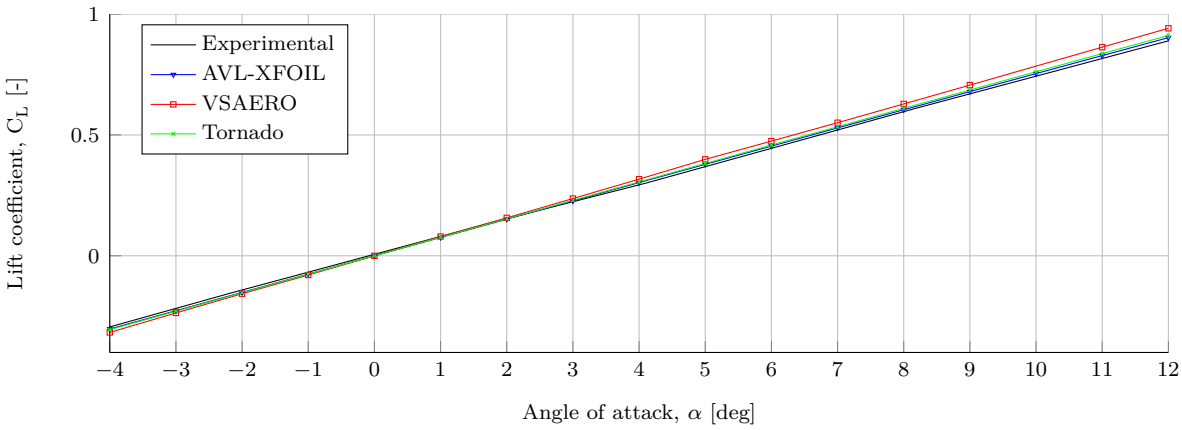

(a) The NACA-00-0-0 wing

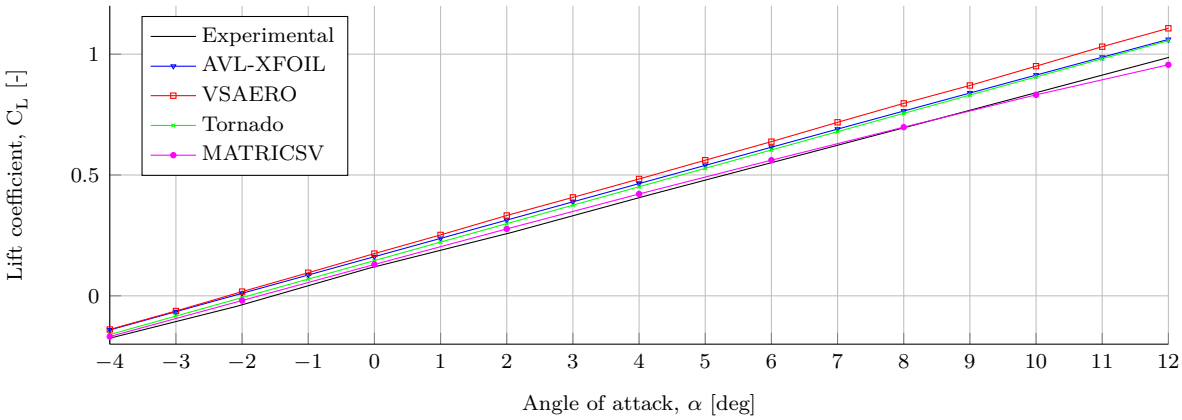

(b) The NACA-24-0-0 wing

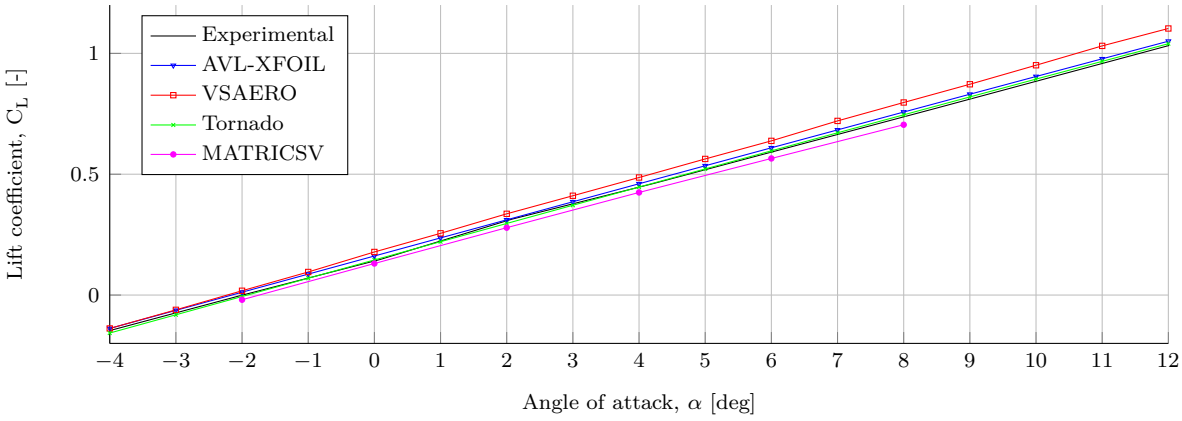

(c) The NACA-24-15-0 wing

Figure 3-5: Angle of attack versus lift coefficient of the NACA-00-0-0 wing, the NACA-24-0-0 wing and the NACA-24-15-0 wing

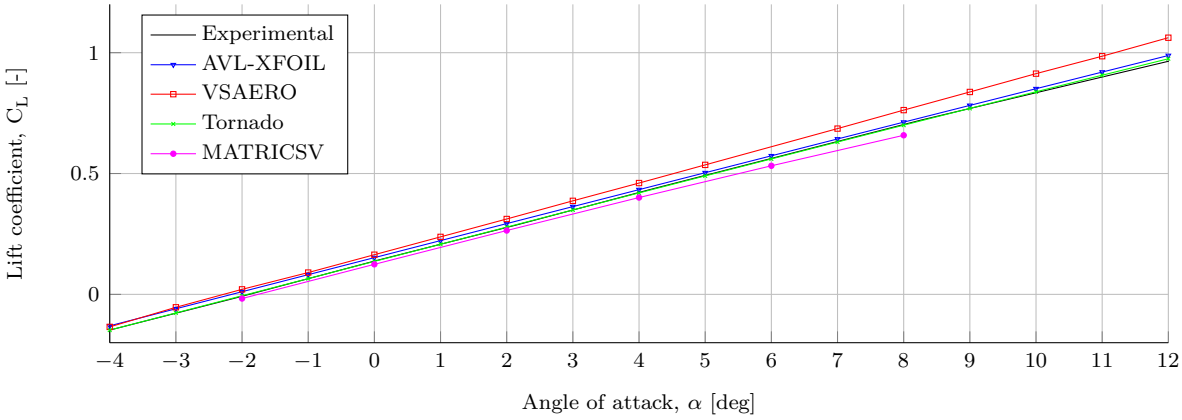

(a) The NACA-24-30-0 wing

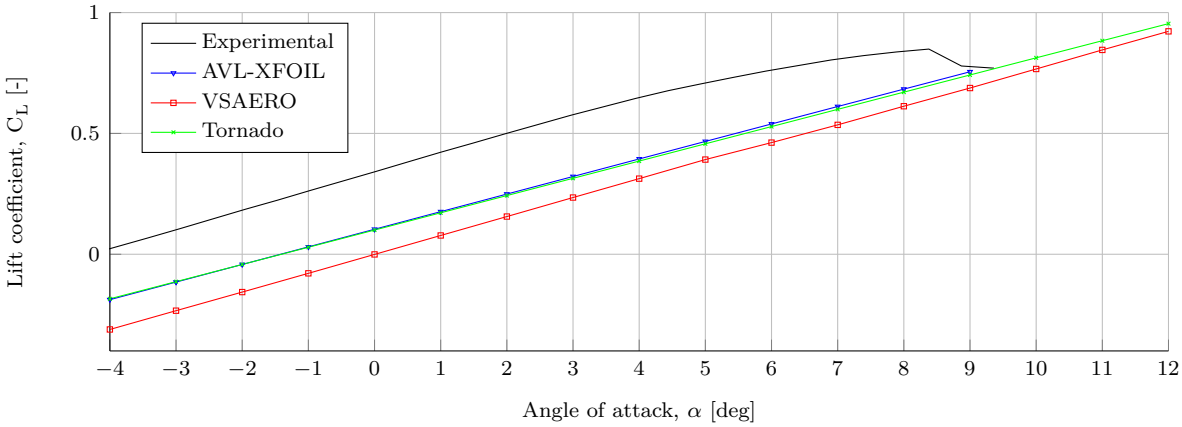

(b) The ZEFT blended wing body

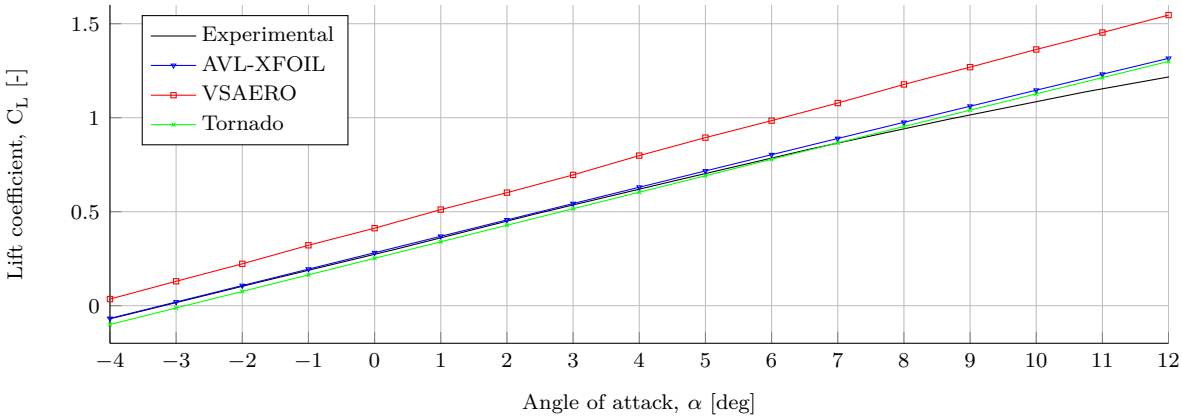

(c) The NACA-2.5-10-44.20 wing

Figure 3-6: Angle of attack versus lift coefficient of the NACA-24-30-0 wing, the ZEFT blended wing body and the NACA-2.5-10-44.20 wing

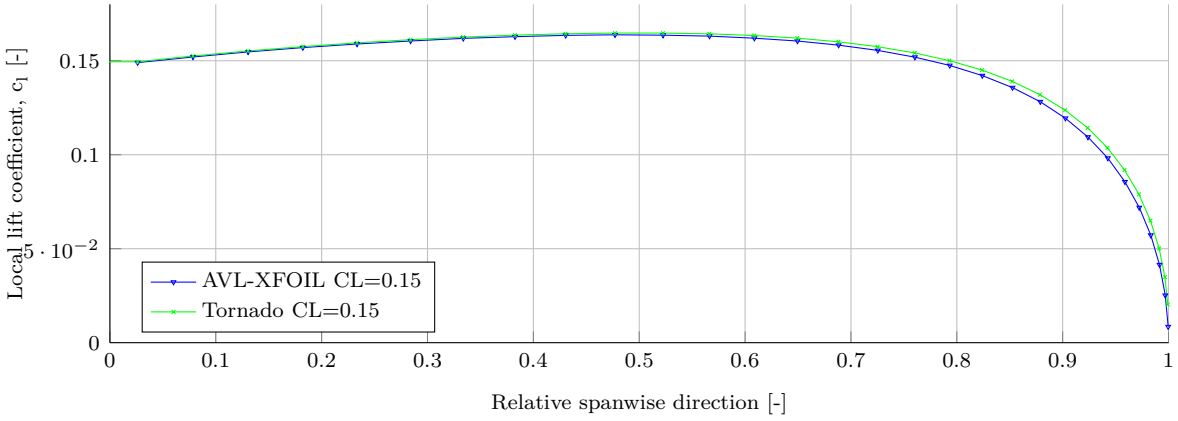

(a) The NACA-00-0-0 wing

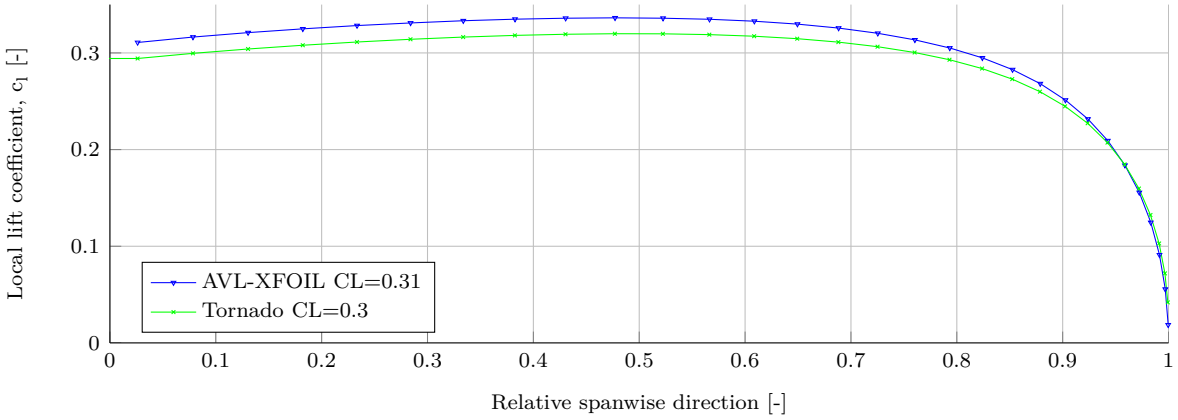

(b) The NACA-24-0-0 wing

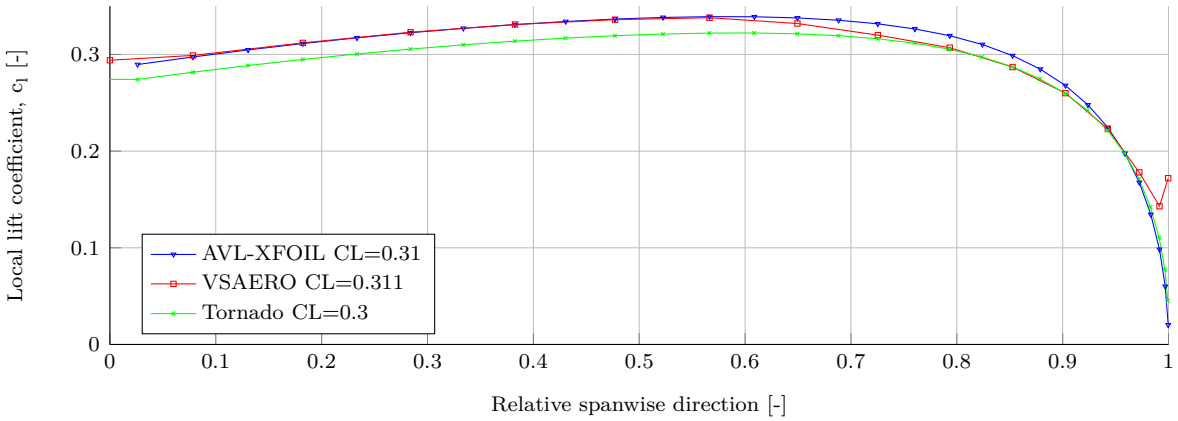

(c) The NACA-24-15-0 wing

Figure 3-7: Lift distribution of the NACA-00-0-0 wing, the NACA-24-0-0 wing and the NACA-24-15-0 wing

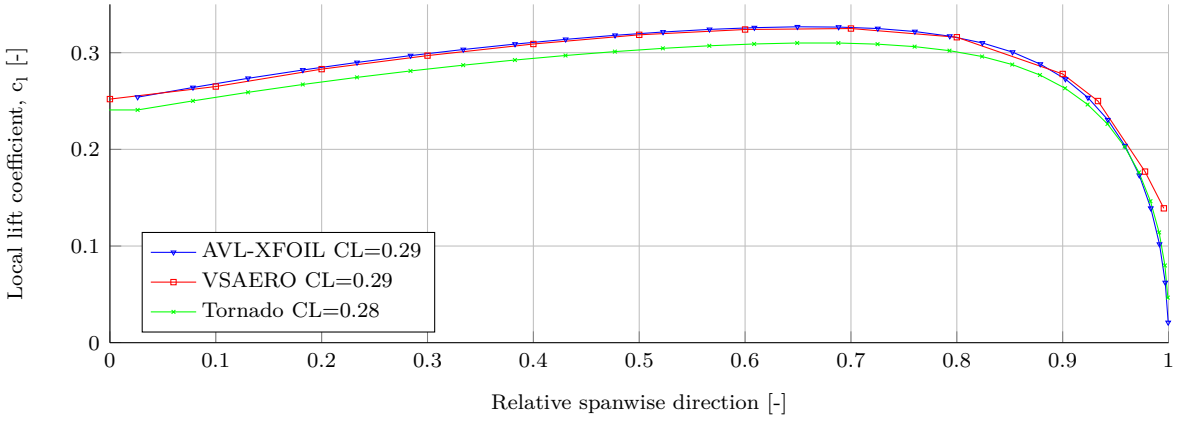

(a) The NACA-24-30-0 wing

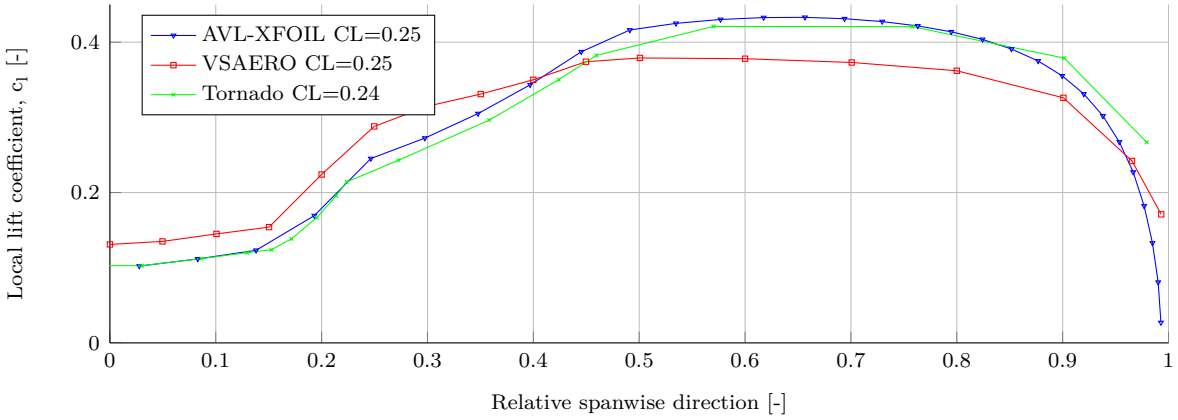

(b) The ZEFT blended wing body

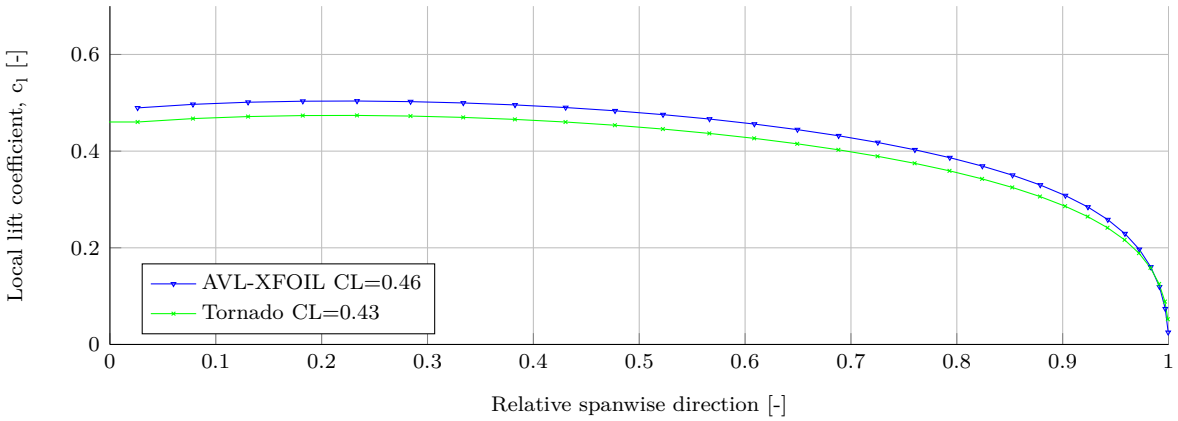

(c) The NACA-2.5-10-44.20 wing

Figure 3-8: Lift distribution of the NACA-24-30-0 wing, the ZEFT blended wing body and the NACA-2.5-10-44.20 wing

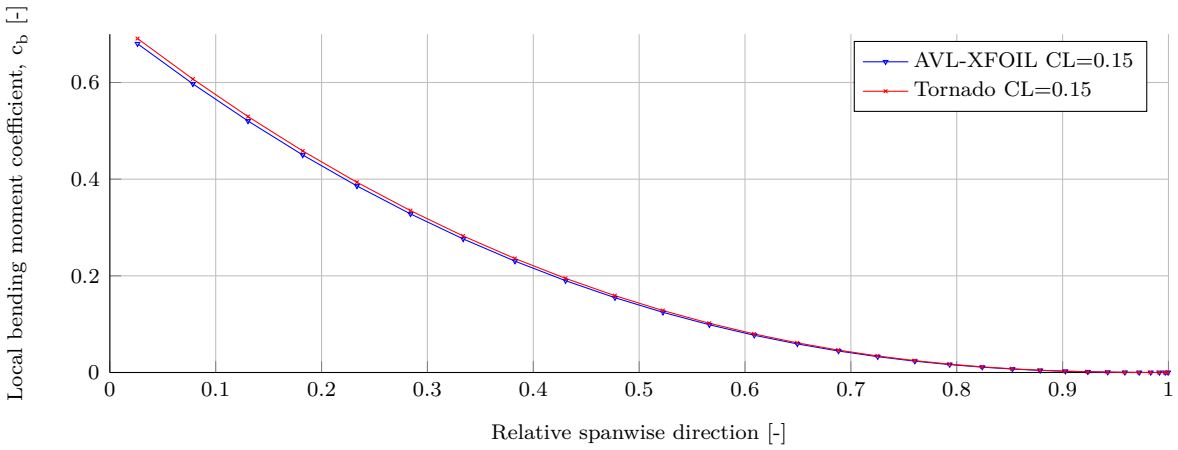

(a) The NACA-00-0-0 wing

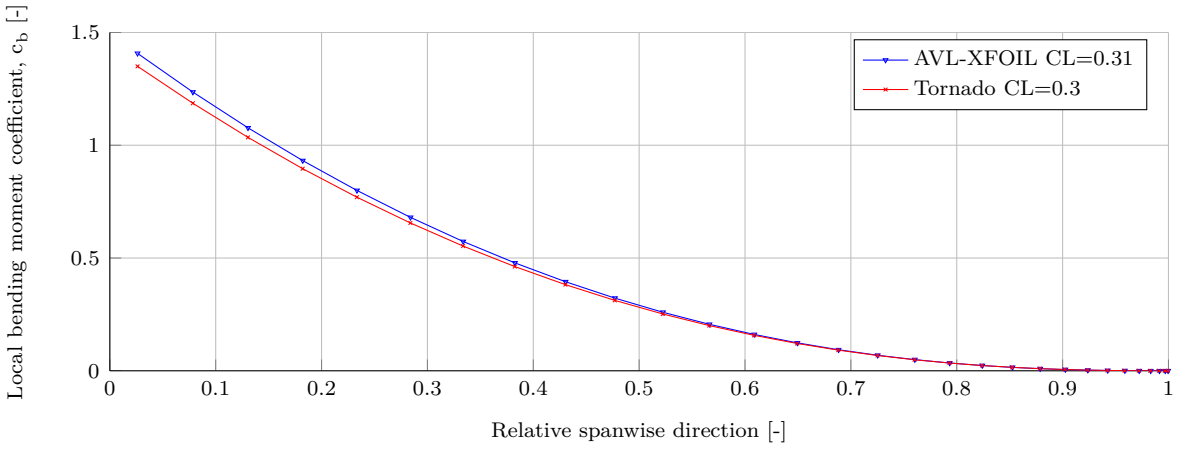

(b) The NACA-24-0-0 wing

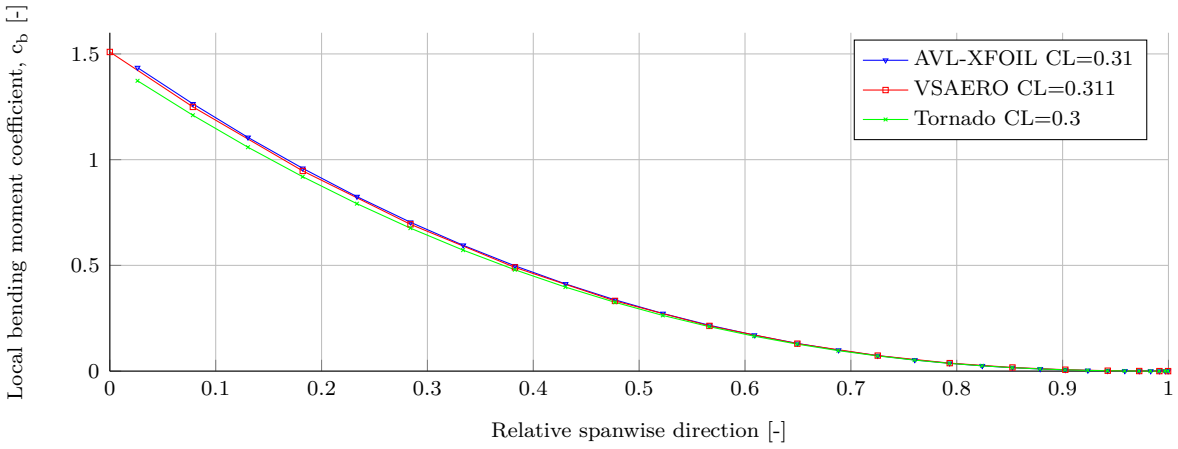

(c) The NACA-24-15-0 wing

Figure 3-9: Bending moment distribution of the NACA-00-0-0 wing, the NACA-24-0-0 wing and the NACA-24-15-0 wing

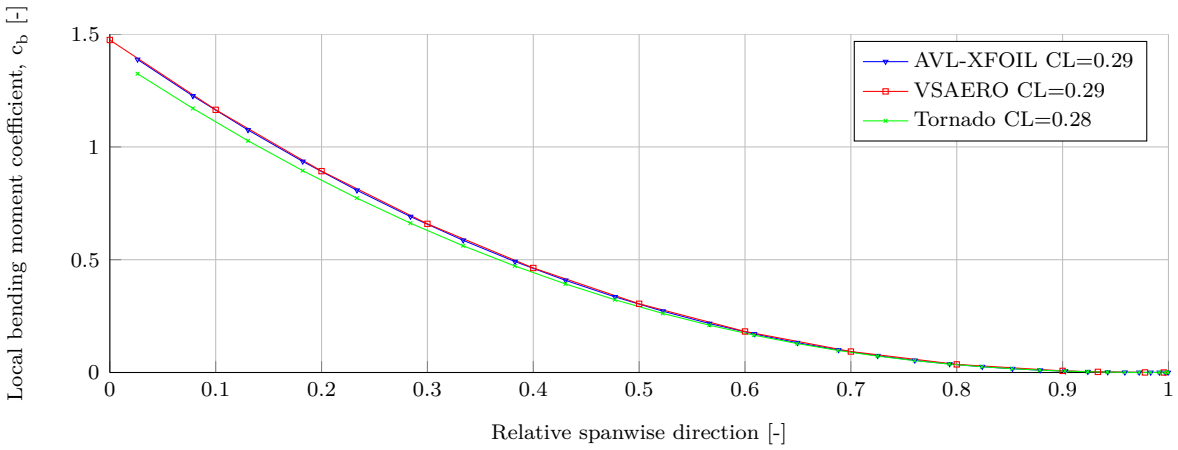

(a) The NACA-24-30-0 wing

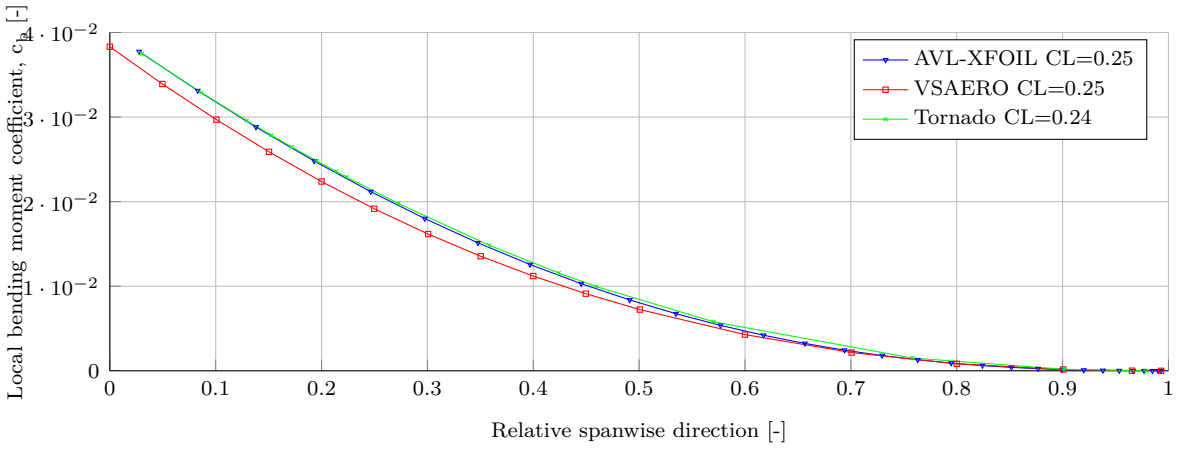

(b) The ZEFT blended wing body

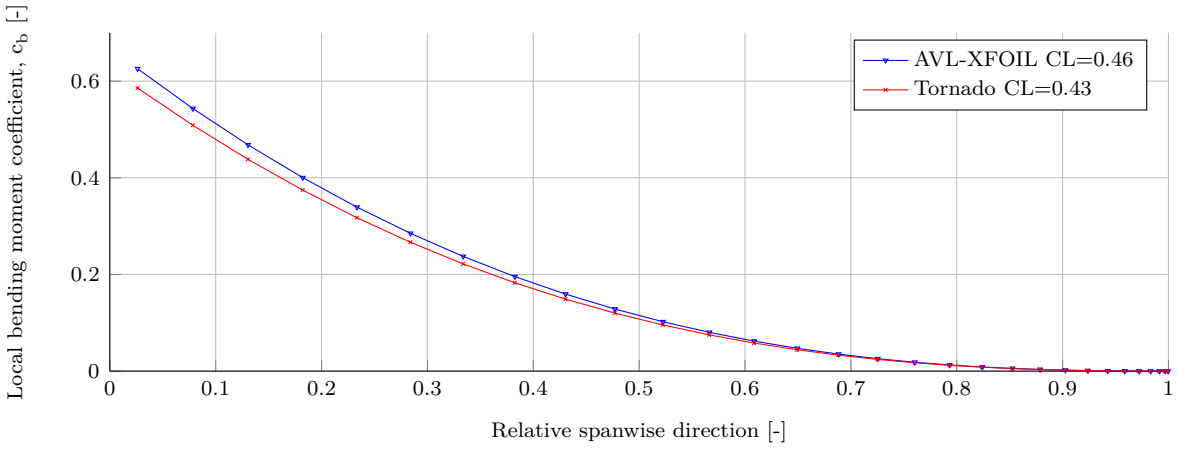

(c) The NACA-2.5-10-44.20 wing

Figure 3-10: Bending moment distribution NACA-24-30-0 wing, the ZEFT blended wing body and the NACA-2.5-10-44.20 wing

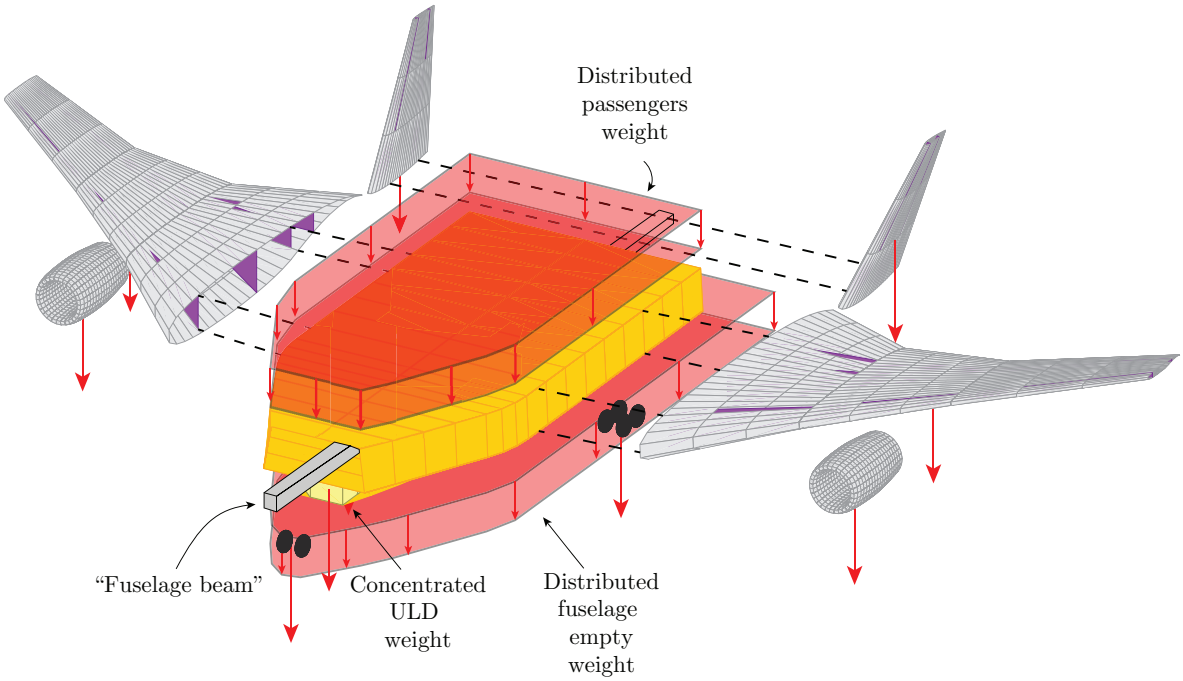

Figure 3-11: An overview of the inertial loads acting on the fuselage itself and on aircraft component attached to the fuselage

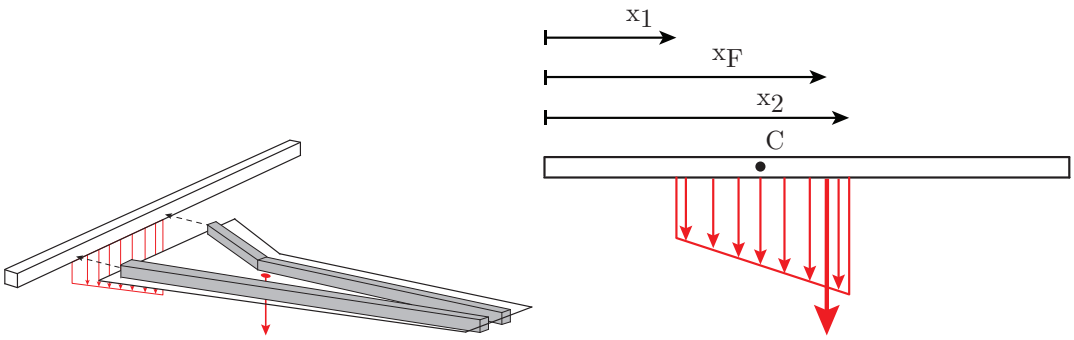

(a) Isometric view **(b)** Side view

Figure 3-12: The transformation of the wing weight to a linear distribution on the fuselage beam acting at the center of the fuselage.

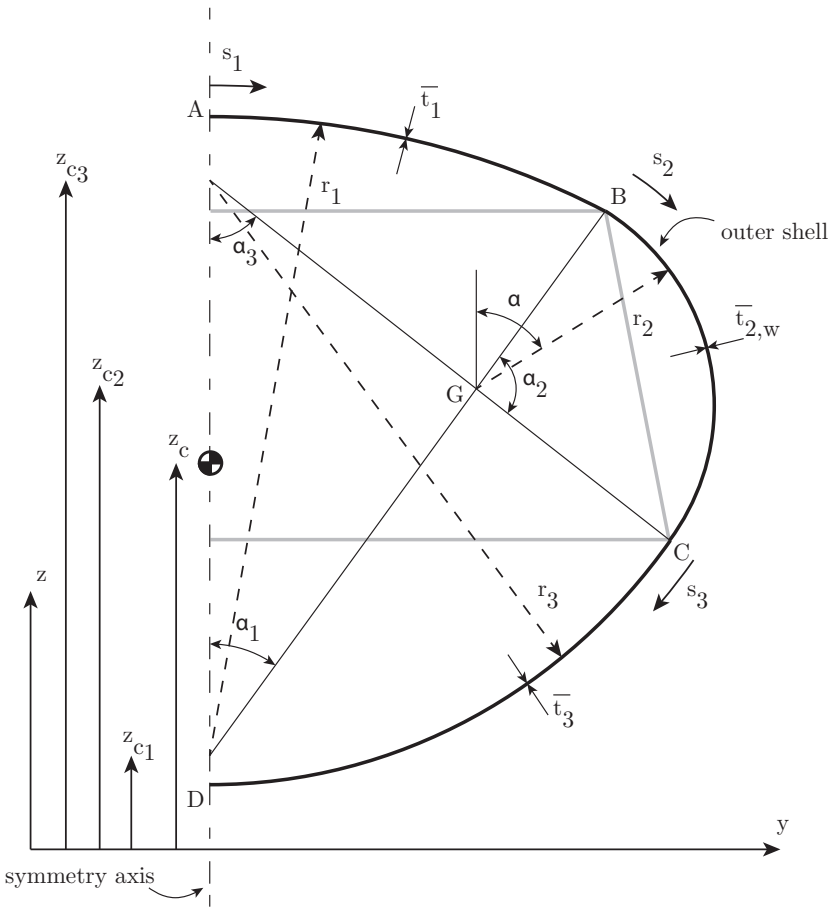

Figure 3-13: Overview of geometric variables for the determination of the shear flow

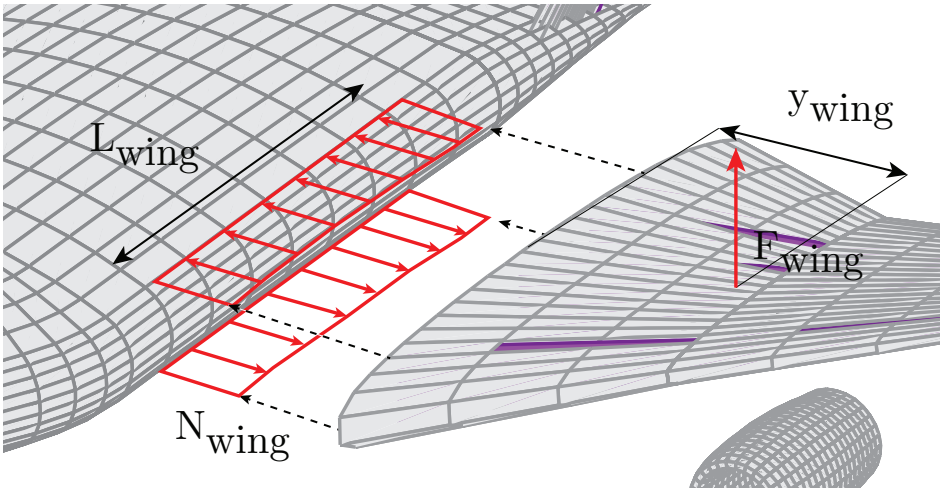

Figure 3-14: Schematic representation of how the wing bending moment is introduced in the trapezoidal structure

Chapter 4

Sizing of structural members

The sizing procedure presented in this chapter has the purpose of estimating the weight of the structural components of the oval fuselage. The sizing procedure is a physics-based weight estimation and therefore this chapter outline follows this steps of a structural design and analysis problem starting with the topology of the structure in Section 4-1. The material used for the structure in Section 4-2. Using the loads determined in Chapter 3 the structural sizing is discussed in Section 4-3.

The fuselage is divided into a finite number of sections and the required size of the structural members of each section is determined separately using two-dimensional structural analysis. For the straight cylindrical sections, the structural sizing of each fuselage sliver can be converted to a weight per unit length. For the spherical and toroidal components, a weight per unit of rotation can be calculated. The summation of these weights over the entire length of the fuselage results in the total ideal weight of these structural elements. Through the use of empirically determined penalty factors the weight penalty associated with windows, passenger doors and cargo doors are taken into account.

The fuselage weight estimation process is carried out in the following four consecutive steps:

1. Estimate the weight of the aircraft parts using a Class 2 weight estimation method
2. Determine the inertial loads and aerodynamic loads acting on the fuselage structure
3. Size the outer stiffened shell and the inner sandwich structure
4. Calculate the weight of the structural components and estimate the nonstructural weight components from empirical data

After the first iteration, the estimated weight is compared with the estimated weight of the Class 2 weight estimation method. If the difference between the two weights is within a given convergence tolerance, the calculation is completed. If this is not the case, the four consecutive steps are repeated but now using the newly estimated weight as its input. After each following iteration the last estimated weight is compared to the previously estimated weight to check for convergence. This process is shown in Figure 4-1 and a more elaborate discussion of this algorithm is found in Chapter 6.

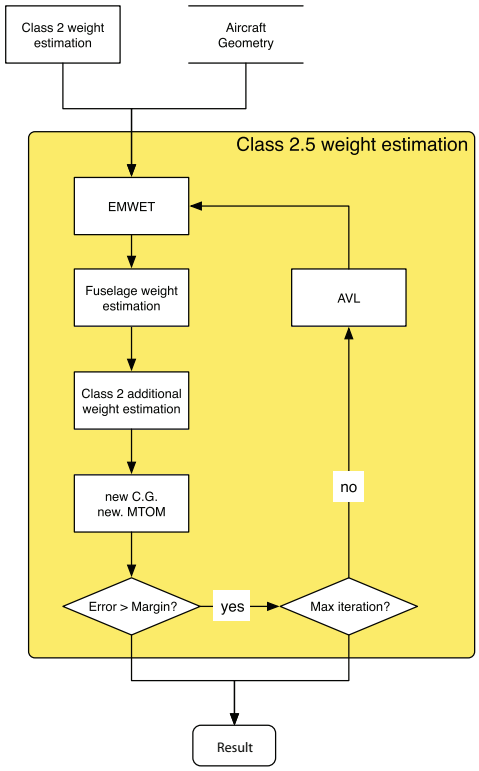

Figure 4-1: Activity diagram of the "Class 2.5 weight estimation" module

4-1 Fuselage topology

The structural design of the fuselage shell is chosen to be a semi-monocoque structure. The semi-monocoque structure consists of a thin-walled outer skin stiffened by stringers in the longitudinal direction to prevent panel buckling and frames in the hoop direction to prevent global buckling of the shell structure. This shell structure is similar to the fuselages of modern transport aircraft. Although recent advancements in the field of structural design show great potential in other topology, the semi-monocoque structure has been extensively used in the past. The advantage from this is that it can be verified with aircraft structures which are currently in operation.

The topology of the trapezoidal structure is different compared to the fuselages of modern transport aircraft. Its function is comparable to the function of a conventional passenger floor, namely to resist the transverse load induced by the weight of the passengers and furnishings. In additional the trapezoidal structure is subjected to axial forces induced by the pressure loads from the outer shell and bending of the wing. Due to the potentially high compressive loads, the trapezoid structure consists of a series of sandwich panels. The sandwich structure consists of two material: a lightweight core material encapsulated by two face sheets of stiff material. The lightweight core material increases the distance of the face sheets away from the neutral axis, thereby increasing its resistance to global buckling in a lightweight manner. While the trapezoidal structure may look like an impenetrable thick structure, the walls are thin compared to floor and ceiling, making the placement of windows feasible.

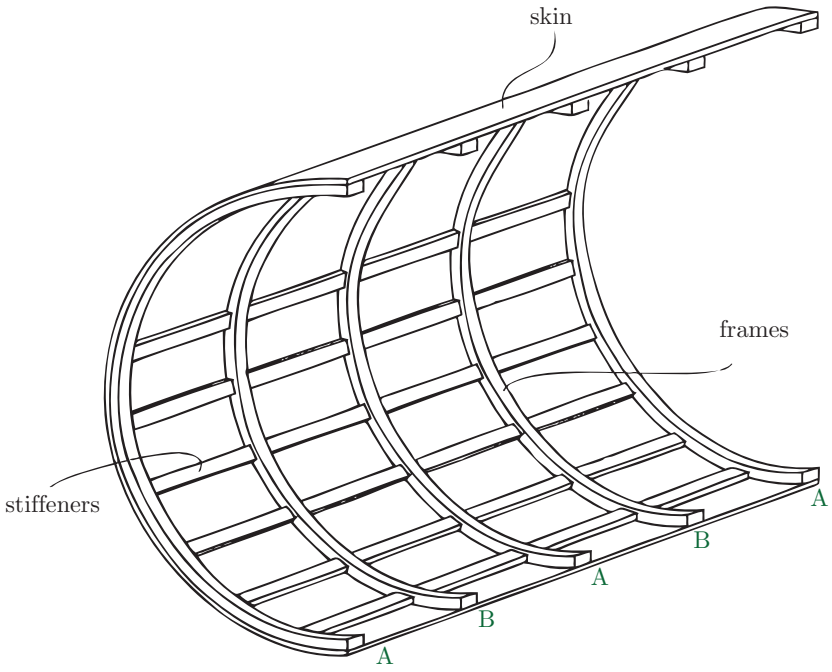

Figure 4-2: Topology of the outer shell consisting of a skin with longitudinal stringers and circumferential frames (derived from [35])

4-2 Material and aircraft design life

The materials that are used in a fuselage structure and the lifetime for which it is designed greatly influence the weight of the fuselage. As most modern aircraft structures are for a large part made out of aluminum alloys, the current trend is to make increasingly more parts out of fiber reinforced plastics. An important difference between these materials is that aluminum alloys behave as isotropic materials while fiber-reinforced plastics are anisotropic materials. The fuselage weight estimation method is aimed at estimating the weight of fuselage structures made out of isotropic materials. This means that the material has equal properties in all directions.

4-2-1 Fatigue strength

The way the lifetime of the structure influences the weight of the fuselage is through fatigue failure. The lifetime of an aircraft is often expressed as the number of flights and the total amount of flight hours. As the lifetime is increased the strength of the material at the end of the lifetime is decreased due to the cyclic loads acting on the material.

Fatigue is taken into account through the selection of the design yield stress of a structural part. The design yield stress of the structural part is the maximum stress occurring during loading such that it does not plastically deform within a specified lifetime. For the fuselage the number of flights is the most important indicator the lifetime. It is equivalent to the number of times the fuselage is pressurized and depressurized generating some of the highest stresses in the fuselage outer shell. The characteristics of this cyclic stress are expressed in

the cyclic stress ratio (R) and cyclic stress amplitude (A):

$$R = \frac{\sigma_{\min}}{\sigma_{\max}} \approx \frac{0}{\sigma_{\max}} = 0 \tag{4-1}$$

and

$$A = \frac{1-R}{1+R} = \frac{1-0}{1+0} = 1. \tag{4-2}$$

In these equations $\sigma_{\max}$ is the maximum stress and $\sigma_{\min}$ is the minimum stress.

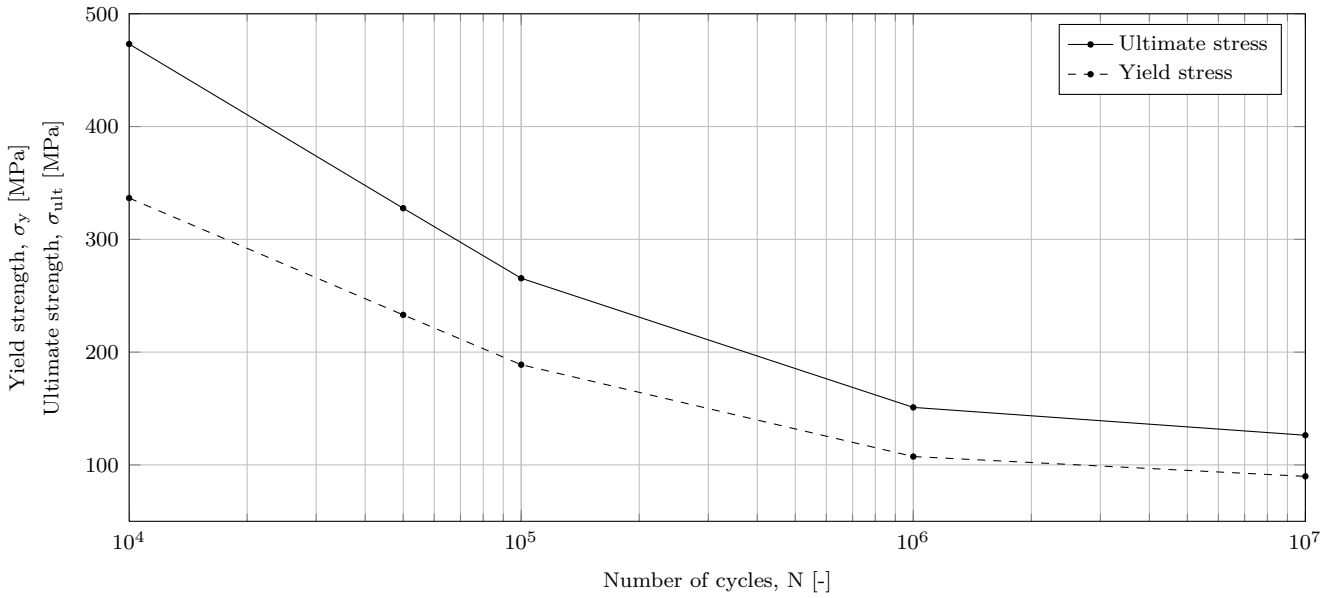

Figure 4-3: Ultimate strength as a function of cyclic loadings ($R = 0$, $A = 1$) for the aluminum alloy Al2024T3 (Alclad) [36] and the derived yield strength

To illustrate this material behavior, the reduction of ultimate strength of the material after a number of cycles is shown in Figure 4-3 for the aluminum alloy Al2024T3 (Alclad). For the determination of the design yield strength of the material it is assumed that the ratio between the yield strength and ultimate strength remain constant during cyclic loading, thus

$$\frac{\sigma_{y_0}}{\sigma_{ult_0}} = \frac{\sigma_{y_{cycles}}}{\sigma_{ult_{cycles}}} \tag{4-3}$$

where σ_y is the yield stress, σ_{ult} is the ultimate stress, the subscript "0" denotes the static properties and the subscript "cycles" denotes the properties after a certain number of cycles.

4-2-2 Number of cycles

A second assumption is that the total lifetime of the fuselage can be expressed in nothing more than the number of flights. This means that the complex loading cycles of different frequency, cyclic mean stress and cyclic amplitude can be condensed into an equivalent number of pressurization cycles. This means in theory that all the load cases happen once during a flight and the aircraft should be able to withstand all the load cases until its last flight, but

should theoretically fail to do so (or start to plastically deform) during its following flight. This means that any damage tolerance such as a crack-growth failure mechanism is included in the maximum number of flights.

Using these assumptions the design yield strength after a number of flights is found from fatigue test data and calculated using Equation 4-3, the number of flights, cyclic stress ratio and cyclic stress amplitude.

4-3 Sizing of structural members

This section explains the sizing procedure. This procedure consists of the determination of the stresses acting in the structural members and their global and local failure modes. Using these criteria the structural members are sized with the objective to minimize the weight of the structural members. First the trapezoidal structure is discussed in Section 4-3-1, next the stiffened skin is discussed in Section 4-3-2 and last the frames are discussed in Section 4-3-3.

In this section the definition *smeared thickness*, $\bar{t}$, is used. The smeared thickness of an structural member attached to the outer shell is the volume of the structural member spanned over a unit area of the fuselage. The smeared thickness of a stringer is therefore defined as

$$\bar{t}_{\text{stringer}} = \frac{A_{\text{stringer}}}{p} \tag{4-4}$$

where A is the cross-sectional area of the stringer and p is the stringer pitch.

The smeared thickness of the frame is defined as

$$\bar{t}_{\text{frame}} = \frac{A_{\text{frame}}}{L_{\text{frame}}} \tag{4-5}$$

where A_{frame} is the cross-sectional area of the frame and L_{frame} is the frame spacing.

The smeared panel thickness of the shell is then

$$\bar{t}_{\text{shell}} = \bar{t}_{\text{frame}} + \bar{t}_{\text{stringer}} + t_{\text{skin}}. \tag{4-6}$$

4-3-1 Trapezoidal structure

The trapezoidal sandwich structure is loaded in both axial tension and compression as well as bending loads. The edge of the trapezoidal member is connected to a neighboring trapezoidal member and the circular outer shell. The conservative assumption is made that this connection behaves as a simply supported connection. This simply supported joint allows rotations but restricts translation. Depending on the detailed design of these corners this might differ.

One sliver of the trapezoidal structure consists of four column beams. It is shown in Figure 4-4 how the horizontal member is modeled as a column beam. The column beam is loaded by a distributed transverse load q in N/m, an axial line load N_{lat} in N/m and an axial line load N_{long} in N/m in the plane of the fuselage section induced by the longitudinal bending of the fuselage, as can be seen in Figure 4-5. The axial load is calculated in Eq. 3-9 and if applicable

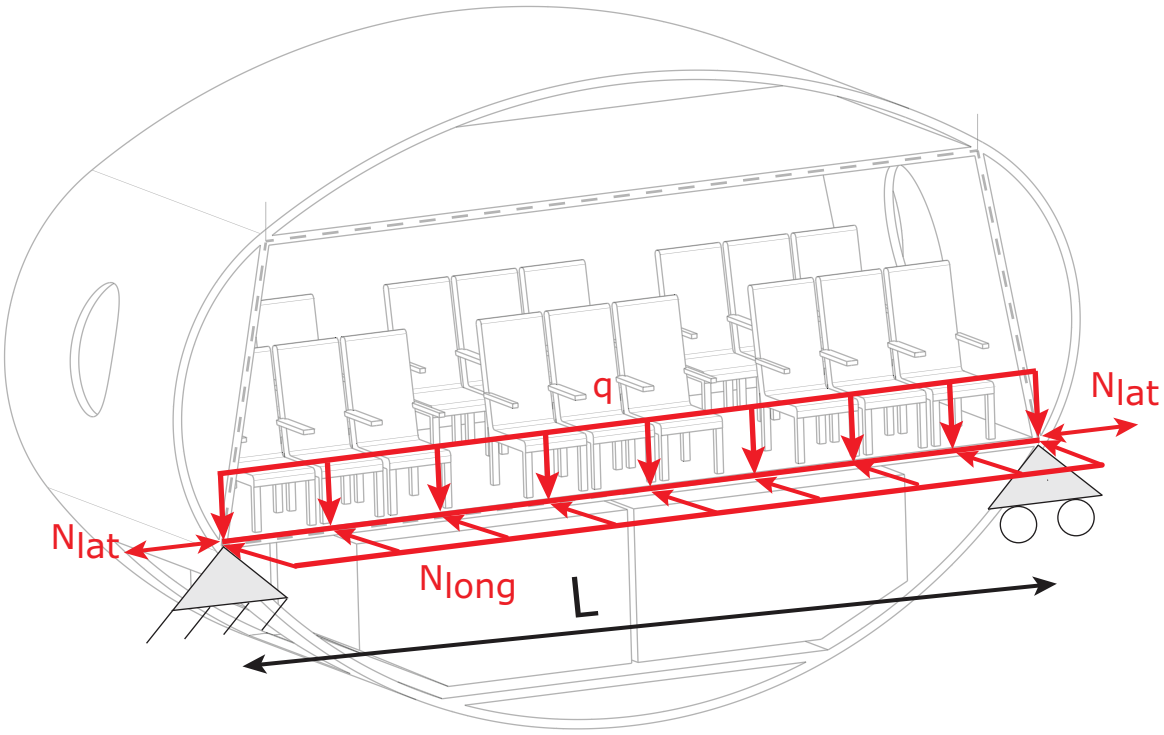

Figure 4-4: A visual representation of the modeling of a structural member as a sandwich column beam

this load is complemented by axial loads introduced by the wing bending. The distributed transverse load is deduced from the weight and location of the passengers and furnishings.

Note that the line load is expressed as the force per length. As the beam of unit depth is considered, this translates to an equal force for N_{lat}.

For sake of completeness the analysis is performed for an eccentric beam. When the eccentricity, e, is zero, the equations below simplify to the relations applicable to a normal column beam. It was seen in Figure 2-3a that the eccentricity is introduced to increase the cabin height without increasing the radius of the circular outer shell on the side of the fuselage.

The loads acting on the beam are depicted in Figure 4-5. In addition to the load cases discussed in Chapter 3, two additional branches are identified for each load case, namely:

1. The case where the distributed load is equal to the weight of the passengers and furnishings

2. The case where the fuselage is empty and the trapezoid is not loaded by a distributed transverse load

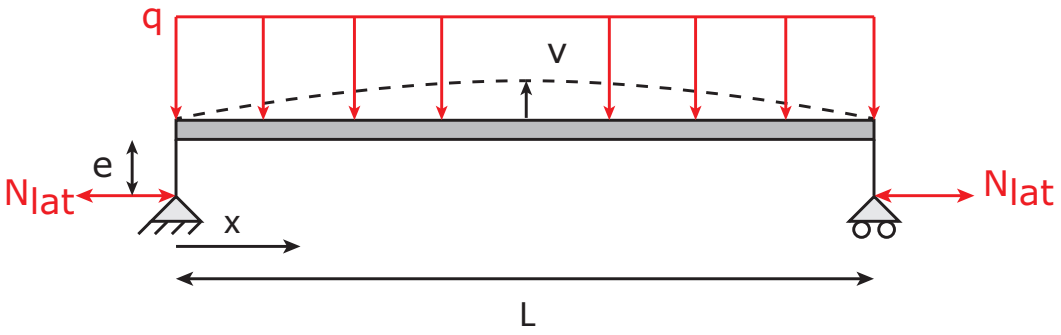

Figure 4-5: Pinned eccentric beam loaded by an axial force and a distributed load

Lateral stress

The stress in the beam in lateral direction is

$$\sigma_{\text{lat}} = \frac{N_{\text{lat}}}{A} + \frac{Mz}{I} = \frac{N_{\text{lat}}}{2t_{\text{face}}} + \frac{Mz}{I} \tag{4-7}$$

where N_{lat} is the lateral line load acting on the beam, A, t_{face} is the thickness of the face sheet, z is the height from the neutral axis of the beam, I is the moment of inertia of the beam and M the moment acting on the beam which is defined as

$$M = \frac{qL}{2} - \frac{qx^2}{2} - N_{\text{lat}}e. \tag{4-8}$$

where L is the length of the beam as depicted in Figure 4-5.

When both a compressive lateral load and a distributed transverse load act on the beam, the deflections caused by the distributed transverse load will induce an extra bending moment in the beam. This extra bending moment is caused by the eccentricity of the deflected part of the beam with the lateral force. Remember that the additional branch of load cases (distributed load on and distributed load off) make it impossible for the combination of eccentricity and distributed load to cancel out.

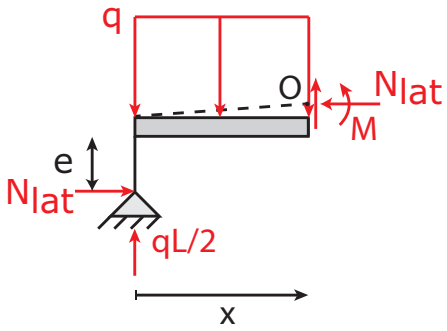

Figure 4-6: The free body diagram of the beam at an arbitrary section

To determine the stress in lateral direction when a compressive axial load and transverse load act on the structure, consider the section in Figure 4-6. The moment about point O is given

by

$$M + N_{\text{lat}}\left(v + e\right) - \frac{qL}{2} + \frac{qx^2}{2} = 0. \tag{4-9}$$

where v is the deflection of the beam. The moment M can be written as

$$M = EI\frac{\partial^2 v}{\partial x^2}, \tag{4-10}$$

where E is the Young's modulus. This results in the differential equation

$$\frac{\partial^2 v}{\partial x^2} + \lambda\left(v + e\right) = \frac{qL}{2EI}x - \frac{qx^2}{2EI} \tag{4-11}$$

with $\lambda = \sqrt{\frac{N_{\text{lat}}}{EI}}$ and boundary conditions:

$$v\left(0\right) = 0 \tag{4-12}$$

$$v\left(L\right) = 0. \tag{4-13}$$

The solution of this differential equation is the sum of the particular and homogeneous solution,

$$v = v_p + v_h. \tag{4-14}$$

The particular solution is of the form

$$v_p = c_1 + c_2 x + c_3 x^2. \tag{4-15}$$

Substituting Equation 4-15 in Equation 4-11 results in

$$2c_3 + \lambda\left(c_1 + e + c_2 x + c_3 x^2\right) = \frac{qL}{2EI}x - \frac{q}{EI}x^2. \tag{4-16}$$

After collecting terms of x this results in,

$$\left(2c_3 + \lambda^2 e + \lambda^2 c_1\right) + \left(\lambda^2 c_2 - \frac{qL}{2EI}\right)x + \left(\lambda^2 c_3 + \frac{q}{2EI\lambda^2}\right)x^2 = 0 \tag{4-17}$$

For Equation 4-17 to be zero, the terms within the brackets should be zero. The coefficients of the particular solution are obtained

$$c_1 = \frac{qx^2}{EI\lambda^4} - e \tag{4-18}$$

$$c_2 = \frac{qL}{2EI\lambda^2} \tag{4-19}$$

$$c_3 = -\frac{2c}{\lambda^2} = -\frac{qx^2}{2EI\lambda^2} \tag{4-20}$$

Substituting Equation 4-18, 4-19 and 4-20 in Equation 4-15 gives

$$v_p = \frac{qx^2}{EI\lambda^4} - e + \frac{qL}{2EI\lambda^2}x - \frac{qx^2}{2EI\lambda^2}x^2. \tag{4-21}$$

The homogeneous solution is of the form

$$v_h = c_4 \cos\lambda x + c_5 \sin\lambda x. \tag{4-22}$$

The unknown coefficients c_4 and c_5 are obtained by substituting Equation 4-21 and Equation 4-22 into Equation 4-14 and solving for the boundary conditions.

$$v(0) = c_4 + \frac{q}{\lambda EI} = 0 \tag{4-23}$$

$$v(L) = c_4 \cos \lambda L + c_5 \sin \lambda L + \frac{q}{\lambda^4 EI} - e = 0 \tag{4-24}$$

Solving for c_4 and c_5 results in

$$c_4 = -\frac{q}{\lambda^4 EI} + e \tag{4-25}$$

$$c_5 = \left(e - \frac{q}{\lambda^4 EI}\right) \tan \frac{\lambda L}{2} \tag{4-26}$$

The homogenous solution is found by substituting Equation 4-25 and 4-26 in Equation 4-22 gives

$$v_h = \left(e - \frac{q}{\lambda^4 EI}\right) \cos \lambda x + \left(e - \frac{q}{\lambda^4 EI}\right) \tan \frac{\lambda L}{2} \sin \lambda x \tag{4-27}$$

$$= \left(e - \frac{q}{\lambda^4 EI}\right) \left(\cos \lambda x + \tan \frac{\lambda L}{2} \sin \lambda x\right). \tag{4-28}$$

The total solution is found by substituting Equation 4-21 and 4-28 into Equation 4-14

$$v = \left(e - \frac{q}{\lambda^4 EI}\right) \left(\cos \lambda x + \tan \frac{\lambda L}{2} \sin \lambda x\right) + \frac{qx^2}{EI\lambda^4} - e + \frac{qL}{2EI\lambda^2} x - \frac{qx^2}{2EI\lambda^2} x^2. \tag{4-29}$$

For the case where $e = 0$, the maximum deflection is always found at $\frac{L}{2}$ and the maximum deflection when no eccentricity in the beam is present is defined as

$$v_{\max} = \frac{q}{EI\lambda^4} \left(\sec \frac{\lambda L}{2} - 1\right) - \frac{qL^2}{8EI\lambda^2}. \tag{4-30}$$

It can be shown using Equation 4-29 and 4-30 that the distributed weight does not affect the buckling load. As $\lambda L \to \pi$, the secant function and tangent function tends to infinity and the deflection function becomes unbounded. With the earlier defined $\lambda^2 = N_{\text{lat}}/EI$, this condition relates to a critical buckling load of $N_{\text{lat}_{\text{cr}}} = \pi^2 EI/L^2$. This condition is similar to the axially loaded beam. However, due to the combined axial load and the distributed load the maximum stress is higher. The stress in the beam in defined as

$$\sigma_{\text{lat}} = \frac{N_{\text{lat}}}{2t_{\text{face}}} + \frac{Mz}{I} \tag{4-31}$$

where M follows from Equation 4-9 as

$$M = \frac{qL}{2} - \frac{qx^2}{2} - N_{\text{lat}} (e - v). \tag{4-32}$$

For the case where $e \neq 0$ the moment M and thus the maximum deflection is not always found at $x = \frac{L}{2}$ and is in addition also evaluated at $x = 0$.

Although it is true that the buckling load is unaffected by the eccentricity, the sizing is significantly affected by this eccentricity. When the beam is either eccentric or loaded by a distributed transverse load, the beam will deflect by the slightest compressive force similar to a imperfect beam. This nonlinear mechanism is similar to a perfect beam with the exception that the bifurcation point is not reached, but asymptotically passed. This is shown in Figure 4-7. Since the bifurcation point is not reached, there is not a specific load where the beam will instantaneously buckle but the load is increased from the moment it deflects similar to a post-buckling state. It may seem that this easily occurs, it should be noted that the trapezoidal members subjected to compressive forces are thick sandwich panels and therefore deflection due to bending are relatively small.

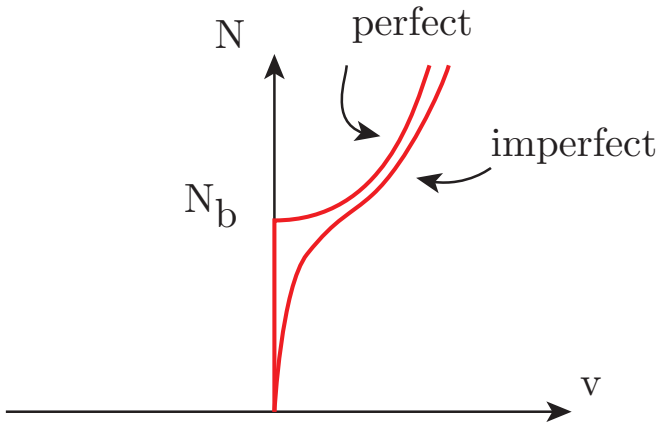

Figure 4-7: The load-deflection diagram for a perfect and imperfect beam

Longitudinal stress

The maximum stress in longitudinal direction due to the fuselage bending is obtained from the longitudinal line load N_b (Eq. 3-12) and the thickness of the sandwich facing sheet t_{face},

$$\sigma_{long} = \frac{N_b}{2t_{face}}. \tag{4-33}$$

Since the longitudinal stress due to bending varies along the height of the section, the maximum line load per load case is used for the sizing of the trapezoidal members. For the "vertical" member two maximum line loads are employed when the members spans from a point above the neutral axis to a point below the neutral axis.

Yield criterion

The lateral and longitudinal stresses in the beam area are used to determine yielding of the face sheets of the sandwich panel. The maximum distortion energy criterion, also known as the von Mises yield criterion, is used [37]. Since the face sheets are thin plates, the plane stress assumption is that $\sigma_z = 0$, $\tau_{z,long} = 0$ and $\tau_{lat,z} = 0$. This results in the following von Mises stress

$$\sigma_v = \sqrt{\sigma_{lat}^2 - \sigma_{long}\sigma_{lat} + \sigma_{long}^2 + 3\tau_{lat,long}^2}, \tag{4-34}$$

where σ_v is the von Mises stress and τ is the shear stress. When the von Mises stress reaches the tensile yield stress, σ_y, it is estimated that the bi-axially loaded structure actually yields.

There is an important difference between the von Mises yield criterion and simply comparing the stress in one direction with the yield stress. The von Mises yield criterion takes into account the reduced strength when the tension is applied in one direction and compression in the other direction. When tension in one direction is twice the tension in another direction the yielding of the material occurs at a 15% higher stress than the uni-axial yield stress σ_y. This can be seen in Figure 4-8.

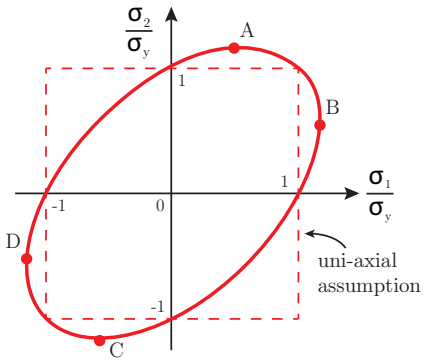

Figure 4-8: The von Mises stress criterion for a bi-axial loading when no shear is present.

Structural stability

The sandwich column beam can buckle in various modes. This analysis accounts for dimpling failure, Eq. 4-35, crimping failure, Eq. 4-36, wrinkling failure, Eq. 4-37, and global buckling failure of thick sandwich panels, Eq. 4-38 [38, 39]. Dimpling is a local buckling mode of the face sheets and only happens when a cellular core material is used, such as a honeycomb core or corrugated material. Crimping is a local buckling mode where the core fails. Wrinkling is the local buckling of the face sheets as a plate with a elastic foundation. These failure modes are shown in Figure 4-9.

Local buckling failure occurs at:

$$N_{\text{dimpling}} = \frac{2E_{\text{face}}t_{\text{face}}^3}{1-\nu_{12}\nu_{21}}\frac{1}{s^2} \tag{4-35}$$

$$N_{\text{crimping}} = t_{\text{core}}G_{\text{core}} \tag{4-36}$$

$$N_{\text{wrinkling}} = 0.79\left(E_{\text{face}}E_{\text{core}}G_{\text{core}}\right)^{\frac{1}{3}} \tag{4-37}$$

where E_{face} is the Young's modulus of the face sheet material, E_{core} is the Young's modulus of the core material, t_{face} is the face sheet thickness, G is the shear modulus, s is the cell size of the core material (for example the radius of the honeycomb shape) and ν the Poisson's ratio.

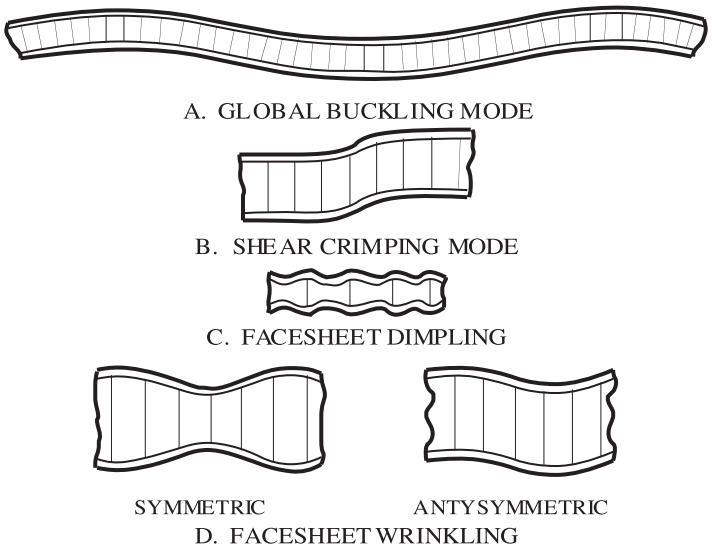

Figure 4-9: The failure modes of a sandwich panel from Ley [38].

Global buckling failure of thick sandwich structures occurs at:

$$N_{\text{global}} = N_{\text{E}} \left(\frac{1 + \frac{N_{\text{E}_\text{f}}}{N_\text{s}} - \frac{N_{\text{E}_\text{f}}}{N_\text{s}} \frac{N_{\text{E}_\text{f}}}{N_\text{s}}}{1 + \frac{N_\text{s}}{N_\text{s}} - \frac{N_{\text{E}_\text{f}}}{N_\text{s}}} \right) \tag{4-38}$$

with

$$N_\text{s} = G_{core} \frac{(t_{core} + t_{face})^2}{t_{core}}$$
$$N_\text{E} = \frac{E_\text{face} \pi^2}{L^2} \left(\frac{t_\text{face}^3}{6} + t_\text{face} \frac{(t_\text{core} + t_\text{face})^2}{2} \right)$$
$$N_{\text{E}_\text{f}} = \frac{E_\text{face} \pi^2}{L^2} \frac{t_\text{face}^3}{6}$$

Sizing

The system of equations is numerically solved to find the face sheet- and core thickness of the beam column that satisfies all the bi-axial stresses and buckling constraints for the lowest mass per unit length. The minimization problem is defined as:

$$\begin{aligned} \min_{t_\text{face}, t_\text{core}} \quad & \rho_\text{core} t_\text{core} + 2\rho_\text{face} t_\text{face} \\ \text{s.t.} \quad & -N_\text{dimpling} \leq N_\text{lat} \\ & -N_\text{crimping} - N_\text{lat} \leq 0 \\ & -N_\text{wrinkling} - N_\text{lat} \leq 0 \\ & -N_\text{global} - N_\text{lat} \leq 0 \\ & \sigma_v - \sigma_y \leq 0. \end{aligned}$$

where ρ is the material density.

4-3-2 Stiffened outer shell

The circular stiffened skin is sized to withstand the longitudinal bending moment without instabilities. The skin is loaded in bi-axial directions by the pressurization loads and the longitudinal bending loads. Two approaches are taken for the buckling analysis: (1) a general panel buckling analysis for a circular panel and (2) a local buckling analysis. The bi-axial stress is used to determine the yielding of the stiffened skin is similar to Section 4-3-1.

The loads that are acting on the circular shell are visualized in Figure 4-10. It was seen in Section 3-6 that the bending stress and line load vary along the vertical axis. For the sizing of the structural members two characteristic loads are used, (1) the maximum compressive load on the structural member is used for the global buckling analysis and (2) the mean normal and shear load is used for the local calculation of the yield criterion and local buckling analysis. Otherwise the structural member would be sized for the maximum load, which only acts on a small portion of the structure and thus the weight of the structural member would be overestimated.

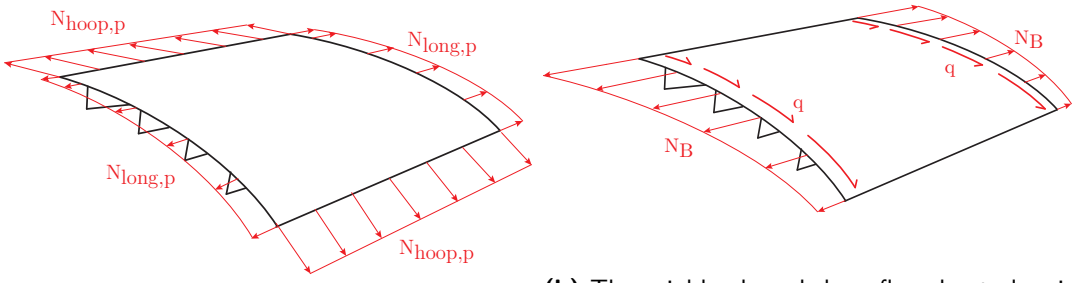

(a) The axial loads due to pressurization

(b) The axial loads and shear flow due to longitudinal fuselage bending and shear

Figure 4-10: The loads acting on the upper part of the stiffened outer shell

General buckling

The general panel buckling analysis studies the circular stiffened skin as a perfect cylindrical shell in bending. The conservative assumption is made that the stiff trapezoidal structure does not help to prevent any buckling of the skin. The buckling load is determined using Eq. 4-40 [40], the critical line load,$N_{\text{cr,shell}}$,of the circular shell is given by

$$N_{\text{cr,shell}} = k_x \frac{\pi^2 D}{L_{\text{frame}}^2} \tag{4-40}$$

where L_{frame} is the frame spacing and k_x is defined by

$$k_x = \frac{4\sqrt{3}}{\pi^2}\theta Z \quad \text{when} \quad Z > 2.85 \tag{4-41a}$$

$$k_x = 1 + 12\frac{\theta^2 Z^2}{\pi^4} \quad \text{when} \quad Z \leq 2.85 \tag{4-41b}$$

where θ is the buckling correlation factor, Z is the Batdorf curvature parameter which is defined by

$$Z = \frac{L_{\text{frame}}^2}{r t_{\text{shell}}}\sqrt{1-\nu_{\text{shell}}^2} \tag{4-42}$$

where $\bar{t}_{\text{shell}}$ is the smeared thickness of the stiffened panel, r is the radius of the stiffened panel and D is the bending stiffness of the plate

$$D = \frac{E_{\text{shell}} t_{\text{eq}}^3}{12\left(1-\nu_{\text{shell}}^2\right)}. \tag{4-43}$$

The equivalent thickness t_{eq}, is the thickness of a flat plate having the same sectional moment of inertia as the stiffened panel.

The correlation factor θ is used to correct for the discrepancy between theoretical and experimental values. Due to imperfections the experimental values are generally lower and therefore the factor θ is lower than unity. The following correlation factor for cylinders loaded in bending is found from experiments [40]:

$$\theta = 1 - 0.731\left(1 - \mathrm{e}^{-\phi}\right) \tag{4-44}$$

where

$$\phi = \frac{1}{16}\sqrt{\frac{r}{\bar{t}_{\text{shell}}}}. \tag{4-45}$$

This equation is derived from experimental data having a fineness ratio $\frac{r}{t} < 1500$ and should therefore be used with caution if fuselages exceed this value.

Local buckling

For the calculation of the local buckling load the stiffened panel is idealized as a collection of j slender rectangular flat plates (strips) having a length equal to the frame spacing, L_{frame}, a thickness, t_j and a width, w_j derived from the stiffened panel cross-sectional shape, Figure 4-11. The curvature is neglected in the local buckling analysis. Although in reality the strips are elastically constraint to the neighboring strips, in this analysis a predefined edge constrain is imposed. The critical buckling load for the strips is then determined using [41]. The critical buckling line load of the individual strip is defined as

$$N_{\text{cr,j}} = \frac{k_{\text{j}} \pi^2 E_{\text{shell}}}{12(1-\nu_{\text{shell}}^2)} \left(\frac{t_{\text{j}}}{b_{\text{j}}}\right)^2. \tag{4-46}$$

The buckling coefficient k is dependent on the type of edge constraints. Each strip is seen as an individual slender plate buckling problem where each of the two edge constraints are either pinned, clamped or free.

When all edges are simply supported, $k = 4.0$. When all edges are clamped, $k = 6.98$. When three edges are simply supported and one is free, $k = 0.43$. When three edges are clamped and one is free, $k = 1.28$.

For the Z-stiffened panel in Figure 4-11a the strips AB and BC are clamped at all edges. Strips BD and DE are simply supported at all edges and strip EF is simply supported with one edge free. For the hat-stiffened panel in Figure 4-11b the strips AB and BC are clamped at all edges, CD and BG are clamped with one edge free and CE, EF and, BF are simply supported at all edges.

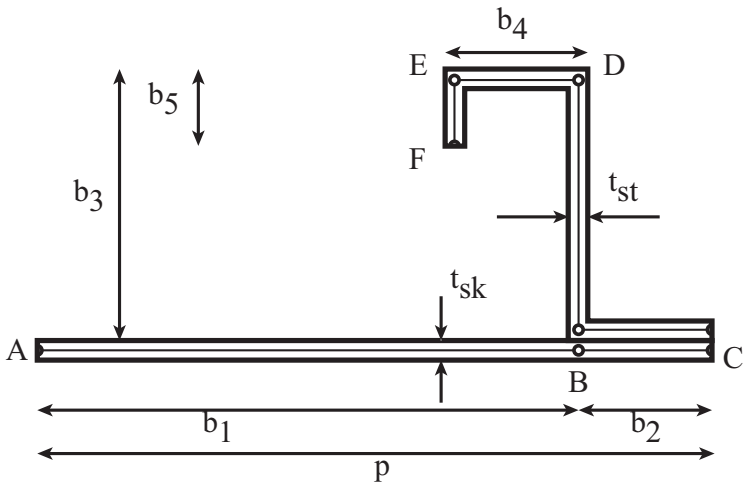

(a) Panel with z-stiffeners

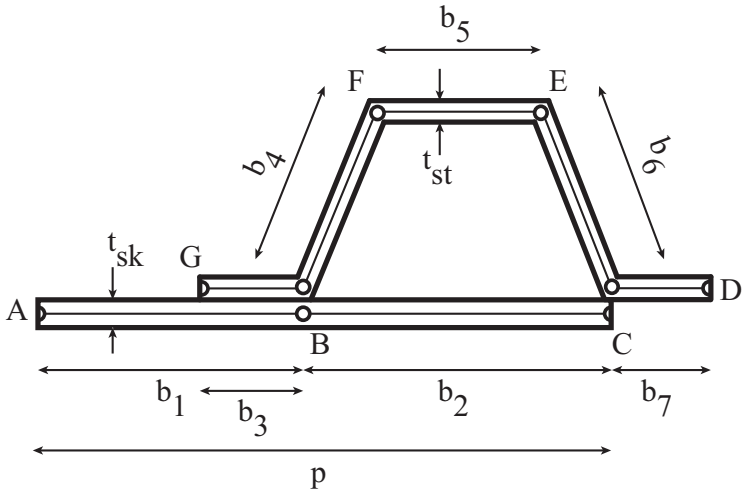

(b) Panel with hat-stiffener

Figure 4-11: Examples the geometry of the stiffened panels divided into five slender flat plates.

Yield criterion

The hoop and longitudinal stresses in the skin are used to determine yielding of the stiffened panel. Using the thin plate assumption the stress through the thickness of the skin are neglected. This results in the following von Mises stress

$$\sigma_v = \sqrt{\sigma_{\text{hoop}}^2 - \sigma_{\text{long}}\sigma_{\text{hoop}} + \sigma_{\text{long}}^2 + 3\tau_{\text{hoop,long}}^2}, \tag{4-47}$$

which should be smaller than the material yield stress σ_y.

For the calculation of σ_{hoop} the thickness of the skin is used since stringer do not contribute to the strength in this direction. For the calculation of σ_{long} the thickness of the stringer and skin are used since the stringers do contribute to the strength of the panel in this direction.

Sizing

The system of equations describing the stresses and buckling modes is numerically solved to find the stiffened cross-section that satisfies all the inequality constraints for the lowest smeared thickness. The minimization problem is defined as:

$$\begin{aligned} \min_{\bar{t}} \quad & \bar{t} \\ \text{s.t.} \quad & -N_{\text{dimpling}} - N_{\text{lat}} \leq 0 \\ & -N_{cr_j} - N_{\text{long}} \leq 0 \\ & -N_{cr_j} - N_{\text{long}} \leq 0 \\ & \sigma_v - \sigma_y \leq 0. \end{aligned}$$

4-3-3 Frames

The frames of the fuselage are, independent of the stiffened skin, sized to prevent general instability of the fuselage due to compressive forces. Existing sizing methods are based on experimental data of circular shells with ring frames [42]. The relation between the required stiffness of the circular frame, the moment applied to the fuselage section and the size of the section are given by

$$C_{\text{fr,circ}} = \frac{(EI)_{\text{frame}} L_{\text{frame}}}{MD^2} > \frac{1}{16000} \tag{4-48}$$

where $C_{\text{fr,circ}}$ is the Shanley frame constant and D is the diameter of the circular fuselage. Although this relation cannot be directly used to size the frames of an oval fuselage, it can be extended for oval fuselage sections. First, the derivation for circular frames is discussed. This derivation is than modified to apply for oval fuselage section.

In the frame analysis a predefined shape of the frame is assumed. This makes the sizing procedure of the frame a closed form solution. The shape of the frame cross-section is given in Figure 4-12 where it can be seen that the geometry is defined by a single variable, a.

The derivation for the circular frame from Shanley [42] is repeated here for sake of completeness. The derivation is modified for the application of frames of the oval fuselage.

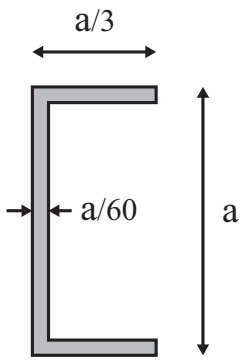

Figure 4-12: The shape of the C-section frame and the relative dimensions

Circular frame

Consider the fuselage topology of Figure 4-2. If one would make a cut through the lower part as it is visualized in this figure, point A and B are the points where the frames are location. A simple strut-spring mode,l shown in Figure 4-13, is set up which represents this longitudinal section cut. The springs represent the location of a frame. The struts represent the stiffened skin of the fuselage. The point A and B correspond to the points A and B in Figure 4-2. From experiments by Shanley [42] it is observed that the general buckling of the frames occurs between the frames. This location is similar to the pinned connection in Figure 4-13.

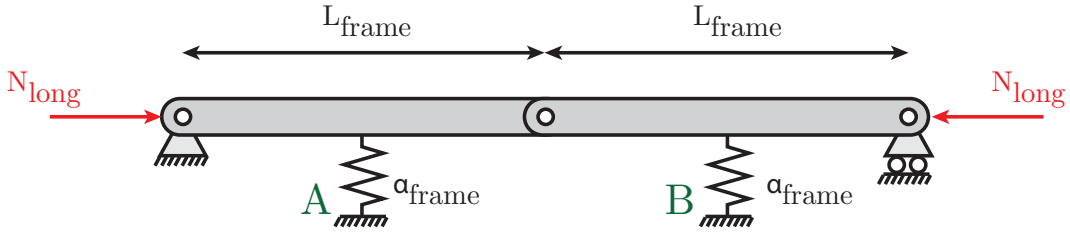

Figure 4-13: Strut-spring model of the frame

The required spring stiffness, $\alpha_{\text{fr,circ}}$, is determined

$$\alpha_{\text{fr,circ}} = \frac{P_1 K_1}{L_{\text{frame}}} \tag{4-49}$$

where P_1 is a force constant and K_1 is a stiffness constant. The maximum line load due to bending for circular fuselages is

$$N_{\text{long,circ}} = \frac{4M}{\pi D^2} \tag{4-50}$$

where M is the longitudinal bending moment applied to the fuselage section and D is the diameter of the fuselage. When multiplied by a fraction of the diameter, D, the line load $N_{\text{long,circ}}$ becomes a force $F_{\text{long,circ}}$

$$F_{\text{long,circ}} = \frac{K_2 M}{D} \tag{4-51}$$

The spring constant, $\alpha_{\text{fr,circ}}$, from the strut-spring model can be translated to the stiffness of a circular frame using [43]

$$\alpha_{\text{fr,circ}} = \frac{K_3 (EI)_{\text{fr,circ}}}{D^3} \tag{4-52}$$

Combining Equation 4-49, 4-50 and 4-51 results in:

$$(EI)_{\text{fr,circ}} = \frac{C_f M D^2}{L_{\text{frame}}} \tag{4-53}$$

In this manner the frame section in Figure 4-12 is sized such that the stiffness, $(EI)_{\text{fr,circ}}$ is equal to the stiffness of the frame. The C-shaped frame has an efficiency factor of

$$k_{\text{frame}} = \frac{I_{\text{fr,circ}}}{A^2_{\text{fr,circ}}} = 5.4 \tag{4-54}$$

Note that the characteristic dimension, a, cancels out in this equation.

The cross-sectional area is then found to be

$$A_{\text{fr,circ}} = \sqrt{\frac{(EI)_{\text{fr,circ}}}{kE_{\text{fr,circ}}}} \tag{4-55}$$

and the smeared frame thickness is then easily obtained as

$$\bar{t}_{\text{frame}} = \frac{A_{\text{fr,circ}}}{L_{\text{frame}}} \tag{4-56}$$

Oval frame

An analogue derivation can be performed for an oval fuselage. First the section is replaced by an oval of equal width w_{oval} and height h_{oval}. The moment of inertia of a thin walled oval is not explicitly defined, however for small deviation from a thin walled circular cross-section the inertia of the thin-walled oval can be approximated by,

$$I_{\text{fr,oval}} = \frac{\pi w_{\text{fr,oval}} h^2_{\text{fr,oval}} \bar{t}_{\text{shell}}}{8} \tag{4-57}$$

This simplification scales the cross-section from circular to elliptical in the direction of the width. This mean that the thickness at the top remains the same, however the thickness at the side of the cross-section increase by a factor $w_{\text{oval}}/h_{\text{oval}}$. This overestimates the moment of inertia slightly for $w_{\text{oval}} > h_{\text{oval}}$ but since the geometry is only thicker close to the neutral axis, this overestimates the inertia by about 10%. When applied to sections where $w_{\text{oval}} < h_{\text{oval}}$ this means that the thickness at the top will be larger than the thickness at the side. Due to this thickness increase away from the neutral axis, the effect on the moment of inertia is significantly larger.

The line load follows from Equation 4-57 as

$$N_{\text{long,oval}} = \frac{4M}{\pi w_{\text{oval}} h_{\text{oval}}} \tag{4-58}$$

and when multiplied by a length relative to the width w_{oval},

$$F_{\text{long,oval}} = \frac{K_2 M}{h\text{oval}} \tag{4-59}$$

Although the stiffness of the oval fuselage section subjected two opposing concentrated loads is different than for a circular section, the same behavior is assumed as in Equation 4-52. The equation is adjusted by replacing the diameter D with two times the radius of the largest of the upper and lower arc, r^3_{max}. Combining Equation 4-49, 4-51 and 4-52 results in the required frame stiffness for an oval fuselage,

$$(EI)_{\text{fr,oval}} = C_f \frac{r^3_{\text{max}} M}{8 h_{\text{oval}} L_{\text{frame}}} \tag{4-60}$$

Similar to the circular frame, the derivation of the smeared frame thickness is determined using the frame efficiency factor k_{frame}

$$k_{\text{frame}} = \frac{I_{\text{fr,oval}}}{A^2_{\text{fr,oval}}} = 5.4 \tag{4-61}$$

Note that the characteristic dimension, a, cancels out in this equation.

Using Equation 4-60 and 4-61 the frame area is,

$$A_{\text{fr,oval}} = \sqrt{\frac{(EI)_{\text{fr,oval}}}{k E_{\text{fr,oval}}}} \tag{4-62}$$

and the smeared frame thickness is then easily obtained as

$$\bar{t}_{\text{frame}} = \frac{A_{\text{fr,oval}}}{L_{\text{frame}}} \tag{4-63}$$

4-4 Structural weight

Using the method discussed in this chapter the required geometry of each structural member to withstand the forces at applied to it in every load case is discussed. From these thicknesses the volume of the section is determined. For the extruded sections this is determined by multiplying the thickness with the depth of the section with respect to the neighboring sections. For the revolved geometry the volume is determined from the swept angle of the revolved geometry. The total structural weight is then determined by multiplying the volume of each structural member by the material density of the structural member.

Chapter 5

Fuselage weight

There are different conventions to define the fuselage weight. The fuselage weight and its components for this weight estimation are adopted from Obert [44]. The fuselage weight is defined as the the summation of the weight of all the structural and non-structural components of the fuselage excluding the furnishings. The furnishings consist of the weight of cabin interior, lavatories, galleys and evacuation systems.

The weight of the fuselage is divided into structural components and nonstructural components. The structural components are the load carrying members such as the outer skin, the floor, ceiling and walls of the fuselage. The size (thickness) of these components have been determined in the previous chapter. The nose and the aft of the fuselage were not determined from the loads. For the nose an empirical method is used. The weight of the aft is derived from the sizing of the outer shell.

The nonstructural weight includes all the systems that are present in the fuselage. Additional weights include weight penalties associated with cut-outs for windows and doors, paint and pressure bulkheads. These are determined from empirical data [45, 46, 47]. To use these empirical relationships, knowledge of the number of doors and windows should be known beforehand. Since this information is not always readily available or is expensive in terms of computational costs, empirical relations are determined from reference aircraft.

5-1 Additional weight

The additional weights are the weight penalties associated with cutouts for windows and doors. The weight of the nose and the aft is also included.

Nose outer shell weight

The weight of the outer shell of the fuselage nose is taken from Howe [46]

$$W_{\text{nose}} = 1.2BS_{\text{nose}}\Delta p\frac{\rho_{\text{skin}}}{\sigma_{\text{skin}}} \quad [\text{kg}] \tag{5-1}$$

B is the width of the nose, [m]
S_{nose} is the wetted area of the fuselage nose, [m^2]
Δp is the differential pressure, [bar]
ρ_{skin} is the denisty of the skin material, [kg/m^3]
σ_{skin} is the allowable working hoop tensile stress, [N/m^2]

Aft weight

The weight of the aft of the fuselage is determined by the previously sized outer skin. Since the aft fuselage is not loaded by pressurization it is assumed that the skin thickness is equal to the minimum gauge thickness, the stringer thickness is equal to the average smeared stringer thickness of the fuselage and the frame thickness is equal to the smeared average frame thickness of the fuselage.

$$W_{\text{aft}} = S_{\text{aft}} t_{\text{aft}} \rho_{\text{skin}} \quad [\text{kg}] \tag{5-2}$$

where
S_{aft} is the wetted area of the aft fuselage outer surface ρ_{skin} is the density of the skin material and

$$t_{\text{aft}} = \bar{t}_{\text{stringer,avg}} + \bar{t}_{\text{frame,avg}} + t_{\text{gauge}} \tag{5-3}$$

with
$\bar{t}_{\text{stringer,avg}}$ is the average smeared stringer thickness, [m]
$\bar{t}_{\text{frame,avg}}$ is the average smeared frame thickness, [m]
t_{gauge} is the average smeared gauge thickness, [m]

Crew floor

The weight of the crew floor is determined from Howe [46]

$$W_{\text{crewfloor}} = (7 + 1.2 B_{\text{nose}}) S_{\text{crewfloor}} \ [\text{kg}] \tag{5-4}$$

where
B is the width of the nose, [m]
$S_{\text{crewfloor}}$ is the surface are of the floor, [m^2]

Windows

A weight penalty associated with the placement of windows is found in Howe [46].

$$W_{\text{windows}} = 90 S_{\text{windows}} \Delta p \quad [\text{kg}] \tag{5-5}$$

where
S_{windows} is the area covered by the windows, [m^2]

Δp is the differential pressure, [bar]

Based on the Boeing 787 Dreamliner, the size of the windows is estimated to be 0.24 m by 0.37 m. The surface area covered by the windows is determined by the number of windows multiplied by the area of a single window.

$$S_{\text{windows}} = N_{\text{windows}} \times 0.24 \times 0.37 \quad [\text{m}^2] \tag{5-6}$$

where
N_{windows} is the number of windows
The number of windows is in the Initiator for a generic aircraft is determined by dividing the length available for the placement of windows by the window spacing. The default setting for this is equal to the frame spacing of 0.5 m. Since the wall and the outer skin should both have windows, there is an option in the method to double the amount of window cutouts.

Doors

A weight penalty associated with the placement of passenger doors is found in Howe [46].

$$W_{\text{doors}} = 60 S_{\text{doors}} \quad [\text{kg}] \tag{5-7}$$

Based on the Airbus A340-600 on average a door is 1.93 m by 1.07. The surface area is determined by multiplying the number of doors by the surface area of a single door.

$$S_{\text{doors}} = N_{\text{doors}} \times 1.93 \times 1.07 \quad [\text{m}^2] \tag{5-8}$$

N_{doors} is the number of doors

The number of doors is in the Initiator for a generic aircraft is determined by relating the surface area of the cabin to the number of doors. The number of doors per unit area of the cabin of the Airbus A380-800 is used. This ratio is 37.9 m^2 cabin area per door.

Cargo doors

A weight penalty associated with the placement of cargo doors is found in Howe [46].

$$W_{\text{cargodoor}} = 10\,(1 + 0.75 B_{\text{cargofloor}})\, S_{\text{cargodoor}} \quad [\text{kg}] \tag{5-9}$$

where $B_{\text{cargofloor}}$ is the average width of the cargo floor, [m]

$$S_{\text{cargodoor}} = 3.0 \cdot N_{\text{cargodoor}} \quad [\text{m}^2] \tag{5-10}$$

The number of cargo doors is determined from the number of cargo bays that are present in the fuselage. Two cargo doors are taken into account per cargo bay. The surface area of the cargo is determined from the size of an unit load device with a margin on all sides of 10% for the loading of these devices. If no unit load devices are used in the cargo bay, but the aircraft has a bulk cargo area, then the height of the cargo bay and the width of 1.6 m is used for the size of the cargo door.

Cargo floor

A weight of the cargo floor is determined from a empirical relation from Howe [46].

$$W_{\text{cargofl}} = 2.6\,(1 + 0.6B_{\text{cargofl}})\,S_{\text{cargofl}}\rho_{\text{cargofl}} \cdot 10^{-3} \quad [\text{kg}] \tag{5-11}$$

where
B_{cargofl} is the average width of the cargo floor, [m]
S_{cargofl} is the cargo floor area, [m^2]
ρ_{cargofl} is the density of the structural material used for the construction of the cargo floor, [kg/m^3]

5-2 Non-structural weight

The non-structural weight include the weight of a weather radar, the windscreen of the cockpit, the cockpit furnishing, paint of the outer shell and an APU.

Weather radar

The weight of the weather radar is adapted from Vos et al. [47] which is bases on a Honeywell Primus 880.

$$W_{\text{radar}} = 20 \quad [\text{kg}] \tag{5-12}$$

Windscreen

The weight of the windscreen is determined from an empirical relation from Howe [46].

$$W_{\text{screen}} = 0.75 S_{\text{ws}} V_d \left(p \cdot 10^{-5}\right) \quad [\text{kg}] \tag{5-13}$$

where
S_{ws} is the area of the wind screen, this is estimated to be approximately 2 m^2 for transport aircraft, [m^2]
V_d is the design diving speed, [m/s]

Cockpit furnishing

The weight of the cockpit furnishing includes the seats for 2 pilots, 1 engineer and 3 fold away seats. This is adapted from Vos et al. [47].

$$W_{\text{cf}} = 200 \quad [\text{kg}] \tag{5-14}$$

Paint

The weight of the pain is estimated to be a factor of the fuselage wetted area, S_{OML}. Vos et al. [47] estimated the weight of the paint to be 0.3 kg/m^2.

$$W_{\text{paint}} = 0.3 S_{\text{OML}} \quad [\text{kg}] \tag{5-15}$$

Auxiliary power unit

The installed weight of an APU is found by Vos et al. to be 2.25 times the dry weight of an APU. The APU of the Airbus A380-800 is chosen as a reference. This APU, the Pratt & Whitney PW980, weighs 417 kg.

$$W_{\text{APU}} = 2.25 \cdot \cdot 417 \quad [\text{kg}] \tag{5-16}$$

5-3 Center of gravity

The center of gravity of the empty fuselage is determined directly from the geometry. It is assumed that the weight is evenly distributed by the planform of the fuselage. Although the weight varies per section, in general the largest mass per projected unit area is situated at the center and therefore this assumption is reasonable.

Chapter 6

Implementation

The fuselage weight estimation is integrated into the Initiator framework of the Delft University of Technology. It is part of the "Class 2.5 Weight Estimation" module which consists of a physics based wing weight estimation tool, called "EMWET" and the physics based "Fuselage weight estimation" presented in this thesis. The author's contribution to the Universal Initiator consists of the "Fuselage weight estimation", "Cabin design", "AVL VLM", "Class 2 weight estimation" and "Class 2.5 weight estimation" module.

This code report consists of a model overview in section 6-1, a user manual in section 6-2 and an explanation of warning and error messages in section 6-3.

6-1 Model overview

The current Universal Initiator has the ability to generate an aircraft from top level requirements and determine aircraft characteristics from a given aircraft design. These features can be used for the optimization of different aircraft configurations to give new insights into the design of unconventional aircraft configurations. When the user requires the generation of an aircraft using only top level requirements and an aircraft configuration the flow of activities is given by Figure 6-1. At the start of the program an aircraft input file and a settings file are fed into the program. A geometry estimation, preliminary sizing and control allocation is performed. The geometry of the aircraft is known after this point.

The next steps in the activity diagram is the "Cabin design" module. This module determines the unit load device which yields the highest packing density and largest cargo volume, the allocation of unit load devices in the cargo bay, the passenger capacity and the number of windows and doors on the fuselage. An activity diagram of this module is shown in Figure 6-2.

Using the aircraft geometry and the results from the cabin analysis the weight estimation can be improved using the "Class 2 weight estimation" module. The weight and lift generated by each aircraft component is obtained from the results of this module and from the "AVL VLM" module. This information, together with the results from the "Cabin design" module

is used for the "Fuselage weight estimation" and "EMWET" module in the "Class 2.5 weight estimation". This weight estimation is iterated until convergence has reached. An activity diagram of this module is shown in Figure 6-3. The last step after the "Class 2.5 weight estimation" is the performance estimation. When this module is completed, the program stops.

An overview of the classes, their properties and their methods are shown in Figure 6-8.

Focusing on the "Fuselage weight estimation" module, three distinct parts can be identified:

Loads
This part of the model determines the loads acting on the structural members due to longitudinal bending, pressurization and if applicable, lateral tension and compression due to wing bending. An activity diagram of this part is shown in Figure 6-5.

Sizing
This part of the model determines the thickness and shape of the structural members.An activity diagram of this part is shown in Figure 6-6 and an activity diagram of the sizing of the skin in particular is shown in Figure 6-7.

Weight
This part of the model determines the weight of the fuselage using the structural sizing, the additional weight and the non-structural weight.

6-1-1 Cabin design

The cabin design determines the passenger capacity from a given density of the passengers per unit area. The number of windows are determined from the frame spacing and the distance along the fuselage where windows can be placed at eye sight height. The cabin design determines the unit load device that results in the highest packing efficiency and cargo volume. When no unit load device fits in the cargo bay a bulk bay is used. The height of the bulk bay is determined using a rectangular cargo volume fitting function. This neglects any corners that could normally be used for a bulk cargo bay.

6-2 User manual

Although the "Fuselage weight estimation", "Cabin design" and " module is integrated into the Initiator framework. Manual input files can be used as input for the module.

6-2-1 Input

The input of the modules is written in the Extensible Markup Language (XML). Example input for the "Fuselage", "Material" and "Container" objects are shown below. Input examples of the "Cabin design", "Fuselage weight estimation", "AVL VLM", "Class 2 weight estimation" and "Class 2.5 weight estimation" are not given since these modules require the complete aircraft input file.

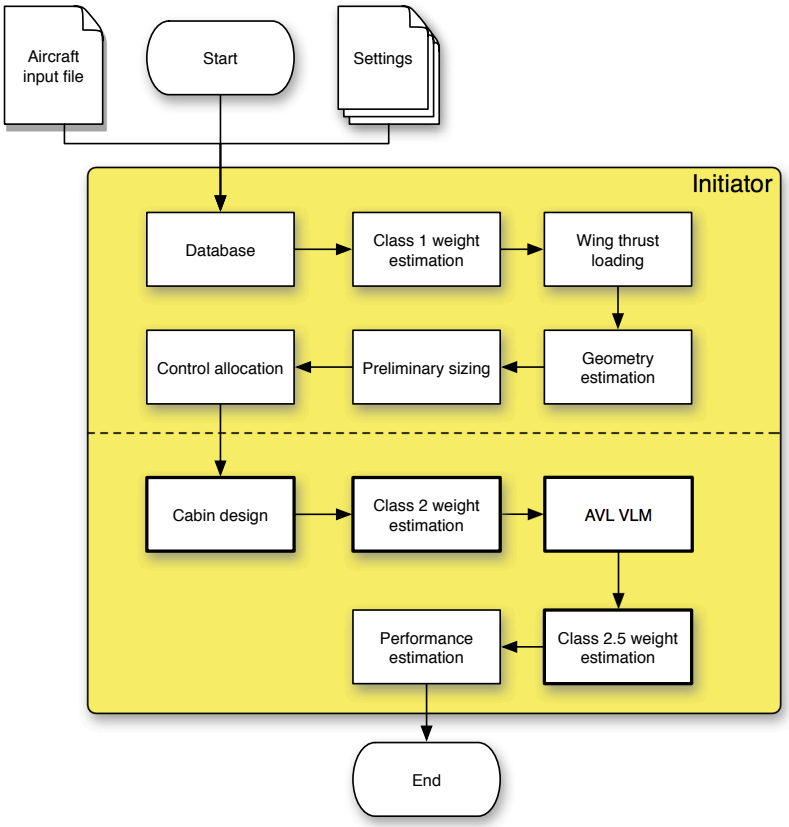

Figure 6-1: Overview of the current Universal Initiator

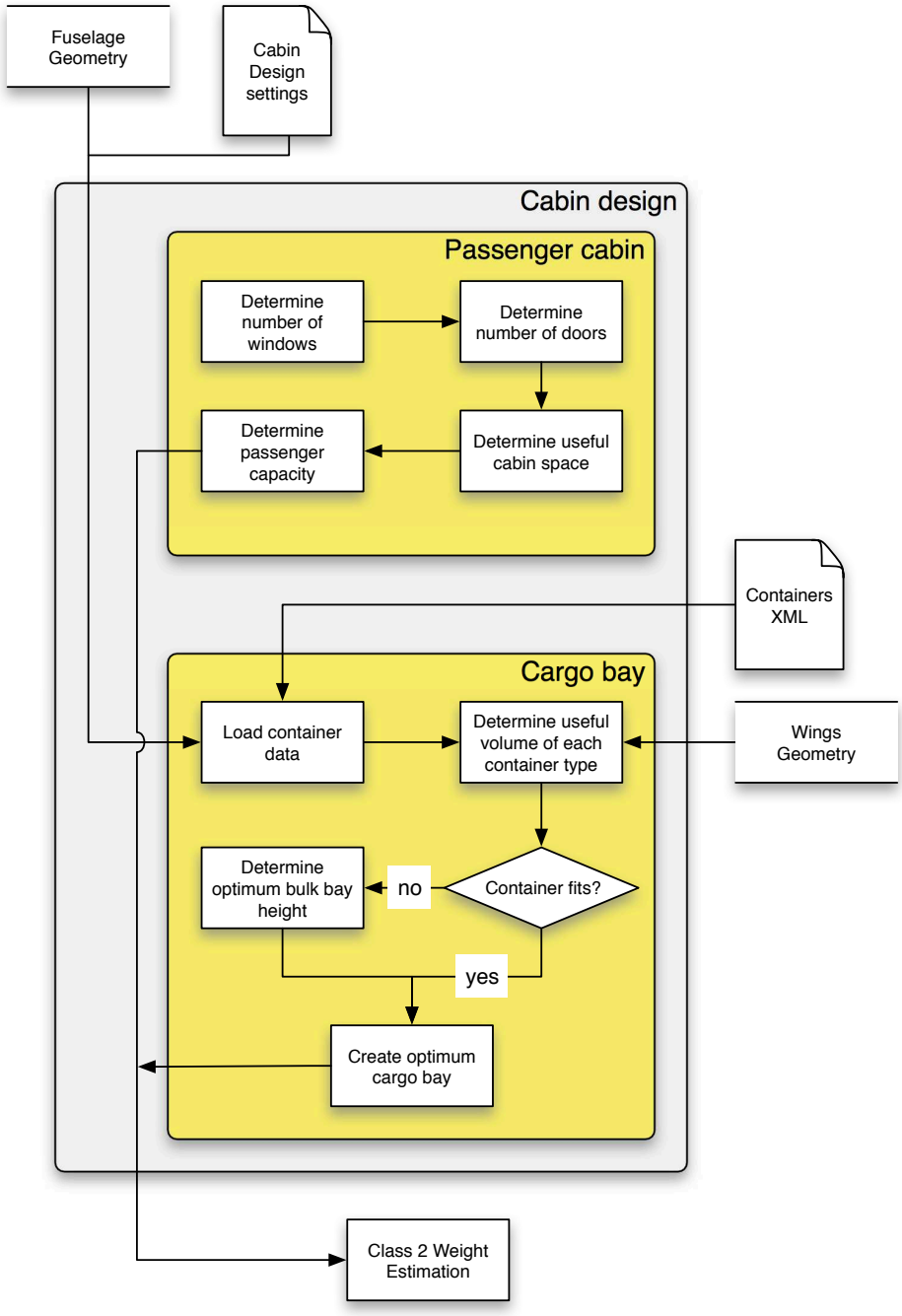

Figure 6-2: Activity diagram of the "Cabin design" module

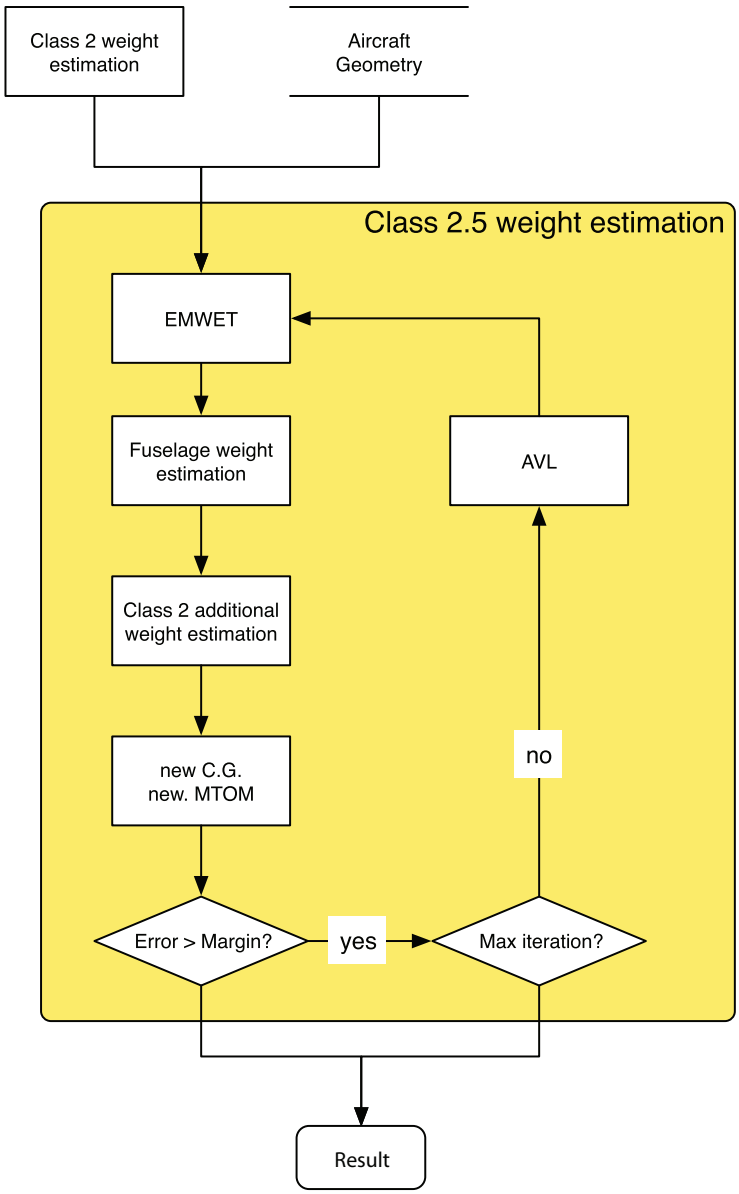

Figure 6-3: Activity diagram of the "Class 2.5 weight estimation" module

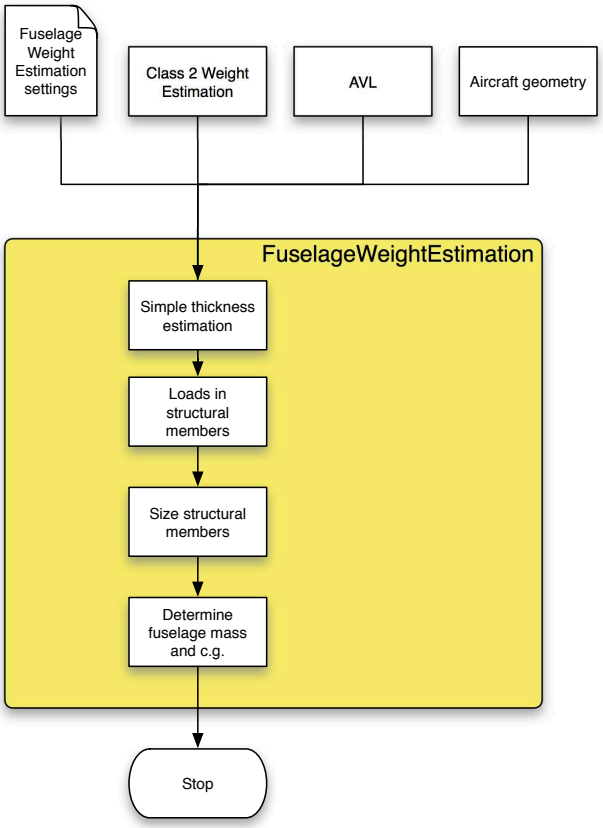

Figure 6-4: Activity diagram of the "Fuselage weight estimation" module

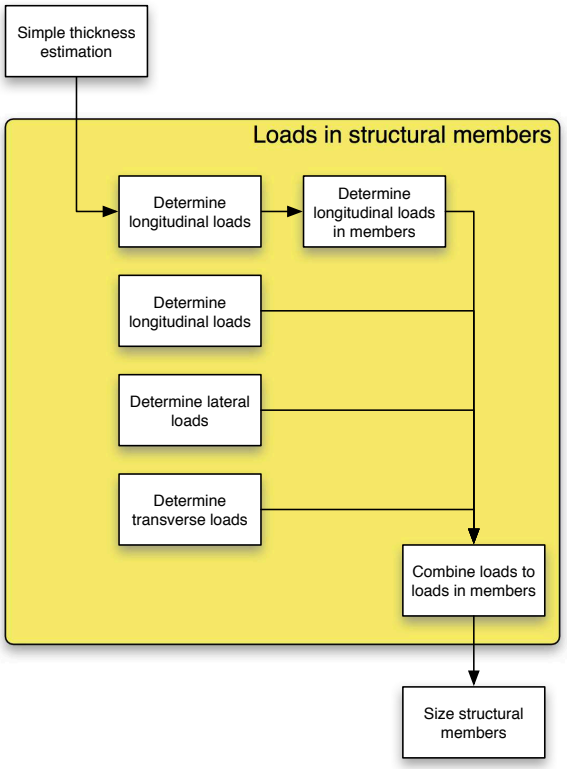

Figure 6-5: Activity diagram of the loads part of the "Fuselage weight estimation" module

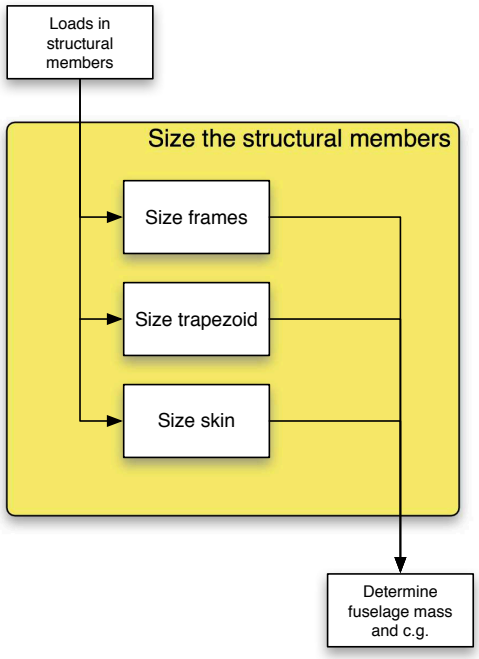

Figure 6-6: Activity diagram of the sizing part of the "Fuselage weight estimation" module

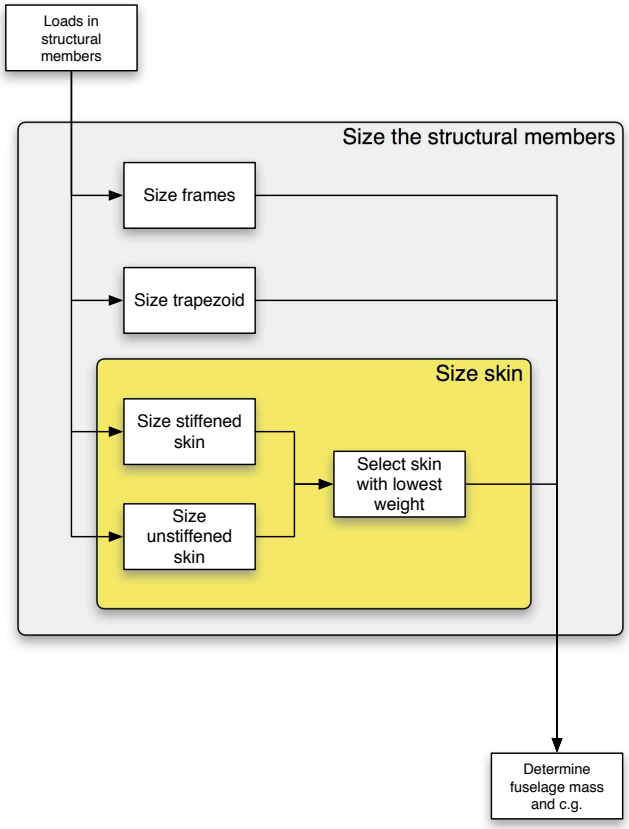

Figure 6-7: Activity diagram of the sizing of the skin in the "Fuselage weight estimation" module

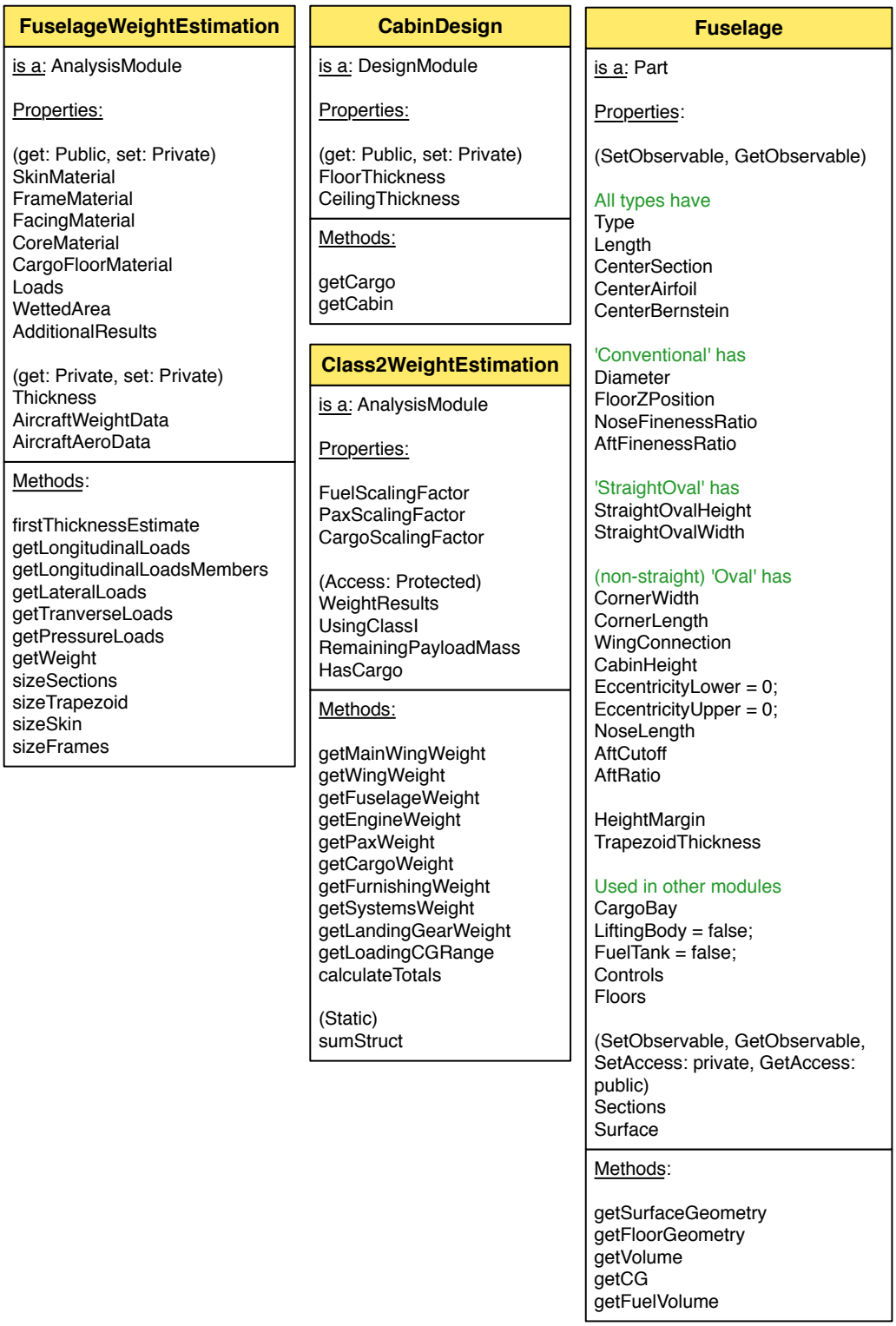

Figure 6-8: Class diagram of the Fuselage, Class 2 Weight Estimation, Fuselage weight estimation and Cabin Design

Fuselage

The input of the "Fuselage" module is very flexible. Three types of fuselages can be modeled:

1. A constant circular fuselage, often called a conventional tubular fuselage. This fuselage is defined by its length and its diameter.
2. A constant oval fuselage, similar to the conventional tubular fuselage although this fuselage can be wider or narrower than its height making it an oval.
3. A oval fuselage. This fuselage can have many shapes, from a twin deck fuselage which is narrower than its height to a blended wing body lifting fuselage which is wider than its height.

Internally these three fuselages are all converted to the parametrization of the oval fuselage. An conventional fuselage is easily modeled using the *length* and *diameter* properties. When an additional property is missing, for example the *NoseLength* is not given as input, the program will use the *DefaultNoseLength* specified in the settings file.

The *CenterSection* is a parametrized shape similar to the shape of a conventional fuselage at the center line of the fuselage. It features a tubular shape where the nose of the fuselage that is drooped down and an aft of the fuselage is swept up. The vector contains five variables. These variables are:

NoseFinenessRatio
: The ratio between the fuselage nose length and the height of the fuselage section

AftFinenessRatio
: The ratio between the fuselage aft length measured from the nose and the height of the fuselage section

Diameter
: The height of the fuselage section

NoseDroop
: The distance of the fuselage nose and the center of the shape divided by the height of the fuselage section.

AftDroop
: The distance of the fuselage top and the center of the shape divided by the height of the fuselage section.

```
1 <fuselage name="Fuselage" type="Conventional">
2   <length>73.08</length>
3   <diameter>6.19</diameter>
4   <NoseLength>6.5</NoseLength>
5   <position>
6     <x>0</x>
7     <y>0</y>
8     <z>0</z>
```

```
    </position>
    <orientation>
      <phi>0</phi>
      <theta>0</theta>
      <psi>0</psi>
    </orientation>
</fuselage>
```

An example of a straight oval fuselage is given below.

```
<fuselage name="Fuselage" type="StraightOval">
    <aftCutoff>0.9</aftCutoff>
    <aftFinenessRatio>0.55</aftFinenessRatio>
    <aftRatio>0.5</aftRatio>
    <cabinHeight>2.7922</cabinHeight>
    <centerSection mapType="vector">0.18;0.45;7.2713;0.15;0.2</
        centerSection>
    <cornerWidth mapType="vector">8.5544;8.5544</cornerWidth>
    <eccentricityLower>0</eccentricityLower>
    <eccentricityUpper>0</eccentricityUpper>
    <floorZPosition>-0.5817</floorZPosition>
    <fuelTank>false</fuelTank>
    <heightMargin>0.2</heightMargin>
    <length>65.0227</length>
    <liftingBody>false</liftingBody>
    <noseFinenessRatio>0.18</noseFinenessRatio>
    <noseLength>6.65</noseLength>
    <orientation>
      <phi>0</phi>
      <psi>0</psi>
      <theta>0</theta>
    </orientation>
    <position>
      <x>0</x>
      <y>0</y>
      <z>0</z>
    </position>
    <straightOvalHeight>7.2713</straightOvalHeight>
    <straightOvalWidth>8.5544</straightOvalWidth>
</fuselage>
```

An example of an oval blended wing body input is given below.

```
<fuselage name="Fuselage" type="Oval">
    <length>40</length>
    <cornerWidth mapType="vector">10;14;14</cornerWidth>
    <cornerLength mapType="vector">0.25</cornerLength>
    <cabinHeight>2.4</cabinHeight>
    <floorZPosition>-1.15</floorZPosition>
    <noseLength>4</noseLength>
    <aftCutoff>0.88</aftCutoff>
    <aftRatio>1</aftRatio>
    <centerSection mapType="vector">0.3;0.35;6;0.15;0.5</centerSection>
    <liftingBody>true</liftingBody>
```

```
12      <position>
13          <x>0</x>
14          <y>0</y>
15          <z>0</z>
16      </position>
17      <orientation>
18          <phi>0</phi>
19          <theta>0</theta>
20          <psi>0</psi>
21      </orientation>
22  </fuselage>
```

Containers

Containers are used in the "Cabin design" module. Currently LD2, LD3, LD3-45 and LD9 are used but any standard container can be added. The nomenclature of the dimensions can be found in Figure 6-9. For containers having two corners at the bottom the boolean *SecondChamfer* can be set to *true*.

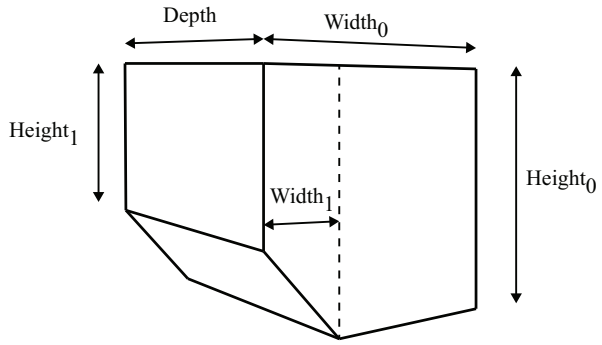

Figure 6-9: The dimensions of the unit load device which are used by the program. Illustration derived from [48].

```
1    <container>
2      <name>LD3</name>
3      <description>LD3 Unit load device</description>
4      <Height0>1.63</Height0>
5      <Height1>1.07</Height1>
6      <Width0>1.98</Width0>
7      <Width1>0.42</Width1>
8      <SecondChamfer>false</SecondChamfer>
9      <Depth>1.53</Depth>
10     <MassFull>1588</MassFull>
11     <MassEmpty>62</MassEmpty>
12     <Volume>4.13</Volume>
13   </container>
```

Materials

Materials are read from the materials.xml file. An example is given below. The fatigue behavior of the material is required. This can be added using two vectors: one vector containing the cycles (fatigueCycles) and one vector containing the strength of the material at the number of cycles (fatigueStrength).

```
1  <material tag="al7075t6bare">
2    <name>Aluminium 7075-T6 Bare</name>
3    <density>2810</density>
4    <poissonRatio>0.33</poissonRatio>
5    <youngModulus>71.7e9</youngModulus>
6    <tensileYieldStrength>505e6</tensileYieldStrength>
7    <tensileUltimateStrength>570e6</tensileUltimateStrength>
8    <compressiveYieldStrength>505e6</compressiveYieldStrength>
9    <shearModulus>26.9e9</shearModulus>
10   <shearStrength>331e6</shearStrength>
11       <fatigueCycles mapType="vector">1e4;5e4;1e5;1e6;1e7</
             fatigueCycles>
12       <fatigueStrength mapType="vector">490.3e6;324.9e6;285.7e6;246.5e6
             ;239.0e6</fatigueStrength>
13 </material>
```

6-2-2 Running the code

The code is started by creating a new Initiator session:

```
1 C = InitiatorController(ovalbwb.xml]);
```

Next the user requests a certain analysis, in this case the "Class 2.5 weight estimation" is requested:

```
1 C.runModule('Class25WeightEstimation');
```

The results can both be retrieved from the ovalbwb.xml file and from the Command Window in the MATLAB Workspace using:

```
1 C.getModuleResult('Class25WeightEstimation');
```

6-2-3 Output

Fuselage

The result of the "Fuselage" module is the geometry of the fuselage. This geometry is given as an ordered set of *Surfaces* and as a set of section parameters. This set of section parameters is the meta data that is used in the "Fuselage weight estimation" module.

Cabin design

The results of the "Cabin design" module contains a structure with the number of windows, number of doors and the number of passengers. Since complex results cannot be written to the XML output, the floor geometry and cargo bay with the location of the unit load devices is written directly to the Fuselage object.

Class 2 weight estimation

The result of "Class 2 weight estimation" module is a standardized aircraft mass structure. The structure consists of a breakdown of the mass per component in the "Parts" variable and a breakdown of specific aircraft masses such as Maximum Take-off Mass, Operative Empty Mass and Fuel Mass in "Total".

AVL VLM

The results of the "AVL VLM" module consist of a structure for each specific simulated flight phase, such as for cruise and for landing. The results of each simulated flight phase contain the aerodynamic coefficients and stability derivatives of the aircraft. The local and sectional aerodynamic coefficients of each individual surface is written to its own structure. The control deflections that are required for the aircraft to trim itself are also written to the results in the *Trim* structure.

Fuselage weight estimation

The results of the "Fuselage weight estimation" module is a structure containing the center of gravity of the fuselage, the mass of the fuselage and a mass breakdown containing all the components of the fuselage. Additional results such as the specific height of the frames and the geometry of the optimized stiffened panel can be accessed in the *AdditionalResults* property of the module object.

Class 2.5 weight estimation

The results of the "Class 2.5 weight estimation" module is similar to the "Class 2 weight estimation" module. The only difference is that the "Fuselage weight estimation" and the "EMWET" module are used for the calculation of the fuselage mass and wing mass respectively.

6-3 Explanation of messages

The program is able to warn the user during execution of the application. These messages are shown in the Command Window. This section gives an overview of the possible warnings and their meaning.

6-3-1 Fuselage

Unkown floor
The requested floor is not present. The available floors are "top", "center" and "bottom".

Unknown fuselage type: ...
The requested fuselage type is not known by the Fuselage module.

Unkown direction
The requested direction of the projection of the fuselage outerpoints is not known. Possible directions are "top" and "side".

FloorZPosition must be between +(fuselage radius) and -(fuselage radius)
The position of the cabin floor in z-direction must be between the top and the bottom of the fuselage outer mold line. The user is only warned when an conventional fuselage is used since other types do not have a clear definition of the fuselage outer mold line at this stage of the program.

Multiple (CenterSection / CenterBernstein / CenterAirfoil) defined
The input of the fuselage is ambiguous. This is solved by making sure the input contains only one the possible definitions of the center profile of the fuselage.

No (CenterSection / CenterBernstein / CenterAirfoil) defined
No center profile input is given. Please specify either a CenterSection, CenterBernstein or CenterAirfoil in the input file.

... is not a property of the Fuselage object
One of the required properties is incorrectly defined in the object and the toOval code.

... is missing for the generation of the Fuselage object
One of the required properties is incorrectly defined in the input file.

Unable to generate fuselage
A check failed during the generation of the fuselage. The shape is not properly defined using the current parametrization.

6-3-2 Cabin design

Using test container for debugging
The program is running in debug mode and warns the user that not all types of unit load devices are evaluated.

6-3-3 Class 2 weight estimation

Required CargoMass does not fit
The required cargo mass is larger than the current cargo capacity of the cargo bays.

Required mission fuel is larger than the capacity of the fuel tanks
The required mission fuel mass is higher than the current capacity of the fuel tanks.

Required Pax does not fit in cabin
The required passenger capacity is larger than the current passenger capacity.

Unkown wing type
The wing type is not supported for the calculation of the wing weight.

6-3-4 AVL VLM

AVL not available on this machine
The AVL program is not installed on the current machine. The program is available on the web [30].

No method to create AVL input for ...
No method is defined for the geometry modeling of the indicated part in AVL.

6-3-5 Fuselage weight estimation

Using fuselage as carry-through structure for ...
The fuselage trapezoid structure is used as a carry-through structure for the MainWing part appended in the message. The program is telling the user that it is using the mass and aerodynamic loads from this wing in the sizing of the trapezoid structure.

Mid-wing is too thin to carry-through cabin floor and cabin ceiling structure
If the mid-wing should be connected to the fuselage for carry-through purposes, the wing root should increase in thickness.

Names of parts are not unique
The names of the parts is not unique. This is a requirement for the program to function properly.

Do not know to which part ... is connected
A wing, connector, engine or landing gear has not a known part or no part at all set as its connected part.

Mass contribution by ... is ignored
The mass of the indicated part is ignored in the determination of the longitudinal loads acting on the fuselage.

Not compatible with a fuel tank in ... part
Method is not compatible with a fuel tank in the indicated part. Currently the fuselage has the option of a fuel tank, however this is not yet build into the initiator.

Do not know in which part the fuel tank is located
A fuel tank is sized in a previous weight estimation method, but this is not supported in the current weigh estimation method.

Not compatible with cargo bay in ...
Method is not compatible with a cargo bay in the indicated part. Currently the wing has the property to contain a cargo bay, however this is not yet build into the initiator.

Not compatible with multiple fuselages
The program found multiple fuselages and warns the user that the method is limited to the analysis of aircraft with only a single fuselage.

Difference in furnishing mass
A difference has been found in the furnishing mass calculated from the distributed longitudinal load and the furnishing mass from the obtained weight data.

...% difference from ... part mass
The calculated mass of the indicated part differs from the mass given by the obtained weight data.

...% mass difference from weight estimation for ... component
The mass of the indicated aircraft component that is calculated from the weight distributions along the fuselage longitudinal axis differs from the obtained weight data of the component. The warning originates from the conversion from mass to mass distribution.

...% CG difference from weight estimation for ... component
The center of gravity of the indicated aircraft component that is calculated from the weight distributions along the fuselage longitudinal axis differs from the obtained weight data of the component. The warning originates from the conversion from mass to mass distribution.

...% CG difference from weight estimation for total CG
The center of gravity calculated using the weight distributions differs from the center of gravity from the weight data.

...% difference from total MTOM
The total mass of the distributed masses differs from the Maximum Take-off Mass.

A deviation between the cruise lift and the aircraft weight is found: ...%
The lift and weight are different. A deviation of 2% is possible due to rounding errors in the results from AVL.

Difference in mass section moment calculation in ...
A difference in moment induced by the distributed mass and by the point mass is found.

Difference in lift section moment calculation in ...
A difference in moment induced by the distributed lift and by the lift vector is found.

Bending moment during cruise is not zero at end of fuselage
The longitudinal bending distribution during cruise is not zero at the end of the fuselage. This is caused by the summation of one of the errors in a mass distribution or lift distribution.

Bending moment during landing is not zero at end of fuselage
The longitudinal bending distribution during landing is not zero at the end of the fuselage. This is caused by the summation of one of the errors in a mass distribution or lift distribution.

Only tripod landing gears are supported, landing load case set to zero
The tripod landing gear condition is true when two main gear have the same x-position and a nose gear is present.

Caution, cylindrical buckling criteria not tested for this ratio, ... > 1500
The cylindrical buckling criteria uses a correlation factor to correlate the theoretical values to experimental values, taking imperfections into account. The experimental data is only valid up to radius to thickness ratio's smaller than 1500.

BoxWing is not supported in Mid-Wing configuration
The user requests the fuselage weight of an aircraft with a box wing attached to the center of the fuselage. However this is not supported by the method.

Number of width must be defined in the switch
The defined stiffener-type is not fully supported in the skin sizing.

Requires w to have a vector length of ... for ...-stiffener
The defined stiffener-type is not fully supported in the skin sizing.

6-3-6 Class 2.5 weight estimation

Converged
The program is running in debug mode and warns the user that not all types of unit load devices are evaluated.

Not converged
The module has not found convergence between the current iteration and the previous three iterations that is within the allowable tolerance and within the given allowable number of iterations. Increase the maximum number of iterations or increase the allowable tolerance.

Part II

Verification and case studies

Chapter 7

Verification

Now that the weight estimation theory and the programmed computer model are discussed, insights can be obtained from this model that describe the weight characteristics of oval fuselages. This section attempts to give these insights. To quantify the quality, accuracy and efficiency of the method several aspects of the method are verified. By verifying the method on multiple components confidence can be gained in the estimation of state of the art oval fuselages without the need of an actual oval fuselage.

First the estimation of forces acting on the trapezoidal structure, discussed in Section 3-2, is verified from a theoretical approach and a finite element analysis. Next convergence of the computer model is discussed along with ways to improve calculation efficiency of the computer model. While there are no existing oval fuselages, a number of aircraft is found of which the fuselage weight is known. These are used to verify the weight estimation. Finally a number of cases are considered where the oval fuselage is incorporated in aircraft design.

7-1 Trapezoidal structure

It was shown in Equation 3-9 that the forces acting on the trapezoidal structure can be determined using force equilibrium. However this force equilibrium neglects the interaction between the dilated outer skin and the flexible trapezoidal structure. To explain this effect consider the case of a circular fuselage section of unit length with radius R and thickness t_{sk} and a horizontal with a floor at its center with length $2R$ and thickness t_{fl}, Figure 7-1.

The passenger floor is unloaded up to pressurization. When pressurized a force is exerted the floor caused by the dilation of the outer shell. The force is determined by modeling their behavior as springs, Figure 7-2. Equating force equilibrium about point N gives,

$$F_{\mathrm{sk}} + F_{\mathrm{fl}} = 0 \tag{7-1}$$

$$k_{\mathrm{sk}} \left(\delta_{\mathrm{p}} - \delta_{\mathrm{n}}\right) - k_{\mathrm{fl}} \delta_{\mathrm{n}} = 0 \tag{7-2}$$

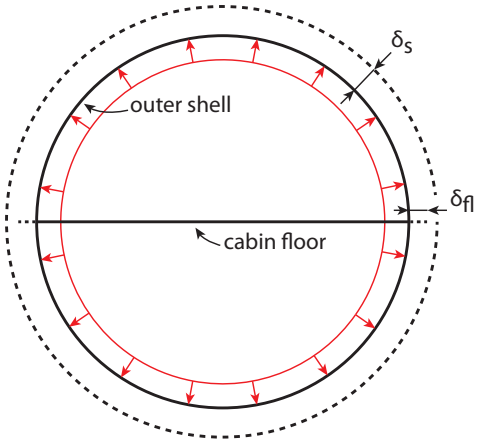

Figure 7-1: A circular cross-section with a cabin floor

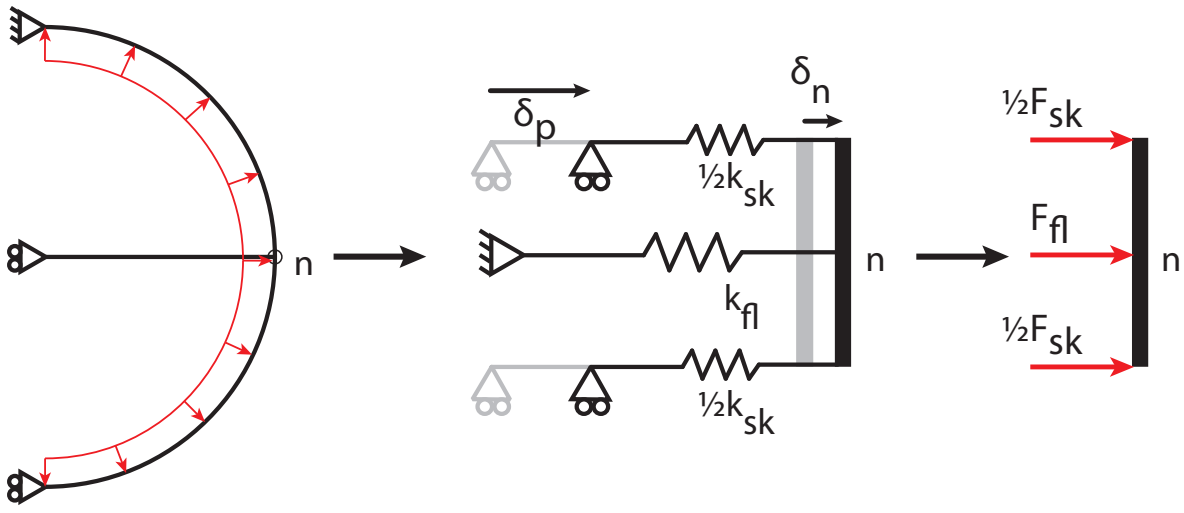

Figure 7-2: The circular cross-section with a cabin floor as a spring system

where F is the force acting on point N, k the spring stiffness and δ the displacement. The subscripts "sk" and "fl" refer to the skin and the floor respectively. Solving Equation 7-1 for δ_{n} results in

$$\delta_{\mathrm{n}} = \delta_{\mathrm{sk}} \frac{k_{\mathrm{sk}}}{k_{\mathrm{sk}} + k_{\mathrm{fl}}} \tag{7-3}$$

where the dilation of a pressurized thin-walled cylinder is found by Fryer [25] to be

$$\delta_{\mathrm{p}} = \frac{pR^2}{2t_{\mathrm{sk}}E_{\mathrm{sk}}} \left(2 - \nu_{\mathrm{sk}}\right), \tag{7-4}$$

the spring stiffness of the shell is found by Timoshenko [49] to be

$$k_{\mathrm{sk}} = \frac{(EI)_{\mathrm{sk}}}{0.139R^3} = \frac{E_{\mathrm{sk}}t_{\mathrm{sk}}^3}{12 \cdot 0.139R^3} \tag{7-5}$$

and

$$k_{\mathrm{fl}} = \frac{(EA)_{\mathrm{fl}}}{R} = \frac{E_{\mathrm{fl}}t_{\mathrm{fl}}}{R}. \tag{7-6}$$

The force on the cabin floor is then calculated from

$$F_{\mathrm{fl}} = k_{\mathrm{fl}}\delta_{\mathrm{n}}. \tag{7-7}$$

Now substituting common values gives the magnitude of force exerted on the floor by the pressure acting on the outer shell. Consider a fuselage section with radius $R = 3$ m, floor and outer shell thickness $t_{\mathrm{sk}} = t_{\mathrm{fl}} = 3$ mm made out of aluminum with a Young's modulus of $E_{\mathrm{fl}} = E_{\mathrm{sk}} = 73$ GPa and a Poisson's ratio $\nu = 0.33$. When pressurized up to a differential pressure $p = 1.2$ bar the dilation, spring stiffnesses and deflection of point N become

$$\delta_{\mathrm{p}} = \frac{\left(1.2 \cdot 10^5\right) 3^2}{2\left(3 \cdot 10^{-3}\right) 73 \cdot 10^9} \left(2 - 0.33\right) = 4.12 \text{ mm}, \tag{7-8}$$

$$k_{\mathrm{sk}} = \frac{73 \cdot 10^9 \left(3 \cdot 10^{-3}\right)^3}{(12)0.139 \cdot 3^3} = 131.30 \text{ N/m}, \tag{7-9}$$

$$k_{\mathrm{fl}} = \frac{73 \cdot 10^9 \left(3 \cdot 10^{-3}\right)}{3} = 18.25 \cdot 10^6 \text{ N/m} \tag{7-10}$$

and

$$\delta_{\mathrm{n}} = 4.2 \cdot 10^{-3} \frac{131.30}{131.30 + 18.25 \cdot 10^6} = 3.0217 \cdot 10^{-5} \text{ mm} \tag{7-11}$$

The force in the floor is then determined as

$$F_{\mathrm{fl}} = 18.25 \cdot 10^6 \cdot 3.0217 \cdot 10^{-5} = 0.5515 \text{ N}. \tag{7-12}$$

For this case the force exerted on the floor is negligible. The floor behaves as a very stiff structure causing the more flexible outer shell to take the dilation in bending.

Now as the floor is placed away from the neutral axis the stiffness of the outer shell in the direction of the cabin floor will increase since it loaded portion will behave more like a strut. To verify that also this effect is negligible a finite element analysis (FEA) is performed on

	Estimated stress [MPa]	FEA nodal stress [MPa]			
		Minimum	%	Maximum	%
Top arc	168.23	167.11	-0.7	169.62	0.8
Side arc	60.64	60.44	-0.3	61.40	1.3
Bottom arc	144.50	143.86	-0.4	145.05	0.4
Ceiling	-72.34	-72.22	-0.2	-72.22	0.2
Wall	70.31	70.07	-0.3	70.26	-0.1
Floor	-56.39	-56.33	-0.1	-56.33	0.1

Table 7-1: Comparison of finite element method with theoretical values

a oval fuselage section with h_1= 1 m, h_2 = 2 m, h_3 = 1.6 m and w = 3 m with structural elements of 3 mm thickness. Similar material is used with a Young's modulus of 73 GPa and Poisson's ratio of 0.33. The fuselage is loaded with a differential pressure of 1.2 bar. The results from the finite element analysis are compared with the estimation from Chapter 4 in Table 7-1 and a stress distribution is shown in Figure 7-3. It can be seen that the finite element values are very close to the estimated values. The neglected effect of dilation results in neglecting bending stresses in the outer shell and a small force in the trapezoid structure. For the present conceptual analysis this is an acceptable difference.

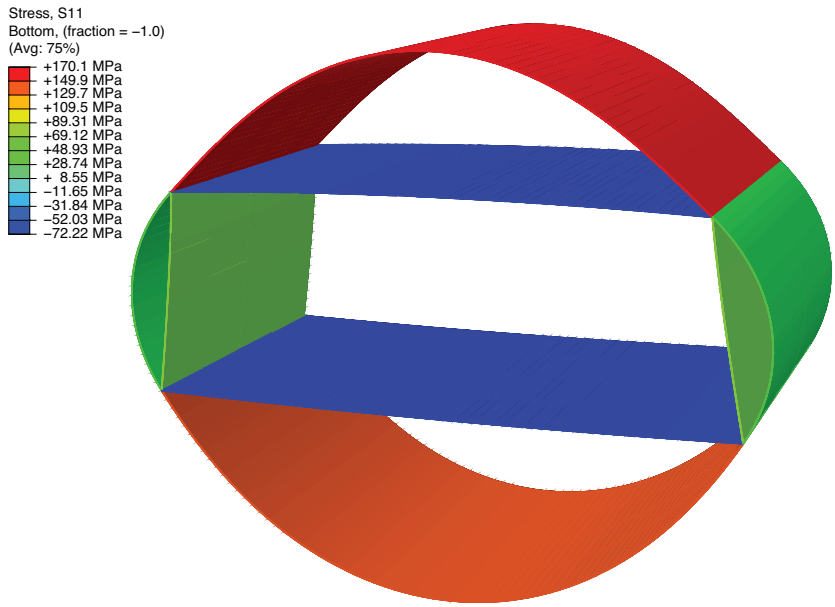

Figure 7-3: Finite element analysis of a pressurized oval fuselage showing the principal stress in the section (p = 1.2 bar)

7-2 Convergence

The fuselage weight estimation discretizes the continuous fuselage structure and sizes each section independent of one another. While the discretization simplifies the problem, it also has an influence on the accuracy of the estimation. This influence is determined for both

a circular fuselage and a lifting oval fuselage. By dividing a fuselage in various numbers of sections and comparing its weight this effect can be investigated. This is done for a circular fuselage as well as an oval fuselage.

Figure 7-4 shows the normalized fuselage weight for different numbers of fuselage sections of a circular fuselage with a length of 68 meter and a diameter of 7 meter. The circular fuselage weight is normalized by converged value of 100 sections. Figure 7-5 shows a similar graph for a lifting oval fuselage with a width of 14 meter and a length of 40 meter. The oval fuselage weight is normalized by the converged value of 214 sections. Note that the two figures show two kinds of convergence: (1) over the vertical axis the convergence is seen of one estimation iterating through the Class 2.5 aircraft weight estimation and (2) the convergence of the final fuselage weight from the Class 2.5 aircraft weight estimation as a function of the number of sections. First focusing only on the final fuselage weight (the red markers), it can be seen

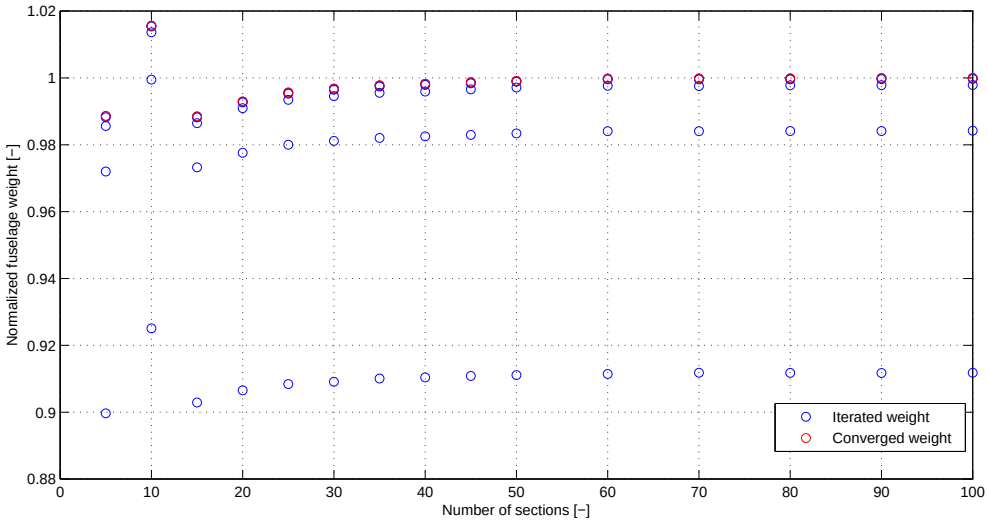

Figure 7-4: The effect of the number of sections used to estimate the weight of a circular fuselage.

that for circular fuselages a discretization of only five sections results in a weight that lies within 2% of the converged weight as a function of the sections. A finer discretization of 15 sections and more reduces this difference to less than 1%. For oval fuselages it can be seen that relatively more sections are required to obtain a result comparable to the circular fuselage. Now focusing on the iterated fuselage weight (blue markers), it can be seen that the trend is similar to the final fuselage weight. These two figures also clearly underline the importance of the iteration of both fuselage and wing weight estimation methods since an error between first and last iteration of 9% and 3% are found for the circular and oval fuselage respectively. For the following weight estimation cases 20 sections are used for the circular fuselage weight estimation and 50 are used for the oval fuselage weight estimation. This means that the precision of the weight is about 1% and 2% for circular fuselage and oval fuselage respectively.

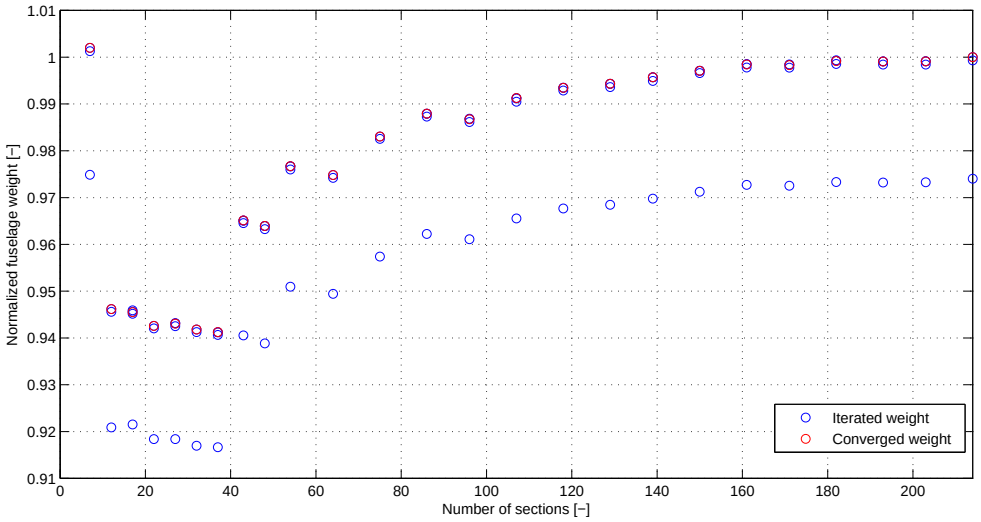

Figure 7-5: The effect of the number of sections used to estimate the weight of a lifting oval fuselage.

7-3 Calculation time

The fuselage weight estimation involves a number of optimization problems which are solved numerically. As described in Chapter 4 this is done for each structural member of each fuselage section (stiffened skin and trapezoidal structure). The optimization of the stiffened skin is the computationally most expensive calculation of these optimization problems. Two ways are found to reduce the computational cost of the sizing of the stiffened skin.

A first modification is the division of the fuselage outer shell sections into barrels. A single barrel spans multiple fuselage shell sections and it is sized for the most critical load case. This can be compared to an aircraft manufacturers design problem where the reduced manufacturing cost of similar parts is traded against higher operational costs. By defining a circular fuselage consisting of 20 sections by 10 barrels reduces the number of evaluations of the optimization problem by half and doubling the number of inequality constraints. This results in a computational cost reduction of 26%.

A second modification is the reduction of the dimensions of the optimization problem. The optimization discussed in Section 4-3-2 involves multiple degrees of freedom. The design space of a Z-stiffener panel spans seven dimensions. This optimization can be simplified by constraining the shape of the stiffener to a single dimension. This reduces the number of dimension in the optimization problem to four namely the skin thickness, stringer thickness, stringer size and stringer pitch. This significantly reduces computational cost of the estimation method. The size of the stiffener is determined from a design of experiments based on 13 reference aircraft, discussed in Section 7-5. The dimensions of the Z-stiffener in Figure 4-11a are defined as a function of the bottom flange w_1 where $w_2 = 2.10w_1$, $w_3 = 0.65w_1$ and $w_4 = 0.26w_1$. It is found that the reducing the optimization problem by three dimensions reduces the computational cost by 17%.

		Aircraft types		
		Conventional	**BWB**	**Cylindrical oval**
Baseline		26.02 $\cdot 10^3$ kg	69.82 $\cdot 10^3$ kg	29.61 $\cdot 10^3$ kg
Number of flights	$5 \cdot 10^4$	-16.58%	-10.50%	-14.76%
	$15 \cdot 10^4$	7.52%	4.48%	6.11%
Stiffener type	hat	0.41%	0.18%	-0.35%
	simplified Z	-0.51%	0.01%	-0.25%
Barrels	20	0.00%	1.21%	0.00%
	10	15.19%	3.38%	9.45%
	5	20.55%	6.52%	19.02%
Frame spacing	1.0 m	-2.50%	-4.02%	-3.40%
	1.5 m	-1.26%	-5.10%	-3.24%
Cabin altitude	+200m	-0.48%	-1.41%	-0.50%
	-200m	0.50%	1.56%	0.30%

Table 7-2: Sensitivity analysis of three aircraft types

7-4 Sensitivity analysis

The proposed method has the ability to provide insights in the effect of the change of any variable used to determine the fuselage weight. An overview of these effects are summed up in a sensitivity analysis. The variables that are varied are the stiffener type, stiffener degrees of freedom, number of barrels, frame spacing, number of flights and cabin altitude. This is done for a conventional aircraft, an aircraft with a BWB aircraft and an aircraft with a oval cylindrical fuselage. The baseline variables consist of the number of flights set to 10^5, Z-stiffeners, no barrels, a frame spacing of 0.5 m and a cabin altitude of 2000 m.

It can be seen in Table 7-2 that the shape of stiffener and and the number of dimensions of the design space, which is reduced in "simplified Z" has little effect on the total fuselage weight. The number of barrels has a great influence on the total weight furthermore it is interesting to see that the effect is larger for tube-wing configurations as is the case for "Conventional" and "Cylindrical oval" than it is for "BWB". This difference could be caused by length effect of the oval fuselage. Figure 7-6 shows a comparison of the longitudinal bending moment distribution of a circular fuselage in a tube-and-wing configuration and an oval fuselage in a BWB. The gradient of the circular fuselage is relatively similar to the oval fuselage. The effect of the subdivision into barrels results in a 30% smaller barrel for the BWB compared to the tube-and-wing aircraft due to the shorter fuselage. The differences in cabin altitude are as expected. The increase in cabin altitude reduces the differential pressure between the cabin and the outside atmosphere reducing pressurization loads and thus reducing weight. The BWB is more sensitive to this change by a factor of three. It can be seen that the method is rather sensitive to changes in frame spacing, although this is not varied in the optimization it might be of interest to include this is future research.

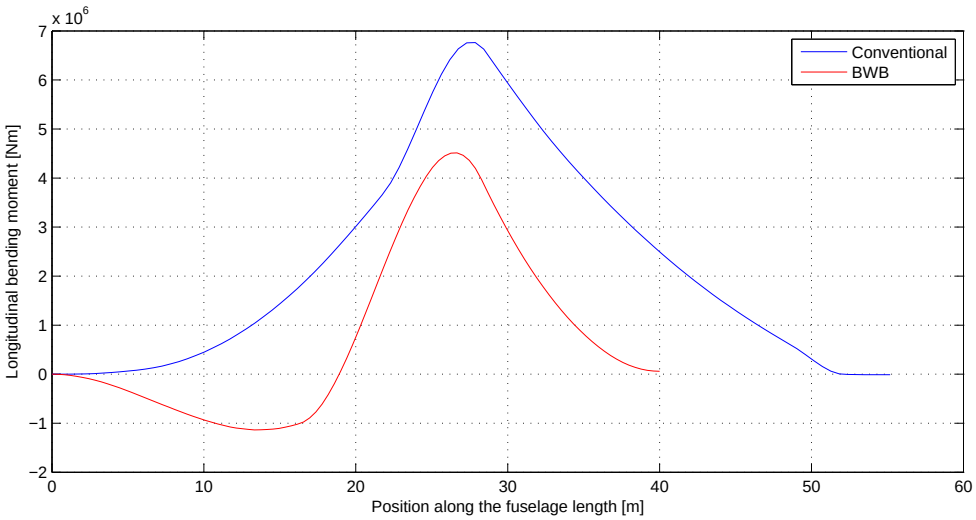

Figure 7-6: Comparison between the longitudinal bending moment distribution of a circular fuselage in a tube-and-wing configuration and an oval fuselage in a BWB

7-5 Conventional fuselages

While the proposed fuselage weight estimation method is specifically developed to estimate the weight of non-circular fuselages in unconventional aircraft configurations. This method can also be used to estimate near-circular fuselages in conventional configurations by slightly adjusting the method. When a cross-section of an oval fuselage, as described in Sec. 2-1, has equal radii, the loads on the trapezoidal inner structure due to pressurization in Eq. 3-9 are zero such that only the transverse distributed load acts on the horizontal members of the trapezoidal inner structure.

In this manner the fuselage weight is compared with actual fuselage weight data [50, 51, 44, 15] and empirical weight estimation methods from open literature [52, 51, 53, 54] of thirteen aircraft. Since little information is available in open literature the aircraft geometry is obtained from three-view drawings and the structural properties are assumed to be equal for all aircraft. The geometry of the aircraft as it is modeled in the Initiator is shown in Appendix E. The skin material used for the estimation of the weight is Alclad 2024-T3. For the trapezoidal sandwich structure Alclad 7075-T6 is used for the face sheets and honeycomb core as core material. The design stress is determined from the S-N for a operational lifetime 100,000 cycles [55], the stiffener shape is a z-stiffener, the frame spacing is fixed at 0.5 m. The cabin altitude is kept at 2000 m during cruise and the cabin differential pressure is kept at 0.11 psi during landing. The load case consists of a load factor of 2.5 and -1.5 during the cruise phase and 2.0 during landing. A safety factor of 1.5 is used on the yielding strength. A distributed transverse load of 17 kN/m is used on the passenger floor [17].

It can be seen from this figure that the proposed method, named Class 2.5 in the graph, at first sight has the same order of accuracy as empirical methods from literature.

It can be seen from Figure 7-7 that the empirical weight estimations themselves show large variations. The proposed method, name Class 2.5, estimates the fuselage weight within the

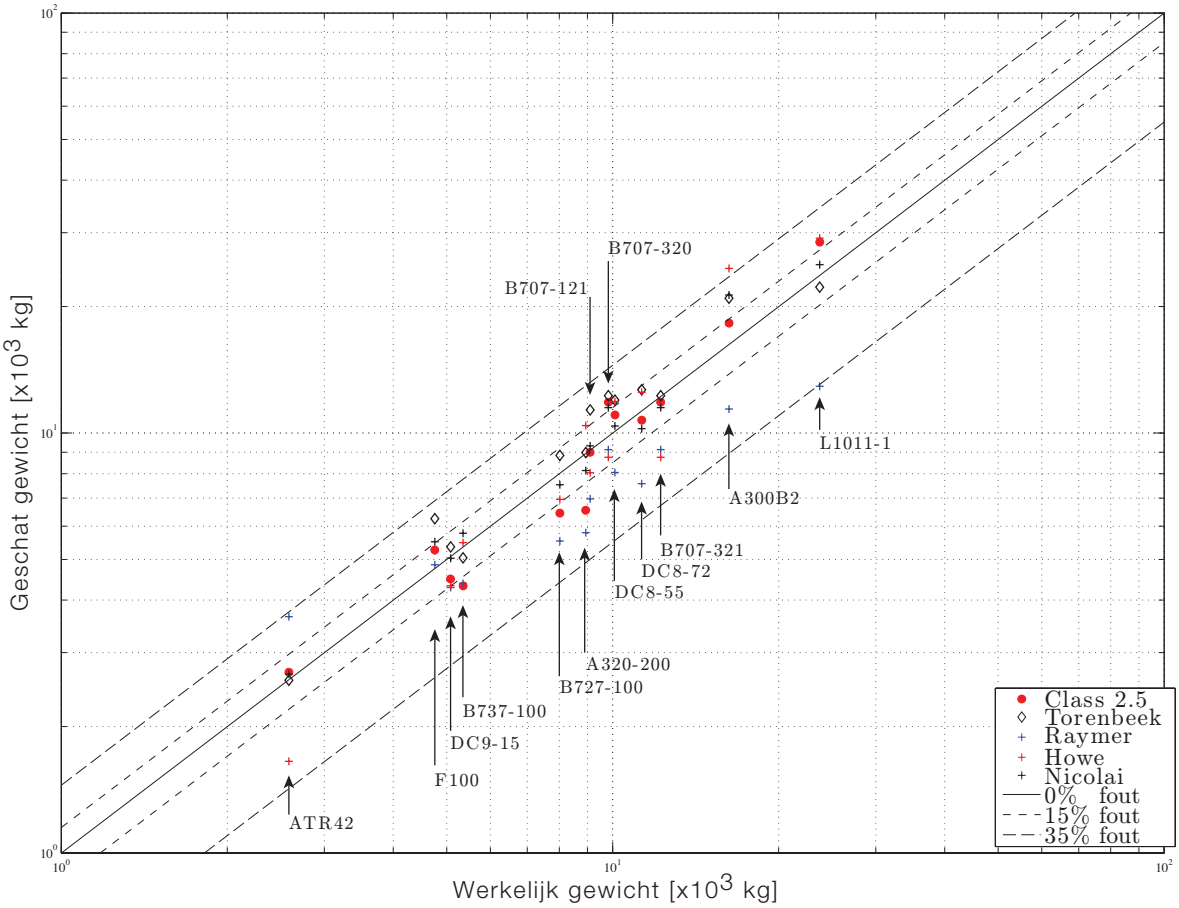

Figure 7-7: The estimated weight of the fuselage using the described method and methods from open literature versus the actual fuselage weight

Method	Maximum error	Mean error	RMS error
Class 2.5	26.7%	-0.7%	12.6%
Torenbeek	31.4%	11.1%	13.1%
Raymer	-45.6%	-18.5%	25.2%
Howe	51.7%	1.3%	19.0%
Nicolai	31.2%	4.2%	9.0%

Table 7-3: The maximum error, mean error and root mean square (RMS) error of fuselage weight estimations methods from open literature and the proposed method

bounds of the empirical estimation methods. From Table 7-3 it can be seen that the Class 2.5 has similar performance compared to empirical methods and the mean error of the Class 2.5 method is small compared to the other methods.

The weight of the cabin floor ranges from 7.4 kg/m^2 (ATR-42) to 18.5 kg/m^2 (L1011-1) and an average of 12.3 kg/m^2 which is about 25% heavier than the rule of thumb of 9.76kg/m^2 for conventional aircraft [50]. The average stringer to shell weight percentage ranges from 33% (ATR-42) to 65 % (Boieng 707-320) with an average ratio of 52% which is less than the expected 75% from [15]. The average frame to shell weight percentage ranges from 0.4% (ATR-42) to 1.2 % (Airbus A300B2) with an average ratio of 0.8%, far smaller than the expected 25% from literature [15]. It is interesting to see in Figure 7-8 that the estimated optimum stringer pitch is close to the industry standard 0.2 m stringer pitch for aircraft with a frame spacing of 0.5 m [50].

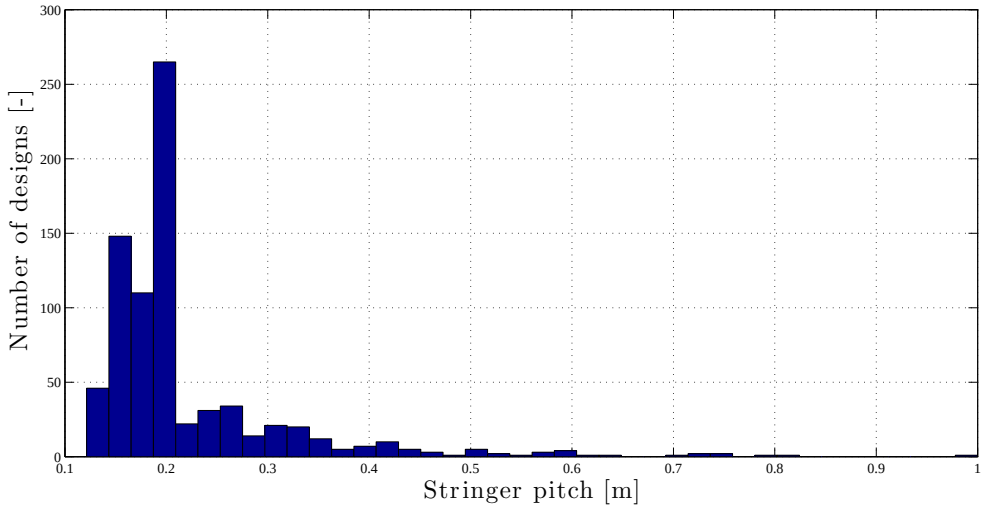

Figure 7-8: The stringer pitch resulted from the optimization problems of 13 aircraft with a circular fuselage

Chapter 8

Case studies

This chapter describes a number cases for which the fuselage weight is estimated using the presented method. First the weight of the fuselage is estimated in three different aircraft configurations. Next examples are given of the flexibility of the oval fuselage parameterization and the ability to estimate the weight of these notably different fuselages. Due to the current work-in-progress state of the Initiator, a sizing study of the oval fuselage in a BWB configuration and a comparison with a circular fuselage in a tube-and-wing configuration could not be performed.

8-1 Aircraft configuration

One of the capabilities of the proposed fuselage weight estimation is its sensitivity for the loads acting on the fuselage. One of the most important loads which has a great influence on the weight estimation is the longitudinal bending. By taking these loads into account as a function of the position along the length of the fuselage the method discriminates between designs where the same fuselage is used in different configurations. To show this four cases are considered: a BWB aircraft with an oval fuselage, a double-deck aircraft, an aircraft with an oval fuselage and a Prandtl plane. All aircraft have been sized with the same load cases as defined in Table 3-1. The longitudinal shear and bending moment along the length of the fuselage of these three different configurations are shown in Figure 8-1, 8-2 and 8-3. The fuselage weight in these three aircraft configurations is 24,845 kg, 20,515 and 19,570 kg for the conventional, canard and Prandtl configuration respectively. This shows a weight reduction of 17% and 21% for the canard and Prandtl configuration respectively compared to the conventional configuration.

8-2 Oval fuselage in aircraft design

The oval fuselage concept can be used to shape a fuselage for a BWB with a single deck (Figure 8-4), a BWB with a double deck (Figure 8-5), an tube-and-wing aircraft with a

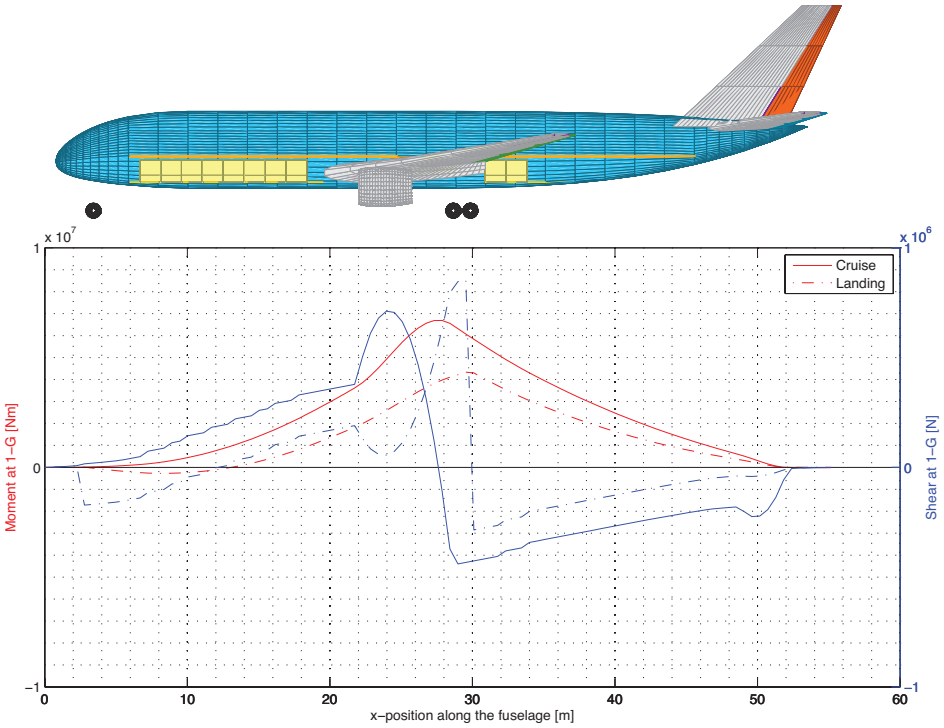

Figure 8-1: The longitudinal shear and bending moment along the length of the fuselage of a conventional aircraft

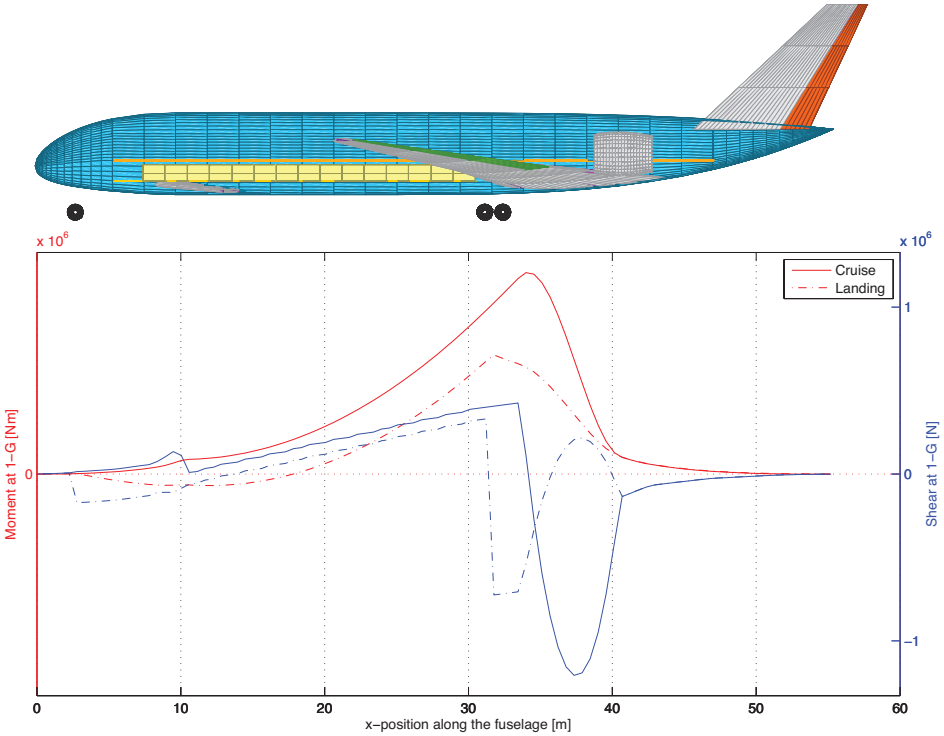

Figure 8-2: The longitudinal shear and bending moment along the length of the fuselage of a canard aircraft

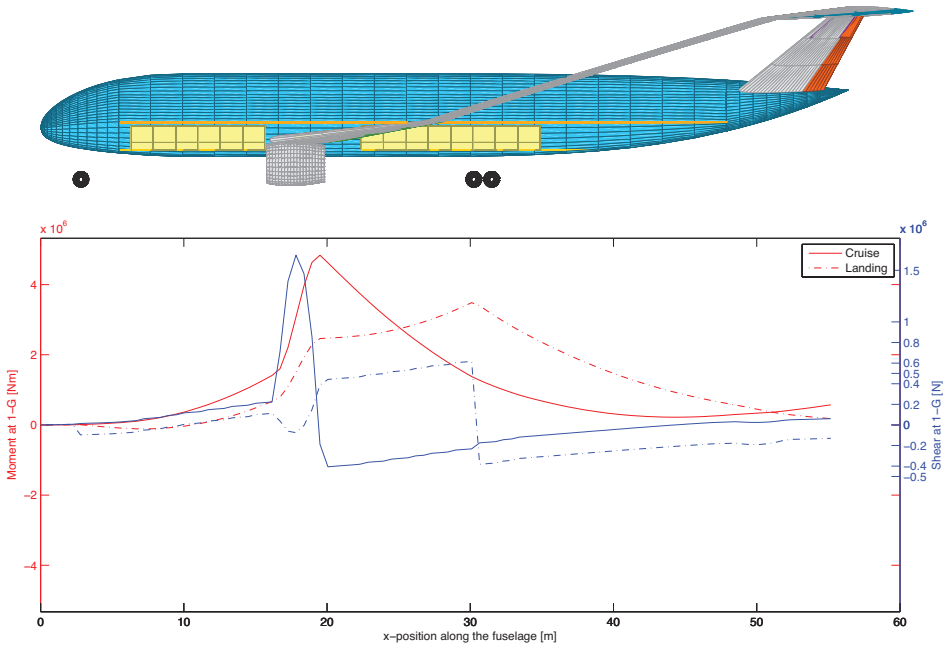

Figure 8-3: The longitudinal shear and bending moment along the length of the fuselage of a Prandtl aircraft

double deck (Figure 8-6) and an oval aircraft in a tube-wing configuration (Figure 8-7).

The aircraft in Figure 8-4 is a BWB aircraft with an oval fuselage which has a cabin area of 357 m^2, capable of seating 460 passengers in two classes. The aircraft has a cargo floor capacity of 31 LD3-45 containers with and has an estimated empty fuselage weight of 69.8 $\cdot 10^3$ kg. It has a wetted area of 1240 m^2.

The aircraft in Figure 8-5 is a hybrid wing body (HWB) with an oval fuselage with a cabin area of 914 m^2 spread over two deck (614 m^2 in the center and 300 m^2 in the top), capable of seating 1180 passengers in two classes. The aircraft has a cargo floor capacity of 112 LD2 containers with and has an estimated empty fuselage weight of 134 $\cdot 10^3$ kg. It has a wetted area of 1910 m^2.

The aircraft in Figure 8-6 is a conventional aircraft with a twin deck fuselage with a cabin area of 683 m^2 (360 m^2 in the center and 323 m^2 in the top) and a cargo floor capacity of 22 LD-3 containers with an estimated empty fuselage weight of 44.4 $\cdot 10^3$ kg. It has a wetted area of 1600 m^2.

The aircraft in Figure 8-7 is an conventional aircraft with an oval fuselage 15% wider than its conventional circular counterpart with a cabin area of 247 m^2 capable of seating 318 passenger in two classes and a cargo floor capacity of 22 LD3-45 containers with an estimated empty fuselage weight of 29.5 $\cdot 10^3$ kg. It has a wetted area of 887 m^2. For comparison, its conventional circular counterpart has a slightly smaller cabin area of 226 m^2 capable of seating 293 passengers in two classes, a wetted area of 845 m^2, room for 20 LD2 containers and an estimated empty fuselage weight of 25.8 metric tonnes, 3.7 $\cdot 10^3$ kg lighter than its oval counterpart.

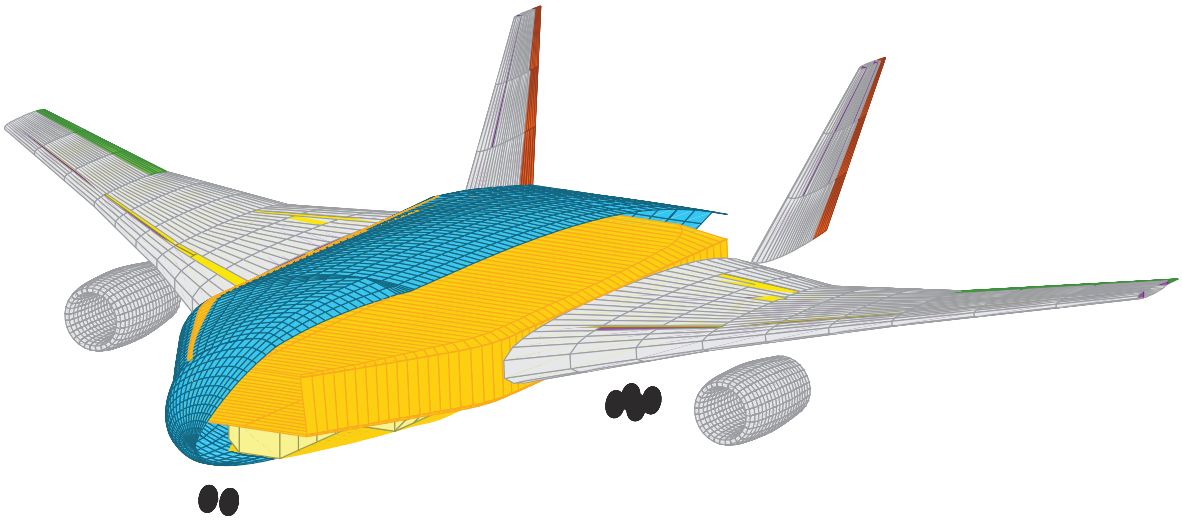

Figure 8-4: A BWB aircraft with an oval fuselage

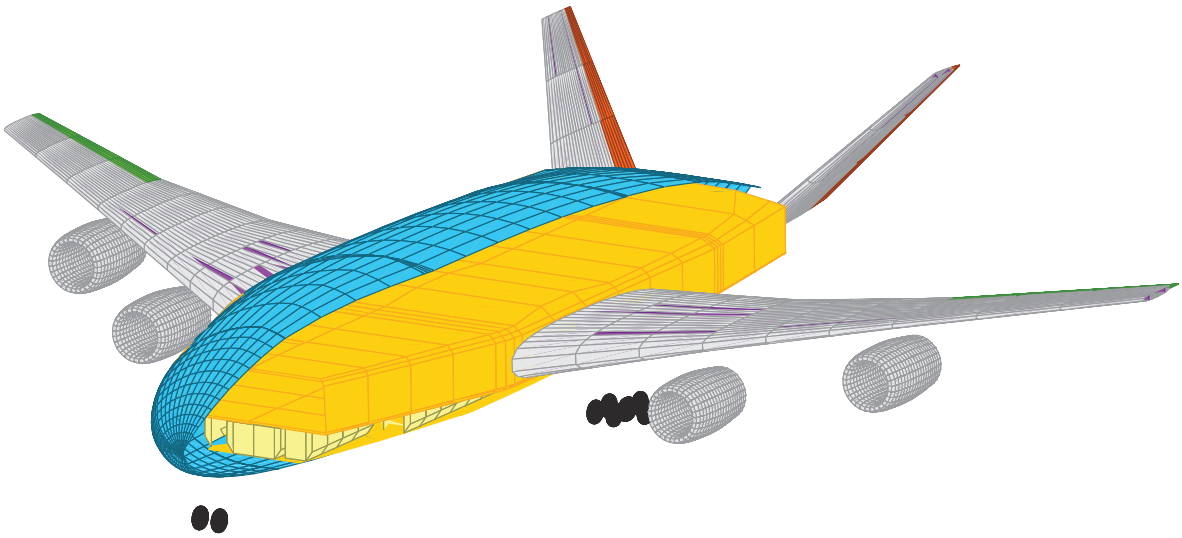

Figure 8-5: A HWB aircraft with an oval fuselage

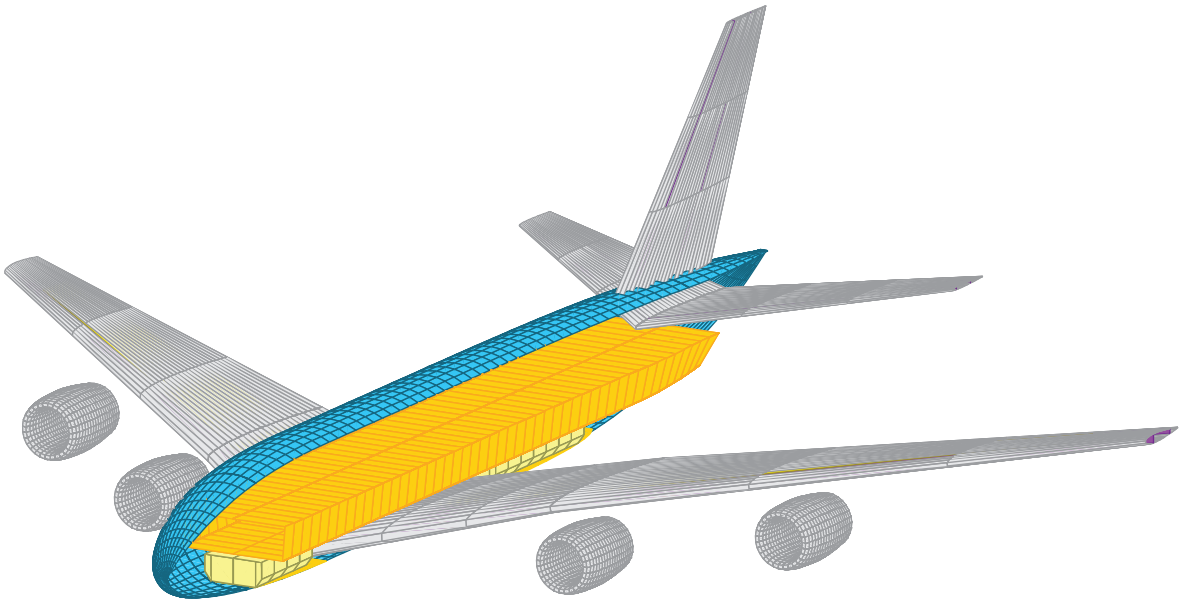

Figure 8-6: A conventional aircraft with a twin deck fuselage

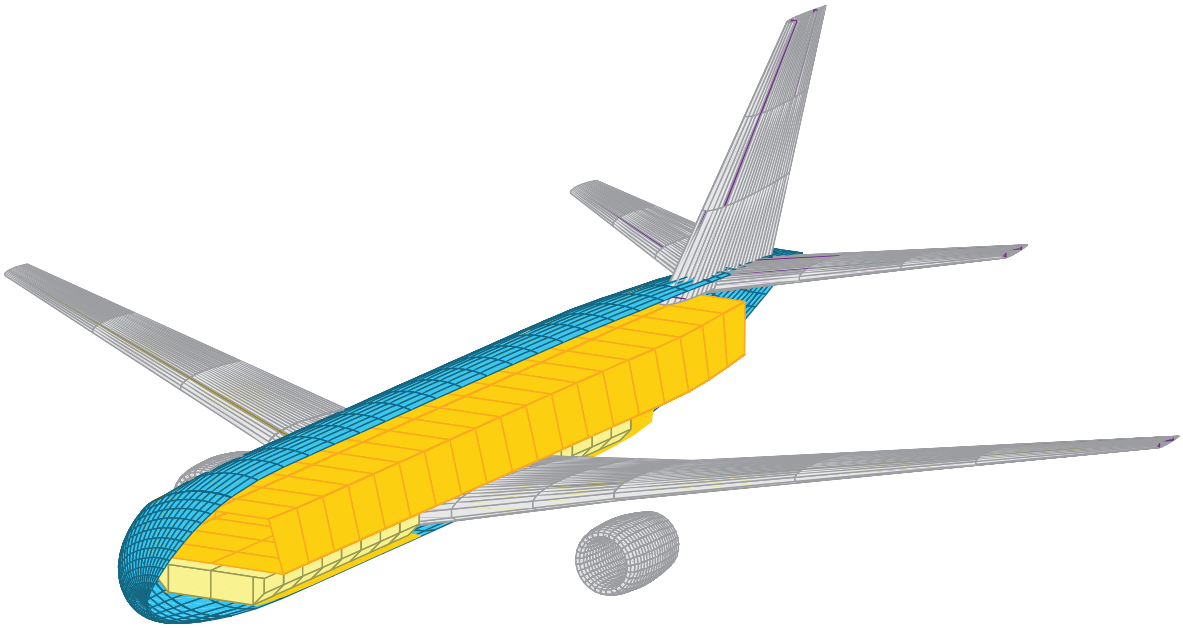

Figure 8-7: A conventional aircraft with an oval fuselage

Part III

Results and conclusions

Chapter 9

Conclusions

The goal of this thesis was to develop a method for the fuselage weight estimation of an oval fuselage in novel aircraft configurations. The motivation for this research is that the Blended Wing Body (BWB) concept has shown great potential in terms of efficiency. One of the problems to overcome in the development of this concept is a structural efficient pressurized cabin that blends well with the aircraft wing. This requires a non-circular fuselage with the design freedom for aerodynamic shape- such as the oval fuselage. An advantage of this concept over other non-circular fuselages is that the oval fuselage features an unobstructed cabin. Based on the research presented in the preceding chapters, a number of conclusion can be drawn.

Parametrization of the oval fuselage

The inside-out approach is taken to describe the cross-section of an oval fuselage. In this manner the three characteristic heights of the fuselage and the width of the floor determine the entire cross-section. A second parameterization method is presented to describe the complex three-dimensional geometry of an oval fuselage using limited number of characteristic dimensions. The three-dimensional shape consists of toroidal, spherical and cylindrical elements. An additional parameterization is presented for the crown and belly curve of the fuselage center section. Although the fuselage geometry is complex, it is still possible to divide the fuselage into a finite number of sections, which form the basis of the fuselage weight estimation.

Fuselage weight estimation method

The presented fuselage weight estimation is based on a simplified structural analysis of each fuselage sections using the plane stress assumption. The method is able to size the fuselage using a set of arbitrary load cases. For the present study these load cases include steady state maneuvering and hard landing conditions.

A comparison of existing aerodynamic models made between the accuracy to predict lift and bending moment. It was concluded that a vortex lattice method provides accurate results for the least computational cost.

By replacing the fuselage by 1-dimensional beam as a surrogate model the applied inertial and aerodynamic loads are translated to moment and shear forces in the individual fuselage sections. The longitudinal bending moment is carried by the outer shell and the trapezoid structure. Shear force is carried by the outer shell and the "vertical" member of the trapezoid structure. In addition to the bending moment and the shear force, the trapezoidal structure is loaded by a distributed transverse load and an axial load induced by the wing bending.

A bottom up approach has simplified the novel concept of the oval fuselage to the isolated design problem of a sandwich panel and a circular stiffened panel. The sizing of the structural members is based on the plane stress assumption. It accounts for the normal stresses and shear stress in-plane. The von Mises yielding criterion is used for this bi-axial loading such that all structural members are stressed. The sizing of the trapezoidal sandwich structure takes the dimpling, crimping, wrinkling and global buckling of thick sandwich panels into account. The sizing of the stiffened panels uses a global buckling criteria based on the buckling of cylinders subjected to bending and a local buckling based on the buckling of slender plates. For the sizing of the frames a method is derived for oval frames based on experimental data of circular frames.

A computer model is created that is able to estimate the weight of the oval fuselage in any aircraft configuration. This computer model is fully integrated in the Initiator of the Delft University of Technology. Since it is shown that circular fuselages can be generated using the proposed parameterization, the computer model can also be used for the estimation of the weight of circular fuselages.

Verification

By means of a theoretical case study and a finite element analysis the assumptions that were made for the estimation of forces due to pressurization on the trapezoidal are verified. The assumptions result in a underestimation of the stress by 2%. Furthermore, the method is verified with actual data of the fuselage weight of conventional aircraft and shows good coherence with both the data and empirical fuselage weight estimation available in open literature. Using limited information about conventional aircraft, on average the estimation error is 12%. This is similar to empirical methods. The passenger floor weight per unit area is similar to values found in literature and the optimum stringer pitch found by the sizing method is equal to the stringer pitch found in modern aircraft.

Two simplifications are proposed to reduce the calculation time of the weight estimation. Reducing the number of unique fuselage barrels by half reduces computational cost by 26%. Reducing the design space dimensions of the stiffened skin sizing procedure from seven to three reduces computational cost by 17%. In a sensitivity study it is shown that the number of barrels significantly affects the fuselage weight, a reduction in the number of barrels increases the weight. It is also found that the reduction of dimensions in the sizing method has little effect on the weight. The sensitivity study also verified that an increased weight is found when the cabin altitude is decreased and an increase in fuselage weight is found when the maximum number of flights is increased.

Case studies

One of the features of the estimation method is that the method is sensitive to the loads acting on the fuselage in different aircraft configurations. It is found that the estimated fuselage weight of a circular fuselage in a canard configuration and in a Prandtl configuration is 17% and 21% lighter compared to the estimated weight of the same fuselage in a conventional aircraft configuration. Comparing different incarnations of oval fuselages it is found that the double deck version of the oval fuselage is the lightest with 65 kg/m^2 of useful cabin area followed by tube-and-wing aircraft with a circular fuselage with 114 kg/m^2 and the tube-and-wing oval fuselage with 119 kg/m^2. It is found that a high capacity Hybrid Wing Body with an oval fuselage and two decks and the Blended Wing Body with an oval fuselage are the heaviest of the five aircraft considered with 146 kg/m^2 and 196 kg/m^2 respectively. It must be stressed that the aircraft presented in the case study are not optimized design. From this case study it should therefore not be concluded that the oval fuselage is not a suitable candidate for the use in Blended Wing Body aircraft or other aircraft.

It can be concluded that the presented fuselage weight estimation for oval fuselages is able to gain insights in the design of aircraft with an oval fuselage. The results from this weight estimation not only include the total weight of the fuselage but also the weight of individual components and the dimensions of the structural members. Due to the physics based approach the method is sensitive to changes in loads, flight conditions and aircraft configurations. The combination of the increased sensitivity to design variables and the flexibility of the parameterization method and the robust computer program makes the method is an essential contribution to the evaluation of novel aircraft during the early stages of design.

Chapter 10

Recommendation

A number of recommendations are given for further research and for further improvement.

Physics based weight estimation It is recommended to use a physics based weight estimation method for the fuselage in the early stages of the aircraft design. The actual loads on the aircraft greatly affect the fuselage weight when different aircraft configurations are considered. In order to obtain reliable results, more effort is needed in the estimation of the required input for such an method, such as a trimmed aerodynamic solution and a valid set of aircraft weight components and their center of gravity.

Calculation time There is a inherent inefficiency in the repetitive evaluation of optimization problems. The use of these optimization techniques to size structural members of an oval fuselage is favored over rules of thumb in design when these rules of thumb are only applicable to circular fuselage. Significant reductions in calculation time could be obtained if a new set of design rules where constructed using a design of experiments using the fuselage weight estimation method.

Initial sizing The initial sizing of the fuselage for a given number of passengers and minimum amount of cargo volume is a procedure that still has to be developed for the incarnations of the oval fuselage. It is found that this is more complex compared to the initial sizing of conventional fuselages.

Three-dimensional effects As this weight estimation is based on the assumption that each section can be analyzed as an isolated sliver of the fuselage. An important subject for future research is the validation of this assumption taking into account the different sets of geometry that are identified and the effect of the trapezoidal structure on the connected fuselage structure to this trapezoidal structure.

Multidisciplinary optimization The increased design freedom of the oval fuselage makes it an attractable subject for the optimization of the fuselage geometry and its integration with wings and other aircraft components. When incorporated in a multidisciplinary design environment the shape of the oval fuselage shape can be optimized to obtain

an efficient balance between the required lift generation, passenger capacity and lowest structural weight.

Appendix A

Empirical fuselage weight estimations

Four different fuselage weight estimation methods for circular fuselages in a tube-and-wing aircraft configurations exist in literature. These and actual fuselage weight data is used to verify the weight from the oval fuselage weight estimation. An overview of these empirical relation are given below.

Torenbeek

According to Torenbeek [51] the fuselage weight is calculated by the following equation:

$$W = 0.23\sqrt{\frac{V_d L_{\mathrm{t}}}{B+H}} S_f^{1.2} \tag{A-1}$$

where
V_d is the dive speed, m/s
L_{t} is the distance between main wing and the tail, m
B is the fuselage width, m
H is the fuselage height, m
S_{f} is the wetted area of the fuselage in m^2

For a pressurized fuselage an additional 8% is taken into account, 4% for fuselage mounted engines and 7% for fuselage mounted main landing gears.

Raymer

According to Raymer [52] the fuselage weight is calculated by the following equation:

$$W = 0.328 K_{\mathrm{door}} K_{\mathrm{lg}} \left(W_{\mathrm{TO}} N_{\mathrm{z}}\right)^{0.5} L^{0.25} S_{\mathrm{f}}^{0.302} \left(1 + K_{\mathrm{ws}}\right)^{0.04} \left(\frac{L}{D}\right)^{0.1} \quad \text{[lbs]} \tag{A-2}$$

where
Kdoor is a penalty factor taking cargo doors into account, equal to 1.12
K_{lg} is a penalty factor taking the main landing gear into account, equal to 1.0 when the main landing gear is attached to the wing, equal to 1.12 when the main landing gear is attached to the fuselage
W_{TO} is maximum take-off mass in lbs
N_z is the maximum load factor including the safety factor
L is the structural length of the fuselage, ft
S_{f} is the wetted area of the fuselage in ft^2
D is diameter of the fuselage, ft

K_{ws} is given by

$$K_{\text{ws}} = 0.75\frac{1+2\lambda}{1+\lambda}B_w \tan\frac{\Lambda}{L} \tag{A-3}$$

where
λ is the taper ratio of the main wing
B_w is the wing span, ft
Λ is the wing sweep at 25% MAC
L is the structural length of the fuselage, ft

Nicolai

According to Nicolai [53] the fuselage weight is calculated by the following equation:

$$W = 200\left[\left(W_{\text{TO}}\cdot N_z\cdot 10^5\right)^{0.286}\left(\frac{L}{10}\right)^{0.857}\left(\frac{D+H}{10}\right)\left(\frac{V_d}{100}\right)^{0.338}\right]^{1.1} \quad \text{[lbs]} \tag{A-4}$$

with: W_{TO} is the maximum take-off mass, lbs
N_z is the maximum load factor including the safety factor
L is the fuselage length, ft
D is the fuselage width, ft
H is the fuselage height, ft
V_d is the dive speed, kts

Howe

According to Howe [54] the fuselage weight is calculated by the following equation:

$$W = c_2\Delta p\,(9.75+5.84B)\left(\frac{2L}{B+H}-1.5\right)(B+H)^2 \quad \text{[kg]} \tag{A-5}$$

with:
c_2 is a constant, 0.79 for transport aircraft
Δp the pressure differential, bar

B is the width of the fuselage, m
L is the length of the fuselage, m
H is the height of the fuselage, m

Appendix B

Sectional properties

An oval fuselage section consists of four arcs making up the outer shell and four straight members making up the trapezoidal structure. The section is symmetric about the z-axis. This chapter describes the derivation for obtaining the centroid and moment of inertia of the oval fuselage section by deriving the centroid and moment of inertia of each member and combining these to obtain the properties of the oval fuselage section.

B-1 Arc

The z-position of the centroid of the arc, $\bar{z}$, depicted in Figure B-1 is determined using,

$$\bar{z} = \frac{\int z \mathrm{d}A}{\int \mathrm{d}A}, \tag{B-1}$$

where $\mathrm{d}A$ can be written as

$$\mathrm{d}A = Rt\mathrm{d}\theta. \tag{B-2}$$

Substituting Equation B-2 into Equation B-1 results in

$$\bar{z} = \frac{\int_{\theta_1}^{\theta_2} z \mathrm{d}\theta}{\int_{\theta_1}^{\theta_2} \mathrm{d}\theta}. \tag{B-3}$$

From Figure B-1 it follows that

$$z\left(\theta\right) = z_r + R\cos\theta. \tag{B-4}$$

The numerator of Equation B-3 then becomes

$$\int_{\theta_1}^{\theta_2} z \mathrm{d}\theta = \int_{\theta_1}^{\theta_2} z_r \mathrm{d}\theta + \int_{\theta_1}^{\theta_2} R\cos\theta \mathrm{d}\theta \tag{B-5}$$

$$= z_r\left(\theta_2 - \theta_1\right) + R\left(\sin\theta_2 - \sin\theta_1\right) \tag{B-6}$$

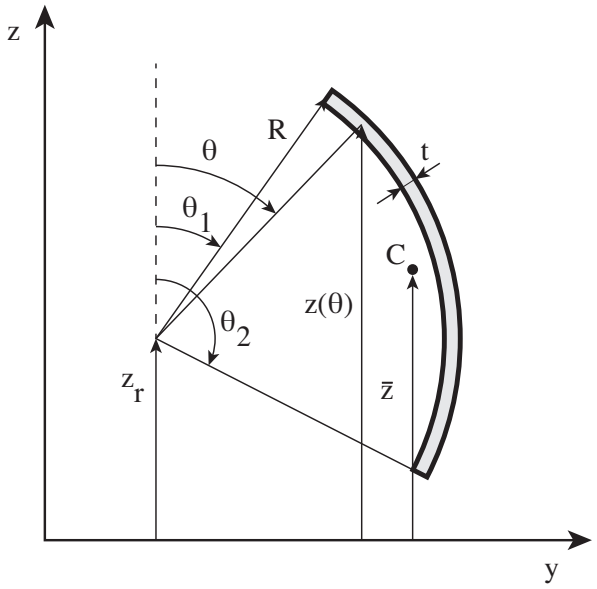

Figure B-1: Schematic view of a thin arc.

and the denominator of Equation B-3 becomes,

$$\int_{\theta_1}^{\theta_2} \mathrm{d}\theta = \theta_2 - \theta_1 \tag{B-7}$$

which results in the centroid of the arc

$$\bar{z} = z_r + \frac{R\left(\sin\theta_2 - \sin\theta_1\right)}{\theta_2 - \theta_1}. \tag{B-8}$$

The moment of inertia about the y-axis is given by

$$I_{\mathrm{yy}} = \int z^2 \mathrm{d}A \tag{B-9}$$

$$= Rt \int_{\theta_1}^{\theta_2} z^2 \mathrm{d}\theta \tag{B-10}$$

where

$$z = z_p + R\cos\theta \tag{B-11}$$

where $z_p = z_r - \bar{z}$. Solving Equation B-9 results in

$$I_{\mathrm{yy}} = \frac{R^2}{4}\left(\sin 2\theta_2 - \sin 2\theta_1\right) + \left(\frac{R^2}{2} + z_p^2\right)\left(\theta_2 - \theta_1\right) + 2Rz_p\left(\sin\theta_2 - \sin\theta_1\right) \tag{B-12}$$

B-2 Trapezoidal

The z-position of the centroid of the horizontal members of the trapezoidal structure is simply the height at which it is located. The moment of inertia of the horizontal member about the y-axis is given by

$$I_{\mathrm{yy}} = \frac{wt^3}{12} \tag{B-13}$$

where w is the width of the horizontal member and t the thickness of the member.

The z-position of the centroid of the slanted 'vertical' members of the trapezoidal structure is located at the vertical midpoint of the member. The moment of inertia of the member about the y-axis is given by

$$I_{\text{yy}} = \frac{th^3}{12\cos\beta}. \tag{B-14}$$

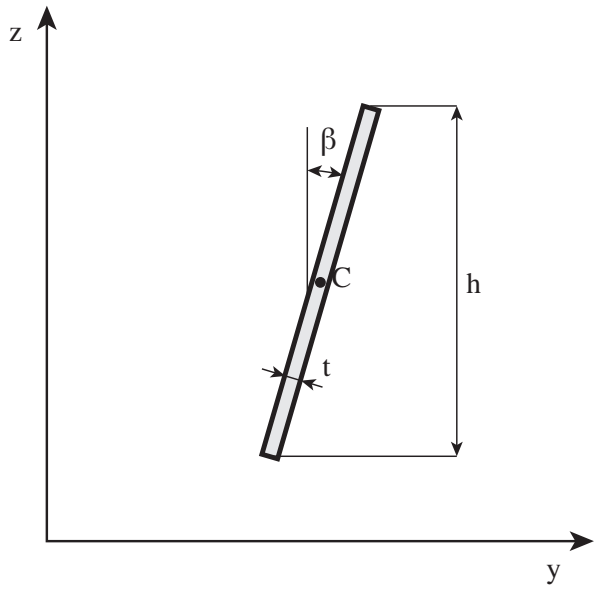

Figure B-2: Schematic view of the 'vertical' member of the trapezoidal structure.

B-3 Oval fusleage

The position of the centroid of the oval fuselage section in the z-direction is obtained from the centroids of the individual members. This position, $\bar{z_{\text{of}}}$ is determined from

$$\bar{z_{\text{of}}} = \frac{\sum_{i=1}^{n} A_i \bar{z_i}}{\sum_{i=1}^{n} A_i} \tag{B-15}$$

where i denotes the individual members including the four arcs and the four members of the trapezoidal structure.

The moment of inertia of the section about the y-axis is obtained using Huygens-Steiner parallel axis theorem as

$$I_{\text{yy,of}} = \sum_{i=1}^{n} I_{\text{yy,i}} + \sum_{i=1}^{n} A_i d_i^2 \tag{B-16}$$

where $d_i = \bar{z_i} - \bar{z_{\text{of}}}$.

Appendix C

Aerodymic drag considerations

The direct contribution of the drag force is neglected in the fuselage weight estimation, as discussed in Section 3. However, it is outputted during the comparison of the different aerodynamic analyses. During these simulations interesting data is gathered of the estimated drag. This section provides the data concerning drag that is estimated by these three aerodynamic analyses.

Although none of the three methods accounts for viscosity one could account for the viscosity effects, pressure drag and skin friction drag through the use of either a two-dimensional viscous solver coupling (e.g. XFOIL, MSES, VGK) where the viscous two-dimensional profile drag is determined and by the use of sweep theory transformed to a semi-three-dimensional drag estimation. This method ignores the three-dimensional pressure relief effects, span wise boundary layer interaction which are important due to the highly curved Blended Wing Body (BWB) center body. Another method for predicting the profile drag is the use of an empirical model (e.g. form factor calculation, Raymer drag prediction, ESDU drag prediction), due to the lack of data from flying BWB designs these models define the aircraft as being a complete wing.

Drag can be divided into a skin friction component and a lift induced drag component. The drag polar from the test cases discussed in Section 3-3-3 is visualized in Figure C-1 and C-2 where the lift coefficient is squared to produce the linear relation. In this figure the slope of the line indicates the Oswald span efficiency and the vertical offset from the origin indicates the profile drag. While the models deviate in the profile drag coefficient, the induced drag coefficient agrees with test data. It can be seen that the profile drag is largely underestimated in VSAERO and roughly equal for AVL-XFOIL and Tornado. It is interesting to see that the empirical drag estimation is approximately similar to the XFOIL analysis although the empirical model does not take the lift coefficient into account. Also a small error can be seen in the lift induced drag of VSAERO where it predicts a negative drag coefficient at zero lift, where it should actually be zero.

Quantitative aerodynamic characteristics are derived from this data and presented in Table C-1. It is seen that there is a rather large difference in the estimated values.The results

obtained from Tornado are empirical values. It is seen that if the AVL-XFOIL analysis would be combined with the empirical drag estimation of Tornado a high accuracy is obtained with little computational cost.

	MATRICS-V	VSAERO	AVL-XFOIL	Tornado
C_{L_α} [deg^{-1}]	4%	6%	3%	4%
C_{D_0} [cts]	15%	44%	33%	**12%**
Oswald factor [-]	6%	11%	**3%**	17%

Table C-1: Mean absolute error of the aerodynamic models

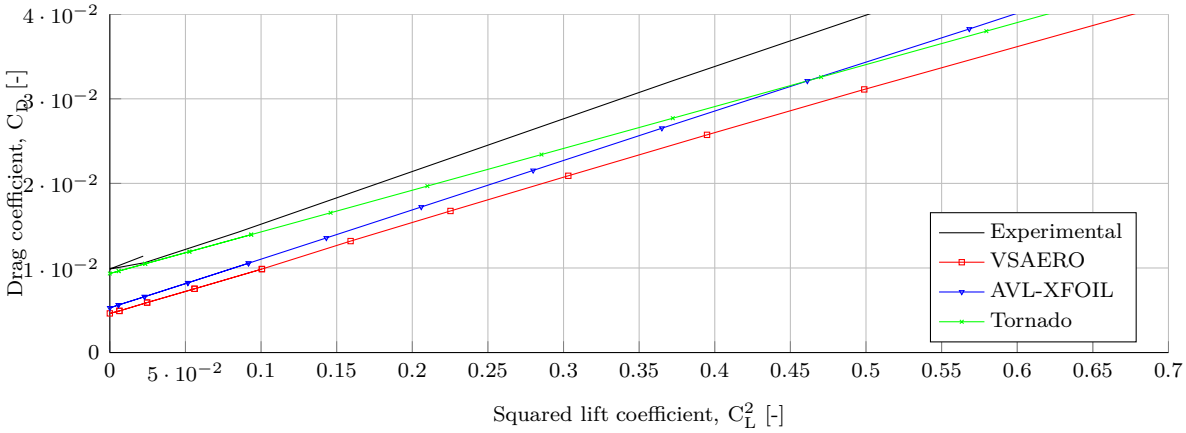

(a) NACA-00-0-0 wing

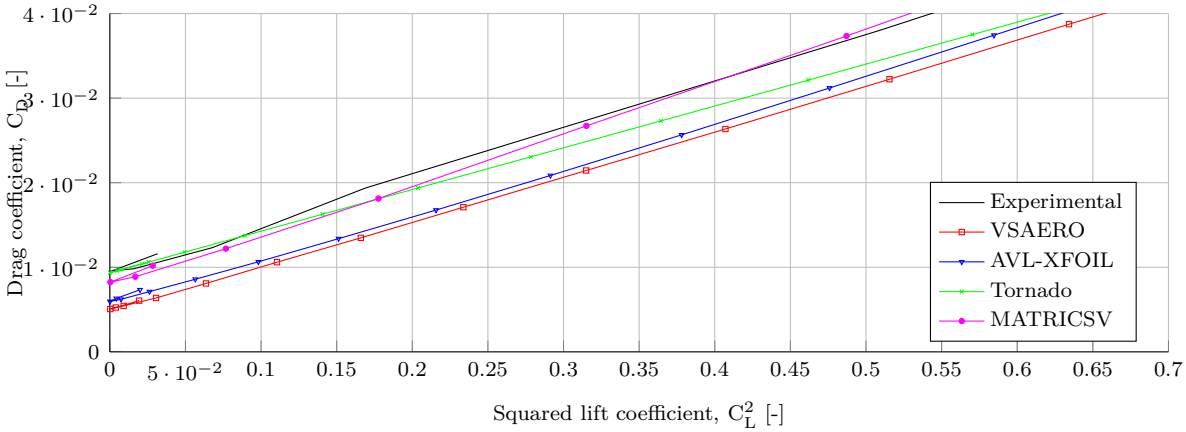

(b) NACA-24-0-0 wing

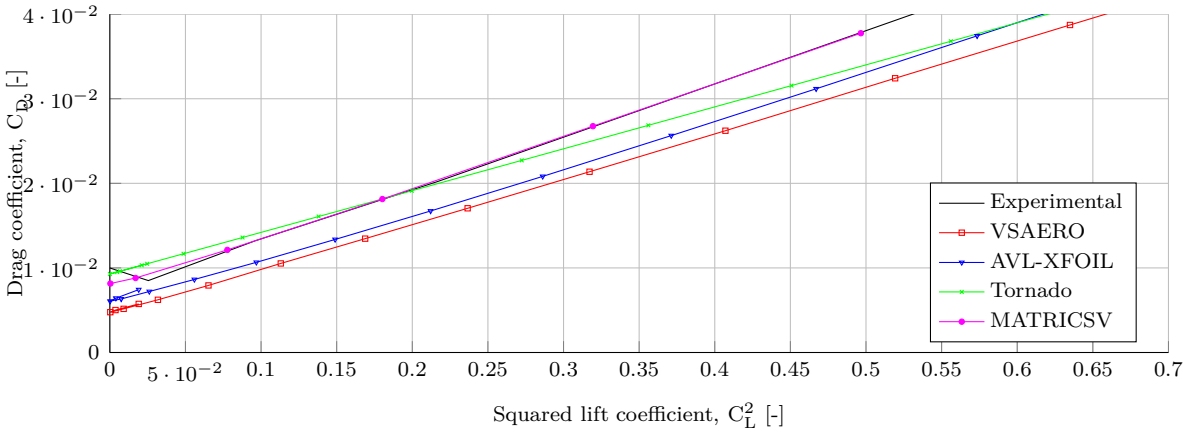

(c) NACA-24-15-0 wing

Figure C-1: The relation between the squared lift coefficient and the total drag of the NACA-00-0-0 wing, the NACA-24-0-0 wing and the NACA-24-15-0 wing

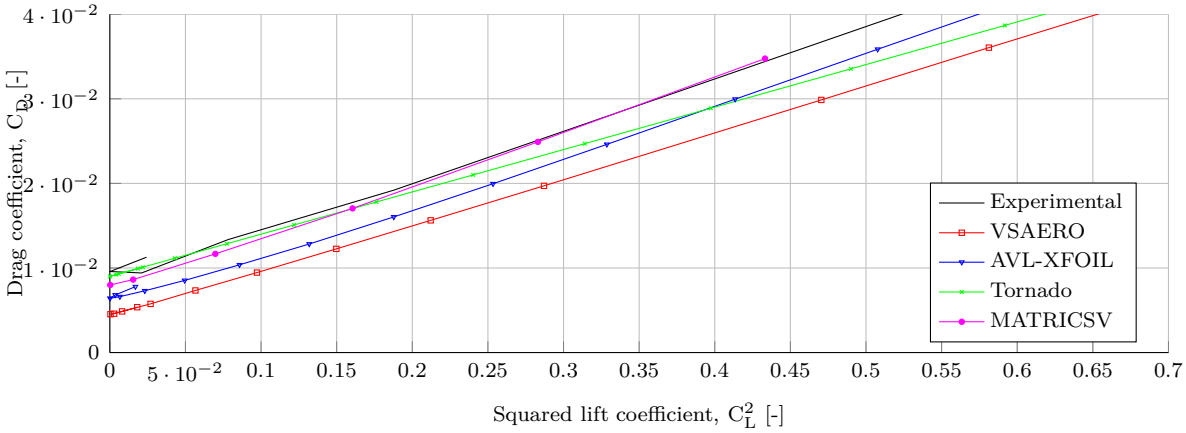

(a) NACA-24-30-0 wing

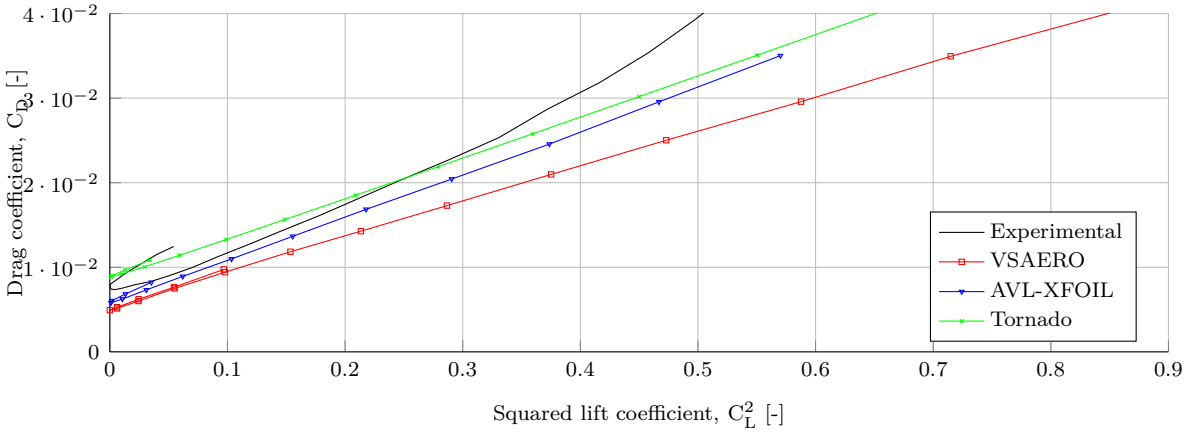

(b) ZEFT blended wing body

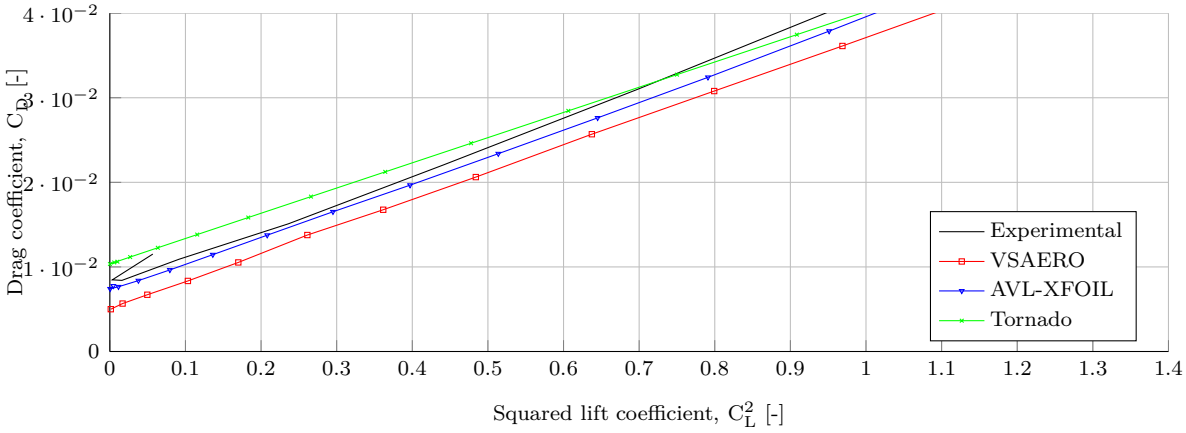

(c) NACA-2.5-10-44.20 wing

Figure C-2: The relation between the squared lift coefficient and the total drag of the NACA-24-30-0 wing, the ZEFT blended wing body and the NACA-2.5-10-44.20 wing

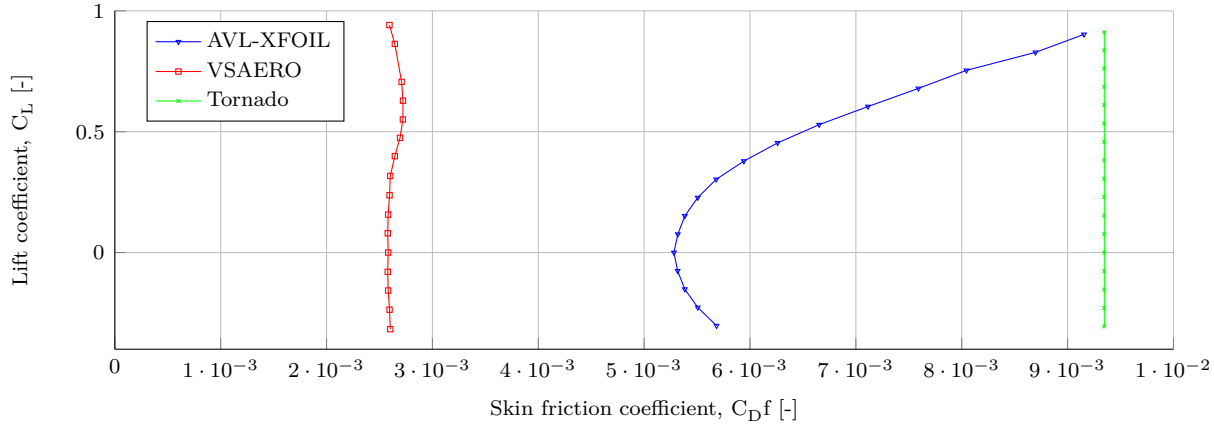

(a) NACA-00-0-0 wing

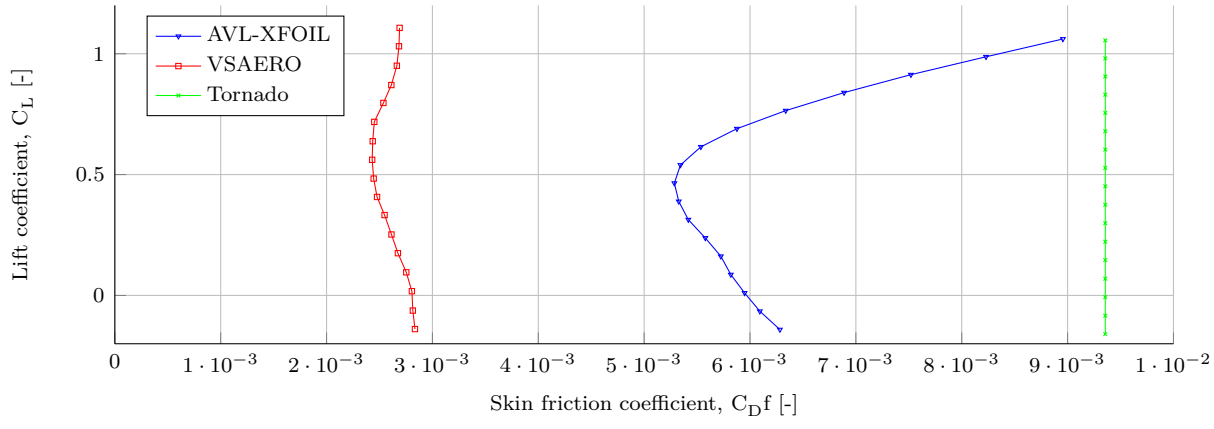

(b) NACA-24-0-0 wing

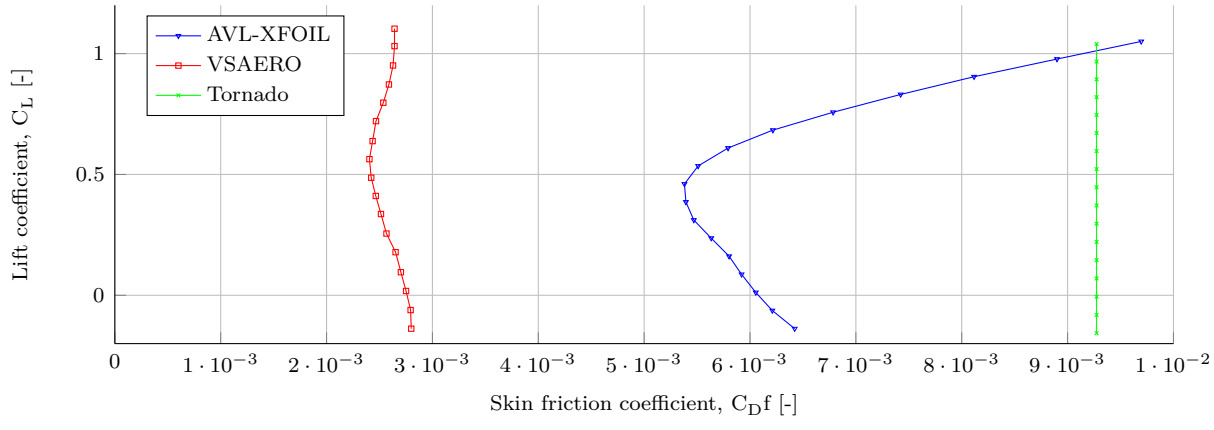

(c) NACA-24-15-0 wing

Figure C-3: The estimated skin friction coefficient of the NACA-00-0-0 wing, the NACA-24-0-0 wing and the NACA-24-15-0 wing

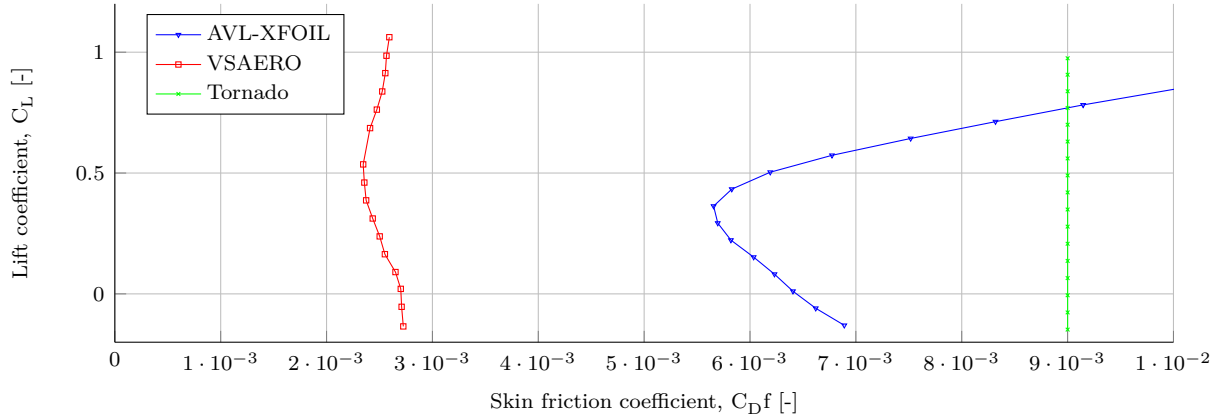

(a) NACA-24-30-0 wing

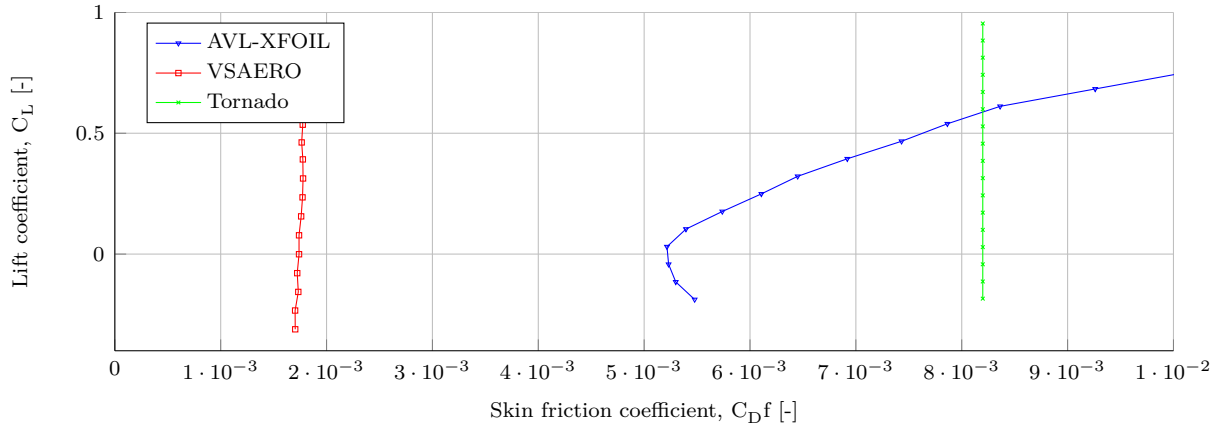

(b) ZEFT blended wing body

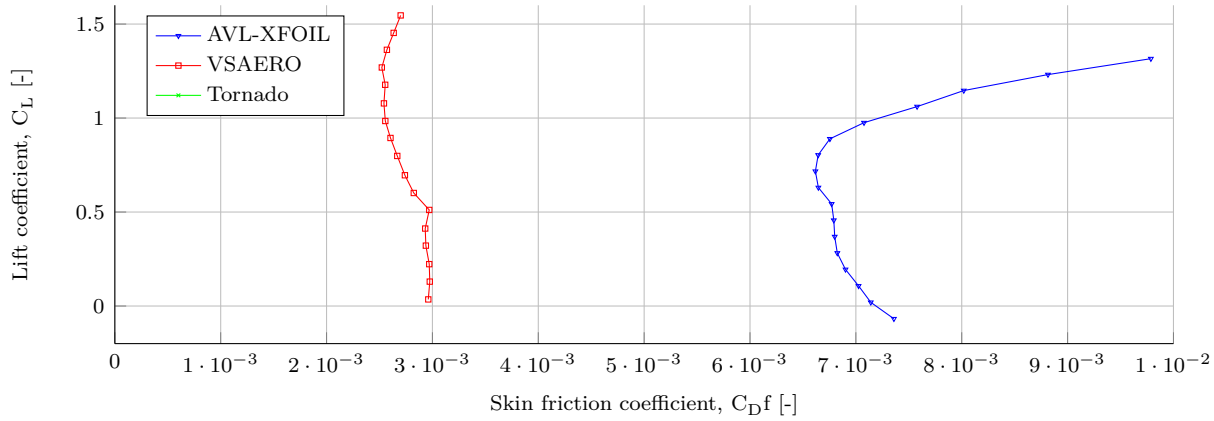

(c) NACA-2.5-10-44.20 wing

Figure C-4: The estimated skin friction coefficient of the NACA-24-30-0 wing, the ZEFT blended wing body and the NACA-2.5-10-44.20 wing

Appendix D

Aerodynamic characteristics of the test cases

For reference, a complete overview of the results of the aerodynamic test case is included.

	Experiment	MATRICS-V		VSAERO		AVL-XFOIL		Tornado	
C_{L_α} [deg^{-1}]	0.074	-	-	0.079	6%	0.075	2%	0.076	3%
C_{D_0} [cts]	95.8	-	-	47.4	-50%	52.7	-45%	86.2	-10%
Oswald factor [-]	0.876	-	-	1.020	16%	0.914	4%	1.071	22%

Table D-1: NACA 00-0-0

	Experiment	MATRICS-V		VSAERO		AVL-XFOIL		Tornado	
C_{L_α} [deg^{-1}]	0.073	0.070	-4%	0.078	7%	0.075	4%	0.076	5%
C_{D_0} [cts]	89.4	74.2	-17%	48.2	-46%	54.0	-40%	86.2	-4%
Oswald factor [-]	0.913	0.844	-8%	0.994	9%	0.954	4%	1.071	17%

Table D-2: NACA-24-0-0

	Experiment	MATRICS-V		VSAERO		AVL-XFOIL		Tornado	
C_{L_α} [deg^{-1}]	0.074	0.072	-3%	0.078	5%	0.074	1%	0.075	2%
C_{D_0} [cts]	83.1	75.0	-10%	45.7	-45%	54.5	-34%	85.4	3%
Oswald factor [-]	0.919	0.876	-5%	0.989	8%	0.938	2%	1.067	16%

Table D-3: NACA-24-15-0

	Experiment	MATRICS-V		VSAERO		AVL-XFOIL		Tornado	
C_{L_α} [deg^{-1}]	0.070	0.067	-4%	0.075	7%	0.070	0%	0.070	1%
C_{D_0} [cts]	89.7	73.3	-18%	43.0	-52%	56.9	-37%	83.0	-8%
Oswald factor [-]	0.904	0.846	-6%	0.974	8%	0.886	-2%	1.055	17%

Table D-4: NACA-24-30-0

	Experiment	MATRICS-V		VSAERO		AVL-XFOIL		Tornado	
C_{L_α} [deg^{-1}]	0.079	-	-	0.077	-2%	0.073	-8%	0.070	-11%
C_{D_0} [cts]	76.3	-	-	52.6	-31%	58.8	-23%	97.5	28%
Oswald factor [-]	0.837	-	-	1.028	23%	0.841	0%	1.027	23%

Table D-5: Blended wing body

	Experiment	MATRICS-V		VSAERO		AVL-XFOIL		Tornado	
C_{L_α} [deg^{-1}]	0.085	-	-	0.095	11%	0.087	1%	0.088	3%
C_{D_0} [cts]	83.2	-	-	51.0	-39%	68.7	-17%	97.8	18%
Oswald factor [-]	0.998	-	-	0.991	-1%	0.957	-4%	1.066	7%

Table D-6: NACA-2.5-10-44.20

Appendix E

Fuselage test cases

The reference aircraft used for the verification of the fuselage weight estimation in Chapter 7 are shown here.

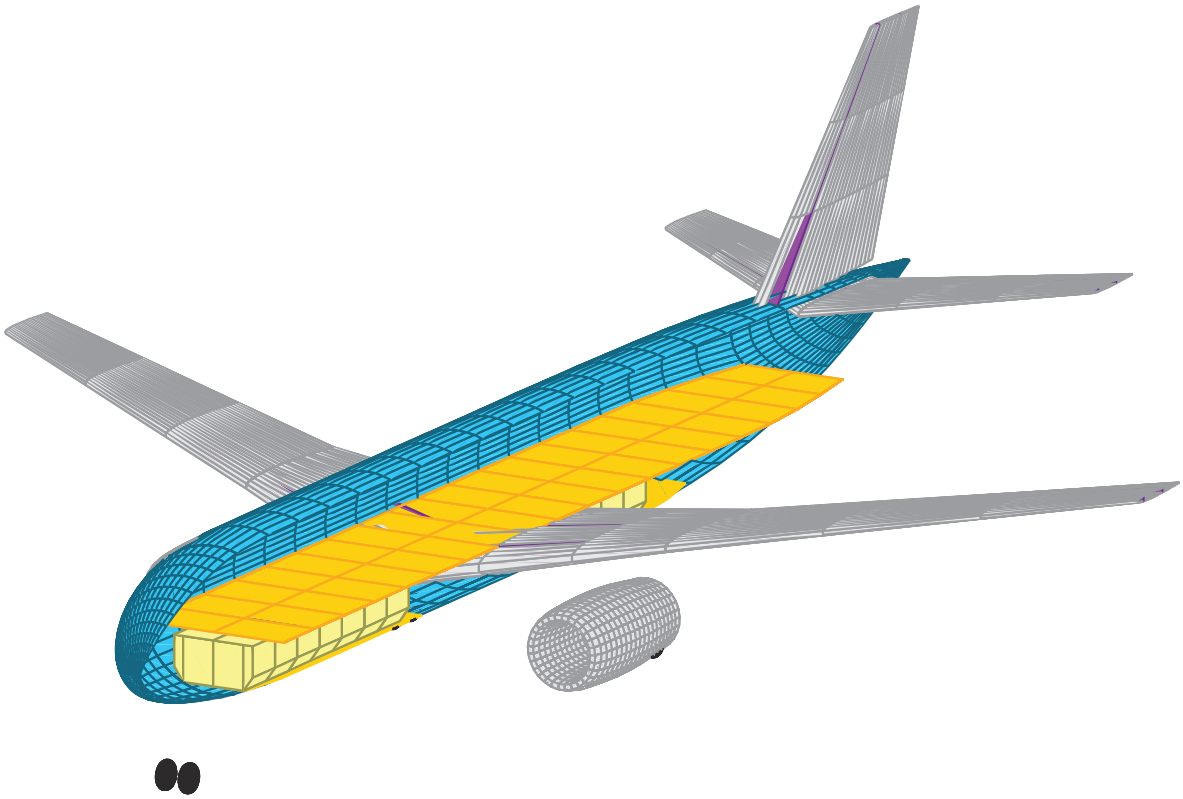

Figure E-1: Airbus A300 B2

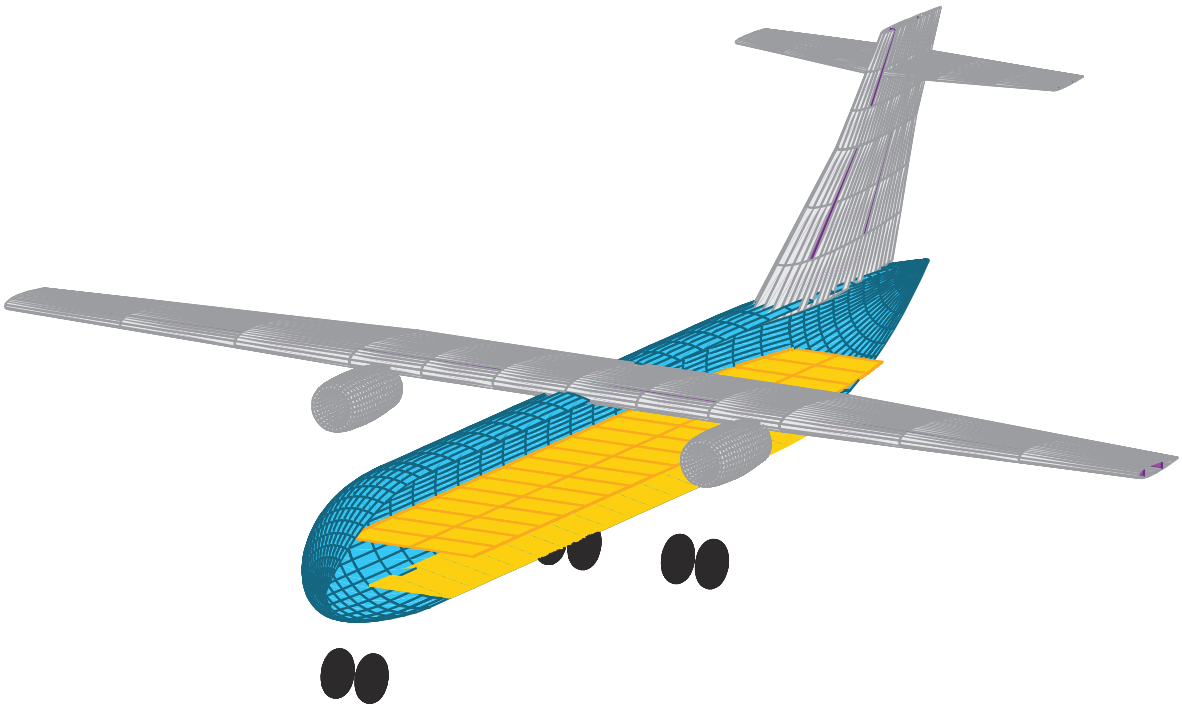

Figure E-2: ATR 42

Figure E-3: Boeing 707-121

Figure E-4: Boeing 707-320

Figure E-5: Boeing 707-321

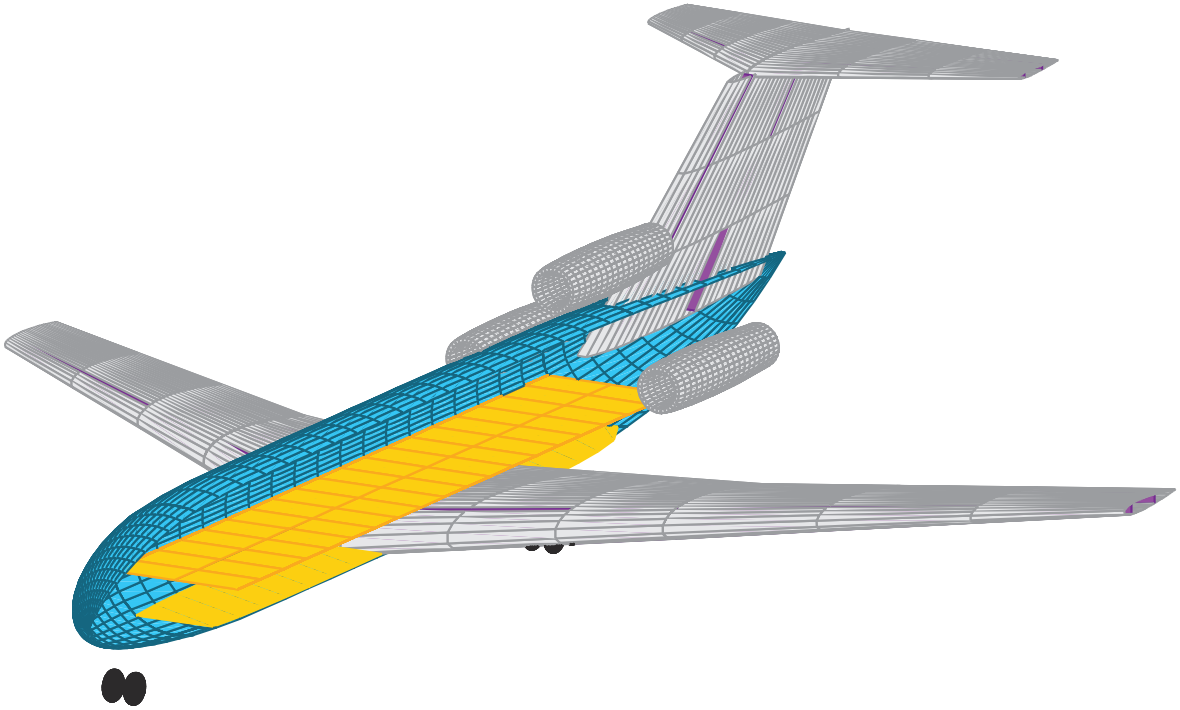

Figure E-6: Boeing 727-100

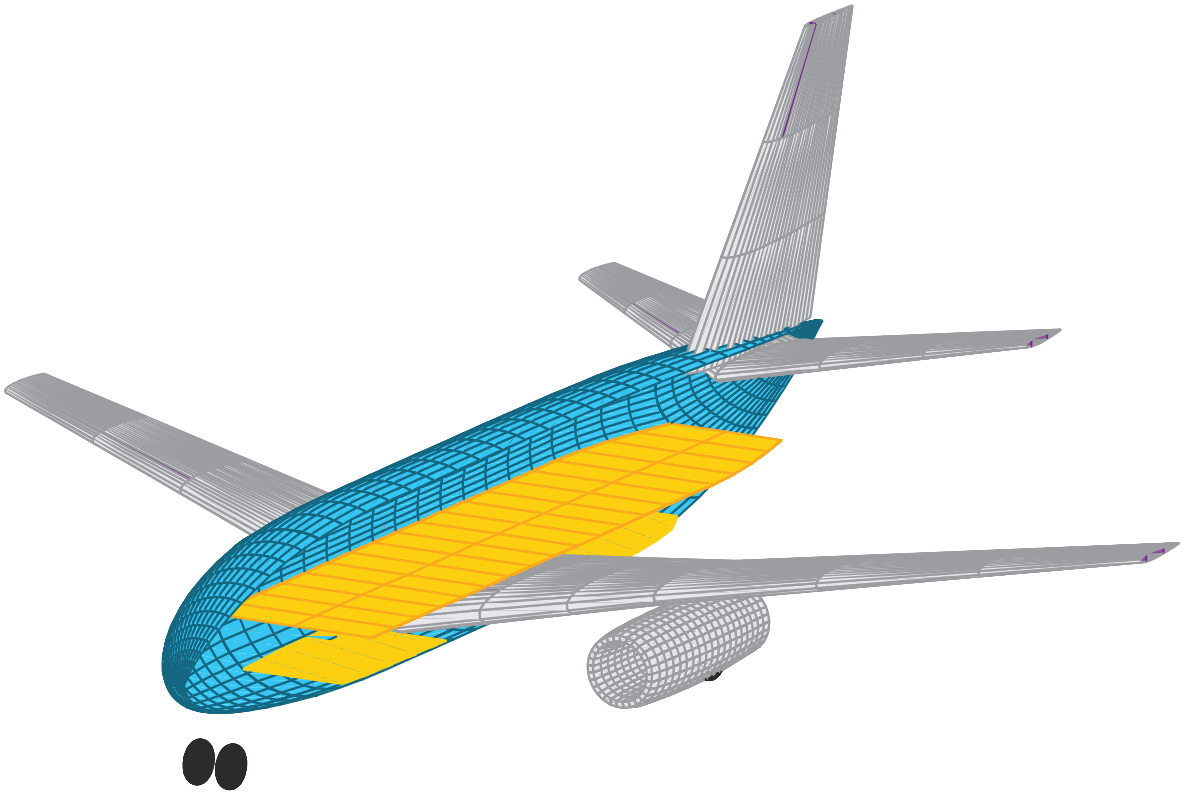

Figure E-7: Boeing 7371-00

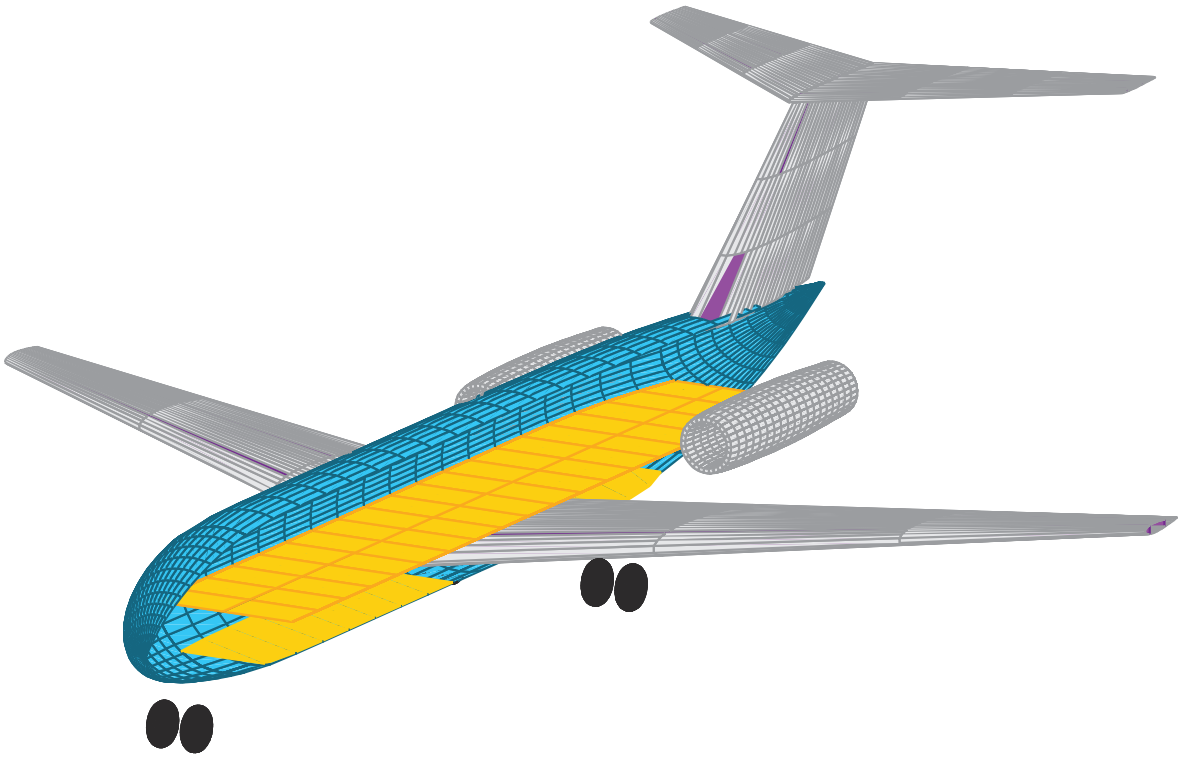

Figure E-8: Douglas DC9-15

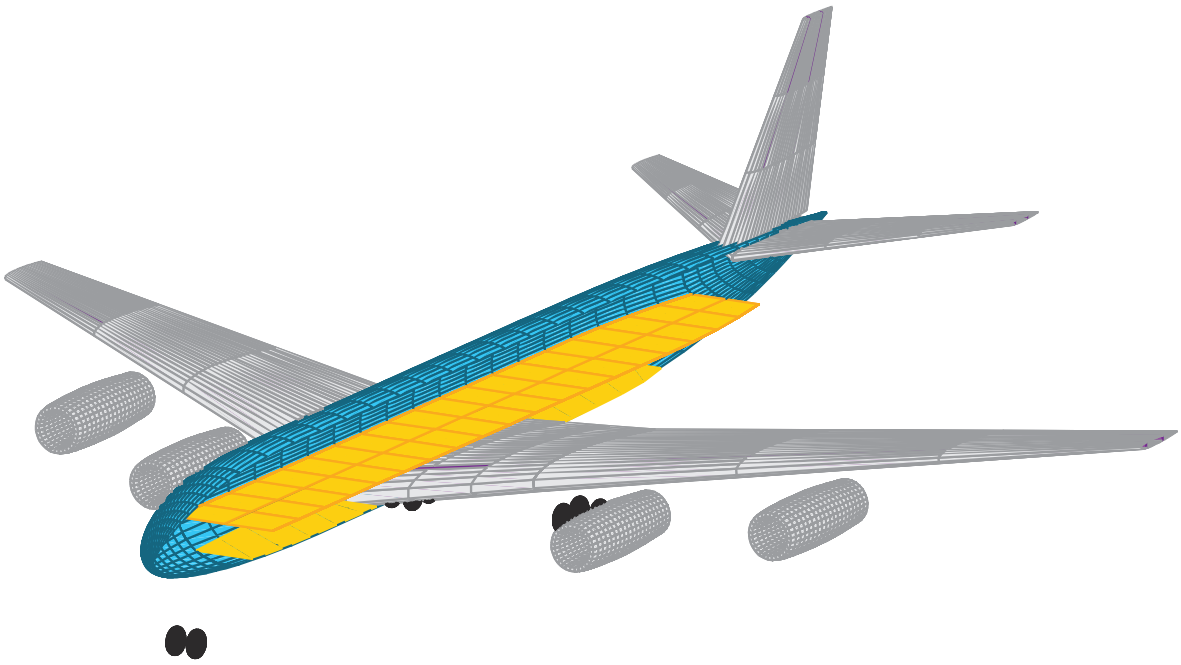

Figure E-9: Douglas DC8-55

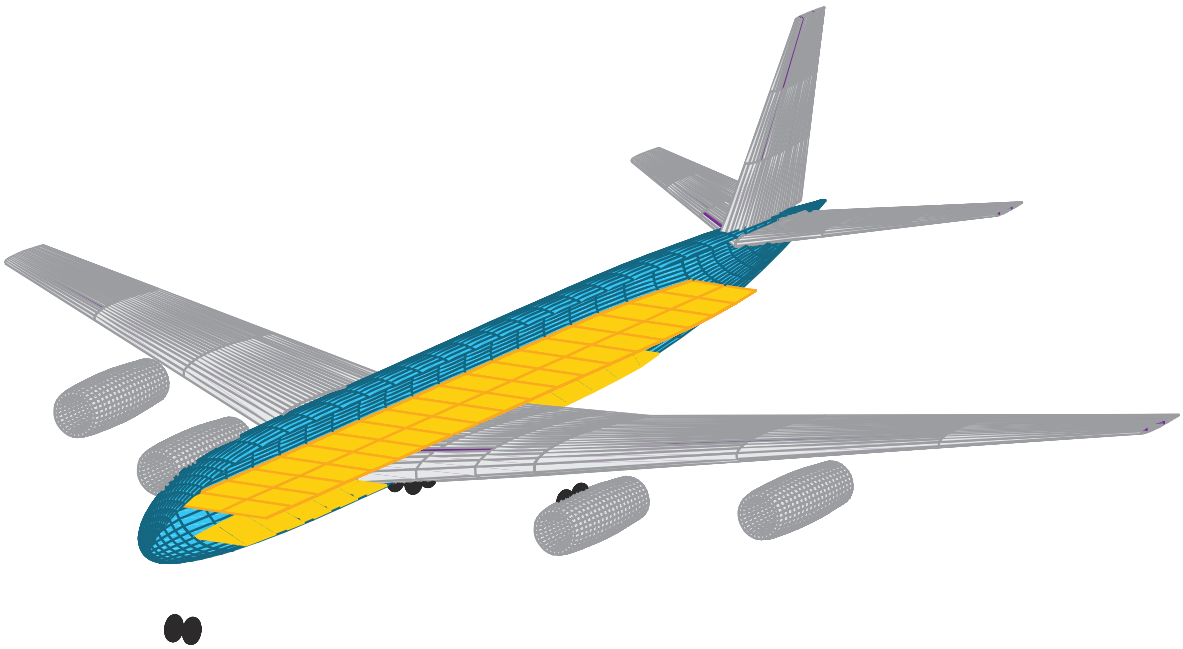

Figure E-10: Douglas DC8-72

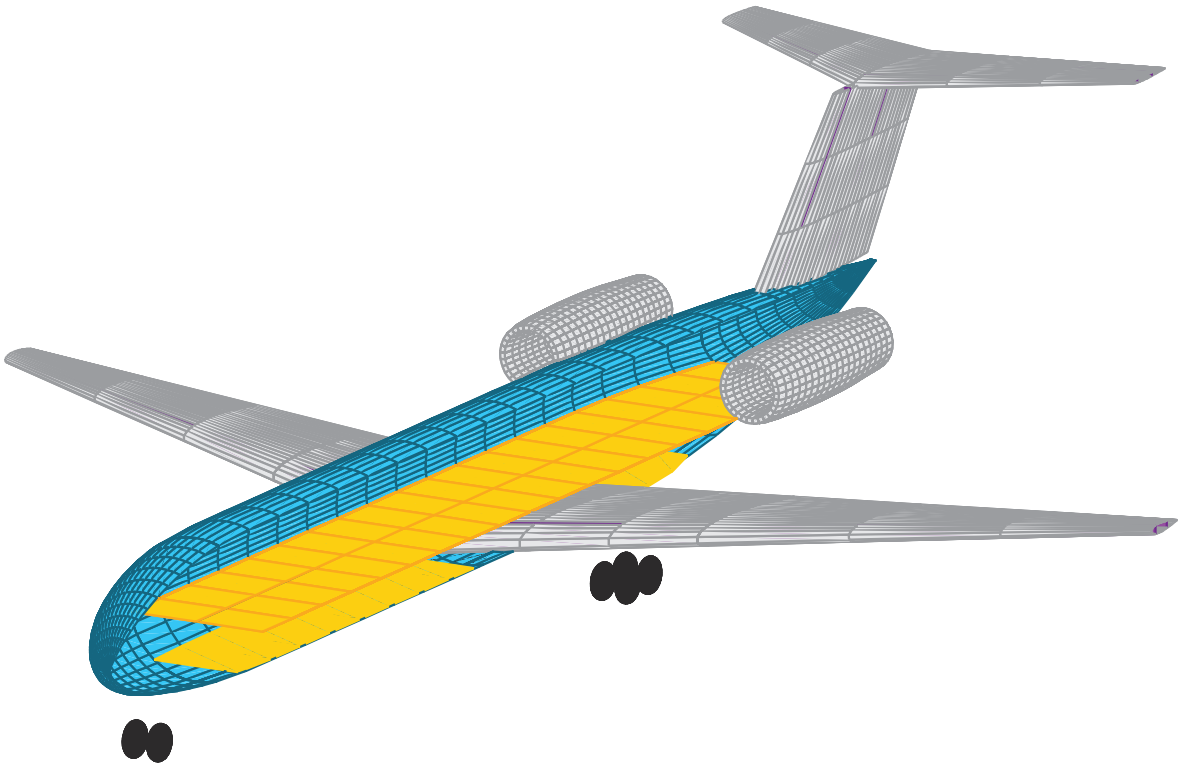

Figure E-11: Fokker 100

Bibliography

[1] M. Potsdam, M. Page, and R. Liebeck, "Blended Wing Body aircraft analysis and design," 1997.

[2] J. A. Pertuze, S. Sato, Z. S. Spakovszky, and C. S. Tan, "N + 3 Aircraft Concept Designs and Trade Studies , Final Report Volume 1," vol. 1, no. December, 2010.

[3] NASA, "Hybrid Wing Body Goes Hybrid," 2013.

[4] C. Hange, "Performance Challenges of Hybrid Wing CESTOL Transports," no. January, 2009.

[5] JSC "Russian Avia Consortium", "Frigate Ecojet," 2013.

[6] R. Wood and S. Bauer, "Flying wings/flying fuselages," in *39th AIAA Aerospace Sciences Meeting & Exhibit*, no. January, p. 25, 2001.

[7] K. Nickel and M. Wohlfahrt, *Tailless aircraft in theory and practice*. Washington: AIAA, 1st ed., 1994.

[8] R. Liebeck, "Design of the blended wing body subsonic transport," *Journal of Aircraft*, vol. 41, no. 1, 2004.

[9] B. Mohr, D. Paulus, H. Baier, and M. Hornung, "Design of a 450-passenger blended wing body aircraft for active control investigations," *Proceedings of the Institution of Mechanical Engineers, Part G: Journal of Aerospace Engineering*, Dec. 2011.

[10] J. I. Hileman, Z. S. Spakovszky, M. Drela, M. a. Sargeant, and a. Jones, "Airframe Design for Silent Fuel-Efficient Aircraft," *Journal of Aircraft*, vol. 47, pp. 956–969, May 2010.

[11] C. Nickol, "Hybrid Wing Body Configuration Scaling Study," *50th AIAA Aerospace Sciences Meeting*, pp. 1–15, 2012.

[12] O. Bergsma, S. Koussios, and A. Beukers, "Pressure vessels & pressure cabins for Blended Wing Bodies," in *ICCM Conference*, p. 12, 2009.

[13] V. Mukhopadhyay, "Blended-Wing-Body (BWB) Fuselage Structural Design For Weight Reduction," *46th AIAA/ASME/ASCE/AHS/ASC Structures, Structural Dynamics & Materials Conference*, no. April, pp. 18–21, 2005.

[14] R. Vos, F. Geuskens, and M. Hoogreef, "A New Structural Design Concept for Blended Wing Body Cabins," no. April, 2012.

[15] M. Chambers, M. Ardema, and A. Patron, "Analytical Fuselage and Wing Weight Estimation of Transport Aircraft," no. May, 1996.

[16] V. Mukhopadhyay, "A Conceptual Aerospace Vehicle Structural System Modeling, Analysis and Design Process," in *48th AIAA/ASME/ASCE/AHS/ASC Structures, Structural Dynamics, and Materials Conference*, no. April, pp. 10–13, 2007.

[17] V. Mukhopadhyay, "Hybrid Wing-Body (HWB) Pressurized Fuselage Modeling, Analysis, and Design for Weight Reduction," pp. 1–14, 2012.

[18] T. Laughlin, J. Corman, and D. Mavris, "A Parametric and Physics-Based Approach to Structural Weight Estimation of the Hybrid Wing Body Aircraft," no. January, pp. 1–20, 2013.

[19] C. Nickol and L. McCullers, "Hybrid wing body configuration system studies," *AIAA Paper*, no. January, pp. 1–12, 2009.

[20] K. R. Bradley, "A Sizing Methodology for the Conceptual Design of Blended-Wing-Body Transports," no. September, 2004.

[21] A. Morris, P. Arendsen, and G. LaRocca, "MOB-a European project on multidisciplinary design optimisation," *24th ICAS ...*, 2004.

[22] R. Vos and J. Van Dommelen, "A Conceptual Design and Optimization Method for Blended-Wing-Body Aircraft," no. April, pp. 1–14, 2012.

[23] B. Kulfan, "A universal parametric geometry representation method - CST," *AIAA Paper*, no. January, pp. 1–35, 2007.

[24] R. Vos, F. Geuskens, and M. F. M. Hoogreef, "A New Structural Design Concept for Blended Wing Body Cabins," in *53rd AIAA/ASME/ASCE/AHS/ASC Structures, Structural Dynamics and Materials Conference
20th AIAA/ASME/AHS Adaptive Structures Conference
14th AIAA*, Structures, Structural Dynamics, and Materials and Co-located Conferences, American Institute of Aeronautics and Astronautics, Apr. 2012.

[25] D. M. Fryer and J. F. Harvey, *High Pressure Vessels*. Chapman & Hall, 1998.

[26] M. I. Gerritsma, *Computational Fluid Dynamics*. Delft University Press, 2002.

[27] L. Prandtl, "Application of modern hydrodynamics to aeronautics," tech. rep., NACA, 1923.

[28] J. D. Anderson, *Introduction to Flight*. McGraw-Hill Professional, 2005.

[29] *Tornado User Manual.*

[30] *Athena Vortex Lattice.*

[31] R. H. Sivells James C; Neely, "Method for calculating wing characteristics by lifting-line theory using nonlinear section lift data," tech. rep., NACA, 1947.

[32] R. F. Anderson, "Determination of the characteristics of tapered wings," tech. rep., NACA, 1937.

[33] K. Schmidt, "CleanEra technology demonstrator." 2012.

[34] J. Mariens, "Wing Shape Multidisciplinary Design Optimization," tech. rep., Delft University of Technology, 2012.

[35] N. Matsui, "Method for producing body structure of fiber-reinforced composite, and body structure produced thereby," Jan. 2003.

[36] S. D. Henry and F. Reidenbach, *Fatigue Data Book: Light Structural Alloys.* Asm Intl, 1995.

[37] R. von Mises, "Mechanik der festen Körper im plastisch- deformablen Zustand," *Nachrichten von der Gesellschaft der Wissenschaften zu Göttingen, Mathematisch-Physikalische Klasse*, vol. 1913, pp. 582 – 592, 1913.

[38] R. Ley, W. Lin, and U. Mbanefo, *Facesheet wrinkling in sandwich structures.* No. January, 1999.

[39] H. G. Allen, *Analysis and design of structural sandwich panels.* The Commonwealth and international library: Structures and solid body mechanics division, Pergamon Press, 1993.

[40] P. Seide, V. I. Weingarten, and J. Peterson, "Buckling of thin-walled circular cylinders," tech. rep., National Aeronautics and Space Administration, 1986.

[41] G. Gerard and N. Y. University, *Handbook of structural stability: Buckling of curved plates and shells, Part 3.* National Aeronautics and Space Administration, 1959.

[42] F. R. Shanley, *Weight-strength analysis of aircraft structures.* (Dover Publications), Dover Publications, 1960.

[43] S. P. Timoshenko and J. M. Gere, *Theory of Elastic Stability.* Dover Publications, Incorporated, 2012.

[44] E. Obert, *Aerodynamic Design of Transport Aircraft.* IOS Press, 2009.

[45] E. Torenbeek, *Synthesis of Subsonic Airplane Design: An Introduction to the Preliminary Design of Subsonic General Aviation and Transport Aircraft, with Emphasis on Layout, Aerodynamic Design, Propulsion and Performance.* Springer, 1982.

[46] D. Howe, "Blended wing body airframe mass prediction," *Proceedings of the Institution of Mechanical Engineers, Part G: Journal of Aerospace Engineering*, vol. 215, pp. 319–331, Jan. 2001.

[47] R. Vos and M. Hoogreef, "Semi-Analytical Weight Estimation Method for Fuselages with Oval Cross-Section," in *54th AIAA/ASME/ASCE/AHS/ASC Structures, Structural Dynamics, and Materials Conference*, Structures, Structural Dynamics, and Materials and Co-located Conferences, American Institute of Aeronautics and Astronautics, Apr. 2013.

[48] HIWTC, "Aircraft unit load device specifications," 2013.

[49] S. Timoshenko, *Strength of Materials, Part 1 and Part 2*. Krieger Pub Co, 1983.

[50] C. Niu and M. C. Y. Niu, *Airframe Structural Design: Practical Design Information and Data on Aircraft Structures*. Airframe book series, Hong Kong Conmilit Press Limited, 1999.

[51] E. Torenbeek, *Synthesis of Subsonic Airplane Design*. Springer, 1982.

[52] D. P. Raymer, *Aircraft Design: A Conceptual Approach*. American Institute of Aeronautics and Astronautics, 2012.

[53] L. M. Nicolai, *Fundamentals of Aircraft Design*. Nicolai, 1975.

[54] D. Howe, *Initial Aircraft Weight Prediction*. 1957.

[55] S. D. Henry, K. S. Dragolich, N. D. DiMatteo, and A. S. M. International, *Fatigue Data Book: Light Structural Alloys*. Asm International, 1994.